Synthesis and Permeation of Large Pore Metal-organic Framework Membranes

by

Alexandra Kasik

A Dissertation Presented in Partial Fulfillment
of the Requirements for the Degree
Doctor of Philosophy

Approved November 2015 by the
Graduate Supervisory Committee:

Jerry Lin, Chair
Amaneh Tasooji
Terry Alford

ARIZONA STATE UNIVERSITY

December 2015

ABSTRACT

Large-pore metal-organic framework (MOF) membranes offer potential in a number of gas and liquid separations due to their wide and selective adsorption capacities. A key characteristic of a number of MOF and zeolitic imidazolate framework (ZIF) membranes is their highly selective adsorption capacities for CO_2. These membranes offer very tangible potential to separate CO_2 in a number of industrially relevant separation processes, such as the separation from CO_2 in flue gas emissions, as well as the sweetening of methane.

By virtue of this, the purpose of this dissertation is to synthesize and characterize two linear large-pore MOF membranes, MOF-5 and ZIF-68, and to study their gas separation properties in binary mixtures of CO_2/N_2 and CO_2/CH_4. The three main objectives researched are as follows. The first is to study the pervaporation behavior and stability of MOF-5; this is imperative because although MOF-5 exhibits desirable adsorption and separation characteristics, it is very unstable in atmospheric conditions. In determining its stability and behavior in pervaporation, this material can be utilized in conditions wherein atmospheric levels of moisture can be avoided. The second objective is to synthesize, optimize and characterize a linear, more stable MOF membrane, ZIF-68. The final objective is to study in tandem the high-pressure gas separation behavior of MOF-5 and ZIF-68 in binary gas systems of both CO_2/N_2 and CO_2/CH_4.

Continuous ZIF-68 membranes were synthesized via the reactive seeding method and the modified reactive seeding method. These membranes, as with the MOF-5 membranes synthesized herein, both showed adherence to Knudsen diffusion, indicating limited defects. Organic solvent experiments indicated that MOF-5 and ZIF-68 were

i

stable in a variety of organic solvents, but both showed reductions in permeation flux of the tested molecules. These reductions were attributed to fouling and found to be cumulative up until a saturation of available bonding sites for molecules was reached and stable pervaporation permeances were reached for both. Gas separation behavior for MOF-5 showed direct dependence on the CO_2 partial pressure and the overall feed pressure, while ZIF-68 did not show similar behavior. Differences in separation behavior are attributable to orientation of the ZIF-68 membranes.

DEDICATION

To Bob,

This degree is just as much yours as mine.

You knew I could do this even when I had moments when I wasn't so sure myself, and

this wouldn't have been possible without your endless love and support.

ACKNOWLEDGMENTS

If it takes a village to raise a child, that certainly extends to doctorate degrees, as well. I have been so blessed to have had countless advocates, cheerleaders and angels help me on this long, strange journey. With that said, I absolutely need to thank my family. From my mom being my biggest cheerleader through all of grad school's ups and downs, to my dad who taught me through his actions my entire life the importance of hard work, integrity and goofiness. As for my brother, I am continually in awe of his strength, physically of course, but also emotionally and mentally. And of course, Bob and Stephanie, who certainly qualify as family at this point.

I feel so lucky to have gotten to work for Prof. Lin. His guidance and endless patience were hugely instrumental in my attaining this degree and it was a privilege to be guided through this PhD by someone so kind and knowledgeable and passionate about his field of study. I also want to thank all past and present members of Prof. Lin's group for their continual encouragement, friendship and support. I consider all of them my friends, and I am so excited to have been able to be a part of such an amazing research group. Also, Fred Pena, whose help and efforts have undoubtedly aided in the graduating of countless students. I am so thankful for every bit of encouragement, support and insight he has given me.

I would like to thank my committee members, Prof. Amaneh Tasooji and Prof. Terry Alford, not only for their time and efforts in their roles as committee members, but also in the impact they had on me as an undergraduate student. It is nothing short of a miracle that the people behind Materials Science and Engineering at ASU could take a kid who never even wanted to go to college and was on the verge of dropping out of

business school and support, encourage and foster such a deep love of the subject matter that it eventually culminated in a doctorate in the subject. I had such an incredible experience at this school, with the people, resources and structuring that I had access to, that I know unequivocally I would not have had this success at any other institution.

Never one to leave a thank you un-thank you'd… I can't omit some of the most important furry, quadrupedal people in my life: Gertie, Chuck, Ursula and my dearly departed Tonk and Pogie. Their continual supply of kisses and wiggles and tear-inducing gas makes life worth living, and I thankful to my wiggly little buddies for their unwavering love and silliness.

Finally, 6 years ago as I began to navigate the nebulous process of leaving full-time work for misadventures in graduate studies, there was a constant guiding light of support and encouragement, Yolanda Murphy. I might be one of the last graduating students to have been lucky enough to have had her as an advisor, and I just want to thank her for her help. She absolutely cared about her students and their success, and I am so fortunate to have been able to know her.

TABLE OF CONTENTS

LIST OF TABLES

LIST OF FIGURES

CHAPTER 1

INTRODUCTION

1.1 General Introduction

Over the last few decades it has become increasingly inadmissible to deny the role human activity is playing in global climate change. As the body of quantifiable, credible and largely unbiased reports on increased levels of greenhouse gases, widespread glacial recession and inexplicable disruptions to natural processes grows, it becomes all the more evident that there will need to be an overhaul of traditional manners of energy creation, storage and utilization in order to sustainably balance the needs of an exploding population with those of our planet (Houghton, 2005).

As the issues associated with global climate change continue to come to light, it is clear that there will likely not be a single solution to reverse, or at least slow, the damage. The answer to some of the more pressing issues will instead be found in the form of a myriad of resourceful materials, novel processes and conscientious changes all working in conjunction. It is in this regard that membranes and membrane processes have the potential to be widely utilized. From reducing the energy consumed in creating clean drinking water, to separating and permanently storing CO_2 found in the atmosphere, to the use of membranes in environmentally-friendly fuel cells, membranes may help lessen the burden of the earth while simultaneously helping meet the needs of its billions and billions of inhabitants (Kim, 2008).

Especially relevant, potentially transformative uses for these ubiquitous materials that will serve as a prominent focus of this introduction are in pre- and post-combustion gas separation, methane sweetening and organic solvent pervaporation. Currently

polymeric membranes are widely used industrially, with inorganic membranes having gained tremendous ground throughout recent years, and lastly metal-organic frameworks have become of huge interest to help bridge some fundamental gaps and issues associated with the use of polymeric or inorganic membranes.

1.1.1 Polymeric Membranes

Polymeric membranes have brought the study of membrane sciences to the forefront of applicability and relevance over the last two hundred years. With their relative ease of synthesis and utilization, polymeric membranes have been found crucial to a number of industries and the use and study of this broad class of membranes has been able to effectively evolve with the needs of a growing society and stave off obsolescence in a way rarely afforded to technologies. It is interesting, however, that of the hundreds of nonporous polymeric membranes that have been studied since the 19th century, relatively few have found strongholds in commercially viable processes, with the most notable of these being cellulose acetate, polysulphone, polyimides and silicon rubbers (Yampolskii, 2012). This is largely due to the field of study being far more diverse and complex than it would initially seem. When studying polymeric membranes a great many considerations must be taken into account; properties such as side-group size, cross-linking, degree of crystallinity and gas transition temperature can result in membranes with dramatically different properties and applicabilities (Yampolskii, 2012). It stands to reason that with the ease of materials synthesis and customizability coupled with a sizeable degree of rational design, polymeric membranes are, and will continue to be, a preeminent membrane technology.

This is certainly the case at this time, as polymeric membranes are used for an overwhelming majority of commercial membrane applications. This is largely due to the reproducible and inexpensive nature of polymeric membrane synthesis, as well as the ease and effectiveness with which they are able to separate an array of systems. From wastewater treatment to biomedical applications, polymeric membranes have proven themselves to be not only invaluable, but also, as in the case of membranes used for hemodialysis, far superior to what nature is capable of achieving (Ulbricht, 2006).

Despite all of the utility these membranes serve, there are still some hurdles for the seamless utilization of polymeric membranes in many relevant gas separation applications. The most widely documented is the frustrating opportunity cost of permeability polymeric membranes exhibit with increasing selectivity, and vis versa, known as Robeson's upper bound (Robeson, 1991). Robeson found that when testing binary systems of He, H_2, O_2, N_2, CH_4 and CO_2, that the permeability of the more permeable of the gases tested varies inversely with the separation factor (Robeson, 1991). This severity of this effect is found to be related proportionally to an increase in the difference between the kinetic diameters of the two permeating molecules in the binary system, and this is illustrated graphically in Figure 1.1. For a membrane to be ideally viable, it would require the highest permeability and selectivity as possible.
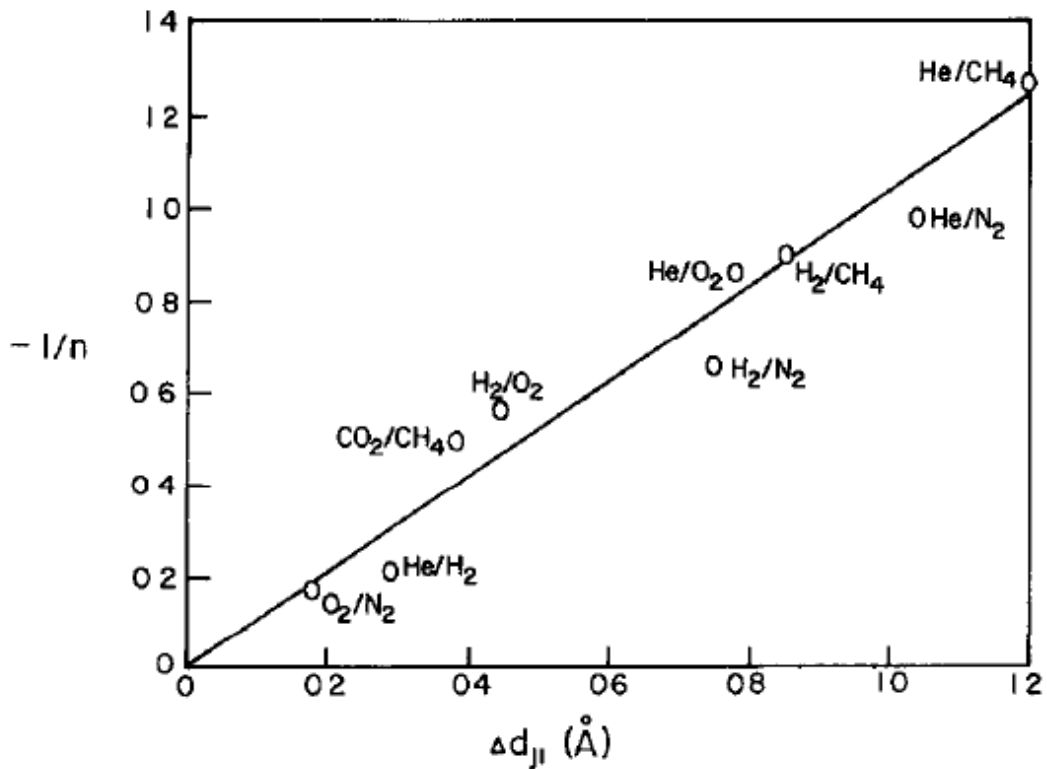
Figure 1.1

Correlation between the slope (n) of the upper bound limit and the difference between the

kinetic diameters of the permeating molecules (Robeson, 1991).

Robeson's Upper Bound Curve, however, is not the only hindrance to wider

spread polymeric membrane usage, there is also the permeability degrading plasticization

and aging that commonly occur in polymeric membranes when separating highly

condensable molecules; CO_2, at industrially relevant pressures and temperatures, being a

condensable molecule (Y. Xiao, Low, Hosseini, Chung, & Paul, 2009). Lower pressure

and temperature experiments typically cannot be extrapolated to feasible pressures and

temperatures at which real life applications would necessitate with much degree of

certainty due to the nature of CO_2 (Wessling, 1991). When separation of binary systems containing CO_2 occurs at higher pressures, there is a dramatic loss of selectivity as the feed pressure is increased. This effect is shown in Figure 1.2 for two polyimide membranes separating a 20/80 mixture of CO_2/CH_4 at pressures from 30 to 70 bar (Wessling, 1991).
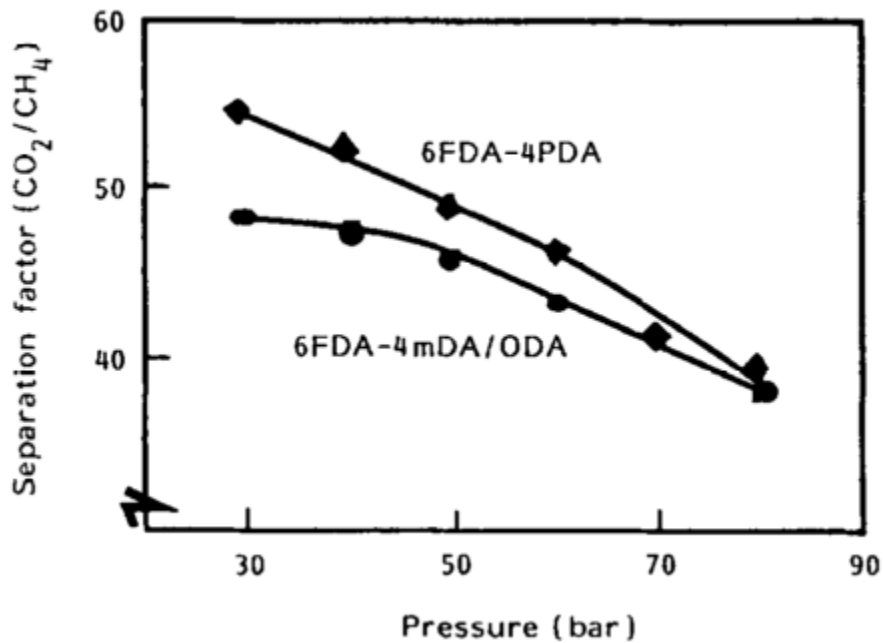
Figure 1.2

Schematic representation of the loss of selectivity evidenced by polymeric membranes with increasing pressures of CO_2 (Wessling, 1991).

The second detrimental effect that occurs in polymeric membranes separating CO_2 is that with an increase in pressure, there is a generally evidenced decrease in permeability for glassy polymers (Wessling, 1991). With more rubbery membranes, this effect is reversed, however, and with enhanced time at certain pressures the CO_2

5

ultimately causes swelling through ingratiating itself into the polymeric matrix. The effect is different depending upon the pressure at which it occurs. Below the critical plasticization pressure the CO_2 is thought to break the bonds between the shorter chains, while above the critical plasticization pressure longer chains begin rearranging as denser chain entanglements begin relaxing. Through both mechanisms the resultant effect is an overall decreased hindrance to molecular diffusion for all permeating species, thereby an increase in permeability, but decrease in selectivity (Wessling, 1991).

While polymeric membranes provide the backbone for a multi-billion dollar membrane industry worldwide, there are clearly some inherent drawbacks and it is in this vein research of inorganic membrane materials has tangentially skyrocketed (Ulbricht, 2006).

1.1.2 Inorganic Membranes

The classification of inorganic membranes is very diverse, and it can encompass metallic, ceramic and completely carbon membranes, as well as non-porous materials and macroporous materials alike. Given the nature of this dissertation, not all permutations of inorganic membrane are linearly relevant and necessary to discuss. The predominant focus herein will be on microporous aluminasilicate membranes known as zeolites. Zeolite membranes have regular frameworks created from silicon and aluminum atoms tetrahedrally coordinated to oxygen atoms. These tetrahedrally coordinated atoms combine to create frameworks of channels and pores of discrete size that make up the variants of zeolites (Tavolaro & Drioli, 1999a). These tetrahedral metallic/oxygen clusters form to create the defining feature of zeolites; their rigid, porous framework. These frameworks can be small, medium, large or ultra large pore in nature and the pore

size is determined by the number of tetrahedra that comprise the rings that make up the pore openings. These rings can either be 6-, 8- or 9-membered for smaller pore zeolites, 10-membered for medium pore zeolites, 12-membered for large pore zeolites and 14-, 18- and 20-membered for ultra-large pore zeolites (Tavolaro & Drioli, 1999b). See Figure 1.3 for a representative illustration of two specific zeolite topologies, MFI, a medium pore zeolite defined by its 10-membered ring, and CHA, a small pore zeolite defined by its 8-membered ring. Given the great variability the size of rings affords zeolite structures; it follows that a large number of zeolite conformations have been discovered thus far, upwards of 190, in fact. It is surprising, however, that of those 190 only 20 have been successfully synthesized into membrane form (Tavolaro & Drioli, 1999a).
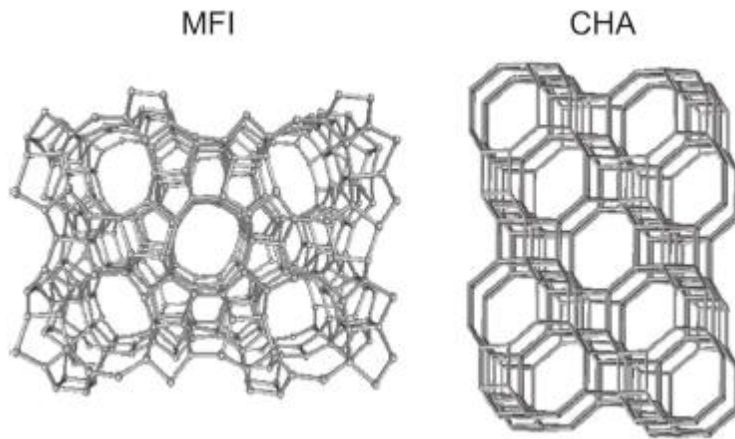
Figure 1.3

Atom stick representation of two different zeolite structures, MFI and CHA that are characteristic of a 10-memberd ring zeolite, ZSM-5, and an 8-membered ring zeolite, SAPO-34, respectively (Yu, Noble, & Falconer, 2011).

As opposed to most polymeric membranes, zeolite membranes are typically "anisotropic" or "asymmetric", that is to say the zeolite layers are thin films deposited or synthesized on a variety of thicker, more structurally sound supports. There has been a remarkable variability in materials used for zeolite membrane supports, everything from stainless steel, to glass, silicon to copper, quartz to $LiTaO_3$, and with this variability the application for which the zeolite membranes may be utilized is greatly broadened (Tavolaro & Drioli, 1999a).

Aside from the wide range of sizes and substrates, these permanently porous materials are also characterized by a remarkable thermal and chemical stability, reports of which date back quite far. For example, Khodakov et al. reported in 1969 the maximum temperatures for which zeolite types A, X and Y were stable to be between 880 and 960°C, and more recently, Garcia-Martinez et al. reported that zeolite Y membranes showed no decrease in pore volume following 4 hours in pure steam held at 788°C (Garcia-Martinez, Johnson, Valla, Li, & Ying, 2012; Khodakov et al., 1969). This stability and relative chemical inertness is quite contrary to that of polymeric membranes, and is a perfect example of why zeolite membranes are a necessary compliment to polymeric membranes. Zeolite membranes exhibit strengths where polymeric membranes exhibit weaknesses. However, zeolite membranes are not without a unique and challenging set of drawbacks. As mentioned previously, there are a finite number of pore size permutations for which zeolite membranes may take, attributable to the finite number of membered rings that comprise existing zeolite structures. A direct consequence of this is a somewhat limited array of pore sizes available, thereby diminishing significantly the possible gas separation processes available to zeolite

membranes (Shah, Mccarthy, Sachdeva, Lee, & Jeong, 2012). Aside from limited pore size/structure customizability, the most predominant drawback to zeolite membranes is the cost-prohibitive nature of scale-up. Zeolite membranes have proven extremely difficult to synthesize free of defects, and this is compounded as the size of the membrane increases. With polymeric membranes synthesis is easy and reproducibility is exceptionally high, but this is not the case with zeolite membranes. Though synthesis avenues have evolved to address hindrances to reproducibility, such as direct synthesis over templating, the cost of synthesizing a large-scale, continuous, high-quality zeolite membrane remains quite astronomical, and one of the only reasons this material is not more commonly utilized in industrial scale separation processes as of yet (Baker, 2004).

It is due to the difficulties associated with the strictly polymeric or strictly inorganic materials that a new class of materials, metal-organic frameworks (MOFs), was developed toward the very end of the 20th century, and has proceeded to become a very prominent and hotly researched area.

1.1.3 Metal-organic Frameworks

Having only first emerged as a research area in the late 20th century, metal-organic frameworks (MOFs) are a relatively new class of microporous material. One of the earlier and more auspicious reports of MOFs was the 1989 publication by Hoskins and Bernard on "Infinite Polymeric Frameworks Consisting of Three Dimensionally Linked Rod-like Segments." Hoskins et al. reported in that work on tetrahedrally coordinated valencies that through linking of rod-like molecules were able to create infinite crystals of cavities and windows (Hoskins & Robson, 1989). Hoskins and Robson continued on to hypothesize that these materials "may show interesting

molecular sieve or ion exchange properties, they may have unusual mechanical and electrical properties and they may, after appropriate functionalization of the rods, provide tailor-made materials for heterogeneous catalysis of a wide range of transformations (Hoskins & Robson, 1989)."

These early permutations of MOFs, such as the one discussed by Hoskins and Robson, were referred to as coordination polymers despite their heavy reliance on a negatively charged Cu atom to allow for tetrahedral formulation and infinite expansion through space (Hoskins & Robson, 1989). This term undoubtedly refers to the type of bonding characteristic to MOF materials; the organic linkers act as a Lewis base and donate two electrons to the metallic tetrahedra which act as Lewis acids, and form covalent coordination bonds (Shah et al., 2012). These materials were soon referred to more inclusively as metal-organic frameworks toward the end of the 20th century. The change in standard nomenclature is shown to coincide with the prevalence of coordination polymers in journal publications, as shown in Figure 1.4. The coining of the term MOF, and the increase of its use as a term as shown in Figure 1.4, was undoubtedly spurred by the evolution of research; as more was understood about the metal centers and the functionality they can exhibit, the more invaluable they became.

Metal-organic frameworks consist of metallic ion secondary building units (SBUs) that are tetrahedrally coordinated to rigid organic linkers (Eddaoudi, Li, & Yaghi, 2000). The materials exhibit permanent porosity, and are characterized by impressively high surface areas. Further interest in the materials stems from the nature of the materials themselves; through altering metallic constituents in the SBUs or the organic linkers used, it is possible to create entirely new MOF materials that can be tailored to meet the

10

needs of a given application. MOF materials truly began to gain research traction when a report on MOF crystals by Yaghi et al. in the late 90's as first published (Rosi, Eckert, Eddaoudi, & Vodak, 2013). Since then, through alterations to the organic linkers used and the SBUs, the field has expanded to countless different conformations of MOF crystals and MOF membrane materials.
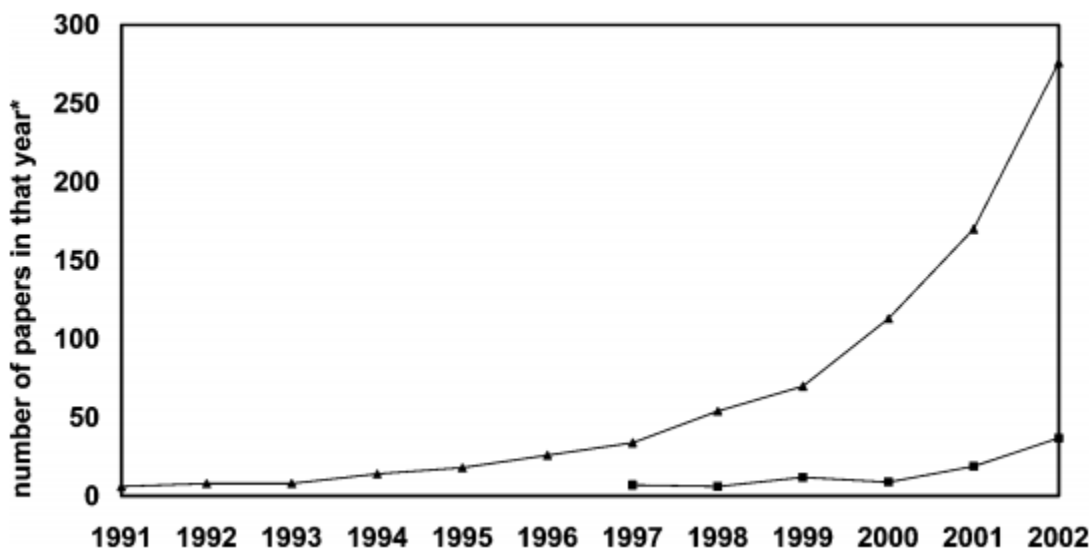
Figure 1.4

Comparative graph showing the prevalence with which coordination polymers (triangles) and metal-organic frameworks (squares) were mentioned in scientific publications (James, 2003).

MOFs encompass a number of subsets, such as isoreticular metal-organic frameworks (IRMOFs), MIL materials developed at the Materials Institut Lavoisier, HKUST materials developed at the Hong Kong University of Science and Technology, zeolitic imidazolate frameworks (ZIFs) and the aforementioned coordination polymers

(CPs) (Shekhah, Liu, Fischer, & Wöll, 2011). There are, of course, a myriad of other means of denoting and referring to MOF materials, however, these are the most common and identifiable and the bulk of the materials referenced in this dissertation should fall under the aforementioned naming schemes.

1.2 Synthesis of MOF Membranes

The notion of customizable microporous materials capable of tackling a wide array of industrially relevant gas and liquid separations with enhanced acuity due to their metallic and inorganic nature is enticing. However, prior to testing the feasibility of these materials in any of these applications, they must first be tangibly synthesized in a usable form. For many MOF applications, this form is as an "asymmetric," or supported, membrane layer on a mechanically sound, porous support. The support is chosen to facilitate a given application, such as high temperature or pressure applications, and typically has a pore size that will not compete with the pore size of the membrane material. Examples of supports are shown in Figure 1.5.
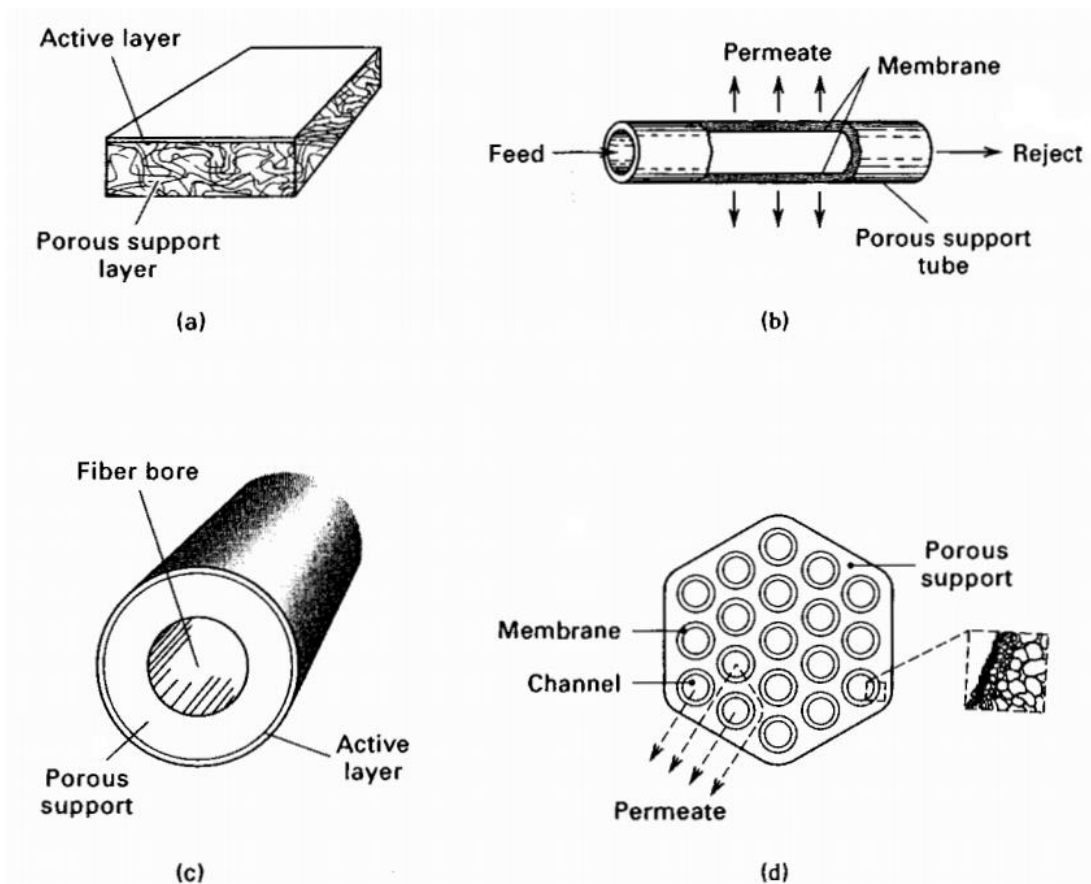
Figure 1.5

Common membrane support shapes: (a) flat asymmetric sheet, (b) tubular, (c) hollow fiber and (d) monolithic (Seader & Henley, 1998).

The general research path these novel microporous materials tend to follow is to initially find numerous reports of MOF crystal synthesis, sorption, structure and stability, both hypothetical and experimental, prior to the emergence of data on membrane synthesis. As the body of knowledge available surrounding a specific MOF crystal becomes denser, usually only then is it possible to find reports of membrane synthesis begin to emerge. Of these synthesis methods, there are further trends. Initially synthesis methods are more traditional and straightforward, and can closely resemble synthesis

techniques widely implemented in the study of inorganic membranes, but as reports on synthesis increase there is a continual evolvement of the processes outlined. As interest in a MOF material grows, so does the body of knowledge outlining membrane synthesis; synthesis techniques tend to become more novel, more streamlined, less energy consumptive, and can grow to cater to a wider array of applications through altering the support and membrane thickness.

The following discussion on MOF membrane synthesis will begin with a widely reported and highly effective method of synthesis with a proven track record of facilitating successful and efficient membrane synthesis for a number of inorganic membranes, the *in situ* method. The *in situ* method, although quite effective, is not the right choice for all asymmetric membrane systems. In this case, a slightly more involved method of synthesis can then be used, seeded secondary growth, which will then be discussed. Seeded secondary growth utilizes the same principle as *in situ*, but adds a preliminary seeding step when heterogeneous nucleation during a single *in situ* synthesis has proven difficult to obtain. And, finally, as research evolves, it is only natural that the combinations of support and membrane, as well as the applications and membrane targets, also evolve and with this synthesis methods change. The final portion of this section on synthesis will provide an overview of the ever-growing number of novel synthesis methods, such as reactive seeding and surface functionalization, which have been reported.

1.2.1 *In Situ* Synthesis

Having been widely studied and utilized in zeolite membrane synthesis, the *in situ,* or direct synthesis method, has had similar success with MOF materials (Y. S. Lin,

Kumakiri, Nair, & Alsyouri, 2007). Although this method differs from that used in zeolites due to the predominantly solvothermal conditions MOFs require, the overall process is one in which a smooth porous support, without any previous modification, is brought into contact with a synthesis solution and held. During the holding step, which is usually at elevated temperatures, nucleation, growth and subsequent intergrowth all occur (Shah et al., 2012; Yao & Wang, 2013).

The first successful synthesis of a MOF material wherein the membrane was continuous and of high enough quality for preliminary gas permeation experiments to be carried out was for MOF-5. Lai et al. performed an *in situ* synthesis analogous to those previously used for zeolite membranes and found that the MOF materials showed strong attraction to the α-alumina support (Yunyang Liu et al., 2009). The robust adhesion of MOF-5 to the support can be attributed to the covalent bonds that form readily between the hydroxyl groups on the surface of the support and the carboxyl groups of the organic ligand (Bertazzo & Rezwan, 2010). It is in this regard that *in situ* synthesis should be considered as a viable option for any carboxylic acid based MOFs, such as MOF-5. However, that is not to say a carboxyl group is necessary for successful *in situ* membrane synthesis, as a number of imidazole based ZIF materials have been successfully synthesized thus far utilizing a direct approach.

Given the similarities between zeolites and their MOF counterparts, zeolitic imidazolate frameworks, it makes sense early attempts at membrane synthesis would centralize around successful methods of zeolite synthesis, such as in situ synthesis. One of the earliest reported attempts at ZIF synthesis by Lai et al. detailed the *in situ* synthesis of a smaller-pore ZIF material, ZIF-69 (Yunyang Liu, Hu, Khan, & Lai, 2010). The

synthesis methodology, which encompassed a 72 hour hold at 100°C and a 30 hour cooling time, yielded exceptionally well-intergrown and overwhelmingly *c*-orientation membranes, as seen in the SEM micrographs in Figure 1.6.
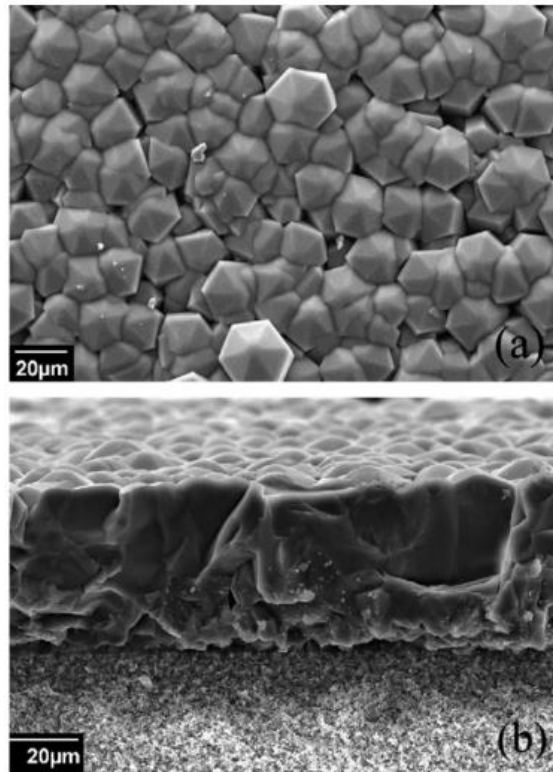
Figure 1.6

SEM micrographs of the (a) top view and (b) cross-sectional view of c-oriented ZIF-69 membrane created by Lai et al (Yunyang Liu et al., 2010).

In situ synthesis methods, although widely used, are not without inherent drawbacks. With *in situ* synthesis, the relationship between the membrane layer and the underlying support is crucial. The support must be smooth and finely polished, an impossibility for tubular-supported membranes, as well as have an appropriate surface

hydrophilicity to incite strong adhesion of nucleating crystals and promote the desired density of nucleation sites (McLeary, Jansen, & Kapteijn, 2006). Not to mention, that in the attempts to foster the needed nucleation density and intergrowth, it may be necessary to synthesize a MOF membrane in an environment wherein the membrane layer can grow to be undesirably thick (McLeary et al., 2006). When any of these issues, or a variety of others, is hindering the successful synthesis of a MOF membrane on a porous support via the *in situ* method, a logical progression of experiment would lead one to attempt synthesis by the seeded secondary growth method.

1.2.2 Seeded Secondary Growth Synthesis

The seeded secondary growth method is another synthesis method that has its roots in traditional zeolite synthesis. Originally proposed after attempts at *in situ* zeolite membrane synthesis were unsuccessful for any number of reasons, this method has served as a remarkably successful starting place for the synthesis of a large number of MOF materials thus far (McLeary et al., 2006).

The process of seeded secondary growth is a two part method that requires first the mechanical application of the relevant membrane materials' seeds followed by a secondary growth step to allow for the intergrowth and impingement of these heterogeneously scattered seeds across the surface of the support. It is carried out first through the synthesis of the MOF crystals. These crystals are then either ball milled or ground if they are much larger than a few microns, or used as is if they are small enough, and inserted into a solvent and mixed thoroughly. This is integral, as the crystal particles must be small to allow for effective seeding, as well as stable sol generation. Once a sol has been created, the process of seeding, or dip coating, occurs when a smoothly polished

support is brought into contact with a sol and suspended in that state of contact for a specified time, on the order of seconds. Upon contact with the sol, differences in capillary pressure cause the sol to enter into the pore and create aggregates of MOF crystals at the surface of the polished support (Y. S. Lin et al., 2007). The effect is generally cumulative, and multiple dip coatings can help create a relatively homogeneously dispersed seeds layer on the support. Although, along with the number of dip coatings, the length of time the support is suspended in a dip coating solution and the concentration of the sol are also important factors to consider when attempting to optimize seeding conditions for a given support/MOF system.

Once seeding is completed, a secondary growth step is needed to create a high-quality membrane layer. Secondary growth allows for the filling of intercrystalline voids and fosters crystal intergrowth through the immersion of a seeded support in dilute synthesis solution and a holding at a typically elevated temperature for an extended period of time (Y. S. Lin et al., 2007). In separating the seed nucleation and dispersal step from the secondary growth step, as opposed to having both occur in the same *in situ* step, can allow for greater control of the resultant membrane. The compatibility of the support to the MOF material has a far greater impact, and in ensuring there is a homogeneous seeds layer covering a large percentage of the support prior to secondary growth allows that step to be carried out in such a way that membrane thickness can be minimized.

Early reports of MOF-5 membrane synthesis show the effect that dip coating can have on the resultant membrane thickness. As was mentioned previously, in 2009 Lai *et al.* synthesized MOF-5 utilizing an *in situ* method, this yielded MOF-5 membranes 25

µm in thickness. It was not until Zhao et al. in 2011 developed a seeded secondary growth synthesis technique for MOF-5 that utilized intimately ground MOF-5 crystals in solution to create a thin, evenly dispersed seeds layer, that MOF-5 membrane thickness jumped down to 15 µm (Yunyang Liu et al., 2009; Z. Zhao, Ma, Li, & Lin, 2011a). This effect was also shown by Lai et al. during ZIF-69 synthesis. The first synthesis method, as outlined in the previously section, created ZIF-69 membranes 50 µm in thickness, however, further attempts at seeded secondary growth resulted in similarly *c*-oriented membranes that were 20% thinner. Further, at times *in situ* synthesis is simply not a viable option for particular MOF/support systems, as research by Nan et al. on HKUST-1 found. When the group compared the two methods of synthesis, *in situ* and seeded secondary growth, it was clear that the *in situ* method resulted in HKUST-1 membranes that were discontinuous and the crystals showed a preference for growth in the solution itself instead of along the support (Nan, Dong, Wang, Jin, & Xu, n.d.).

Seeded secondary growth has been proven as a method of facile, reproducible synthesis for a number of support/MOF material systems, as well as a viable option when seeding via *in situ* synthesis renders the membranes thicker or less continuous than required for the intended membrane purpose. Further, seeded secondary growth has evolved to become a viable method to synthesize membranes on tubular supports and fibers.

This is seen by Venna et al. when the inside of a tubular alumina support was rubbed with dry ZIF-8 seeds prior to secondary growth (Venna & Carreon, 2010). The supports were then hydrothermally treated in the secondary growth solution for 5 hours at 150°C to create low defect, tubular ZIF-8 membranes. The resultant high-quality, 0.8µm

thick membrane layers exhibited remarkably high permeances of CO_2 (Venna & Carreon, 2010). Seeded secondary growth on tubular fibers has also been reported for ZIF-90 on chemically-resistant low-plasticization Torlon polyamide fibers (Yao & Wang, 2014). Instead of a dry rub application of seeds, as with ZIF-8, these polyamide fibers are dip coated in a ZIF-90 seeds solution prior and then secondary growth is carried out (Venna & Carreon, 2010; Yao & Wang, 2014). The results show this method yields highly reproducible, chemically-stable ZIF-90 membranes that exhibit single component gas permeance data that surpasses what is predicted with Knudsen diffusion (Yao & Wang, 2014).

1.2.3 Novel Synthesis Methods

Not all MOFs have proven synthesizable via permutations of the two previously outlined general synthesis methods. In lieu of this more novel synthesis methods have been developed to address deficiencies in existing synthesis methods. The first method to be discussed herein is a straightforward and highly useful alteration to established synthesis techniques through the incorporation of a surface modification to the support. Through the incorporation of a surface modification step, it has been possible to synthesize thinner membranes, higher quality membranes and membranes on surfaces previously thought to be unhospitable to membrane growth. This continual manipulation and extrapolation of existing membrane synthesis methods to better fit the needs of the specific MOF/support system has been widely instrumental in furthering membrane innovations.

This is exemplified in the sheer volume of reports on surface modification that have been reported for MOF materials. In fact, some of the earliest reports on ZIF

membrane synthesis outline surface modification steps. In 2005 Hermes and et al.

outlined the first method of membrane synthesis for MOF-5 that utilized self-assembling

monolayers (SAMs) to bridge the gap between MOF-5 crystals and the Al_2O_3 support

(Hermes, Schröder, Chelmowski, Wöll, & Fischer, 2005).   Around the same time,

McCarthy et al. utilized a thermally activated process of dropping the relevant imidazole

linker in solution on a support held at 200°C to create covalent bonds between the surface

aluminum atoms of the α-alumina support and the nitrogen atoms within the relevant

imidazole linker (Mccarthy, Varela-guerrero, Barnett, & Jeong, 2010).   An example of

the process used is shown in Figure 1.7.   McCarthy et al. found that traditional

solvothermal synthesis on unmodified α-alumina supports were not successful in

synthesizing ZIF-7 or ZIF-8, but they were able to create continuous and high-quality

membranes following a single solvothermal synthesis step on the modified supports

(Mccarthy et al., 2010).
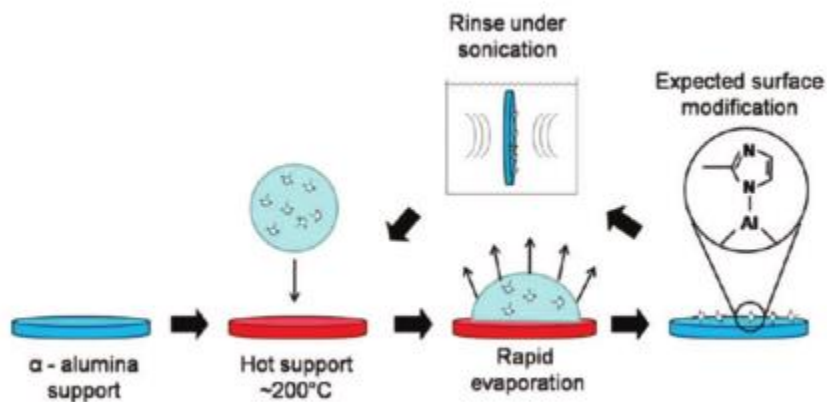
Figure 1.7

Illustrated schematic of ligand surface modification for ZIF materials (Mccarthy et al.,

2010).

Surface modifications, much like synthesis methods, are not always universally applicable for every support/MOF combination. While ZIF-90 is receptive to the previously outlined APTES surface modification, it is hypothesized that many MOF linkers would not be able to provide the linkage groups needed in order to form strong bonds with the APTES surface layer (Q. Liu, Wang, Caro, & Huang, 2013). By virtue of this, Lui et al. set out to create a more universal method of surface modification that could in theory be extrapolated to other MOF materials regardless of any linkage groups that may or may not be already present in the material. To do this, inspiration was drawn from marine mussels, which have adapted to non-discriminately bond to any number of available surfaces under harsh conditions (Waite, 1999). From Teflon to glass, steel and paraffin, the ability of marine mussels to form these immediate bonds in harsh environments not only has helped ensure their survival, but it also has substantial implications in chemistry and materials science alike (Q. Liu et al., 2013; Waite, 1999). Liu et al. utilized this premise to make highly adherent, continuous ZIF-8 membrane layer on alumina supports. The marine-inspired membranes were made through surface functionalization by polydopamine, as shown in Figure1.8. The ZIF-8 membranes were found to have remarkably reproducible quality and mechanical properties, with three independently synthesized ZIF-8 membranes showing an H_2/CH_4 selectivity of 31.3 ± 0.55 (Q. Liu et al., 2013).
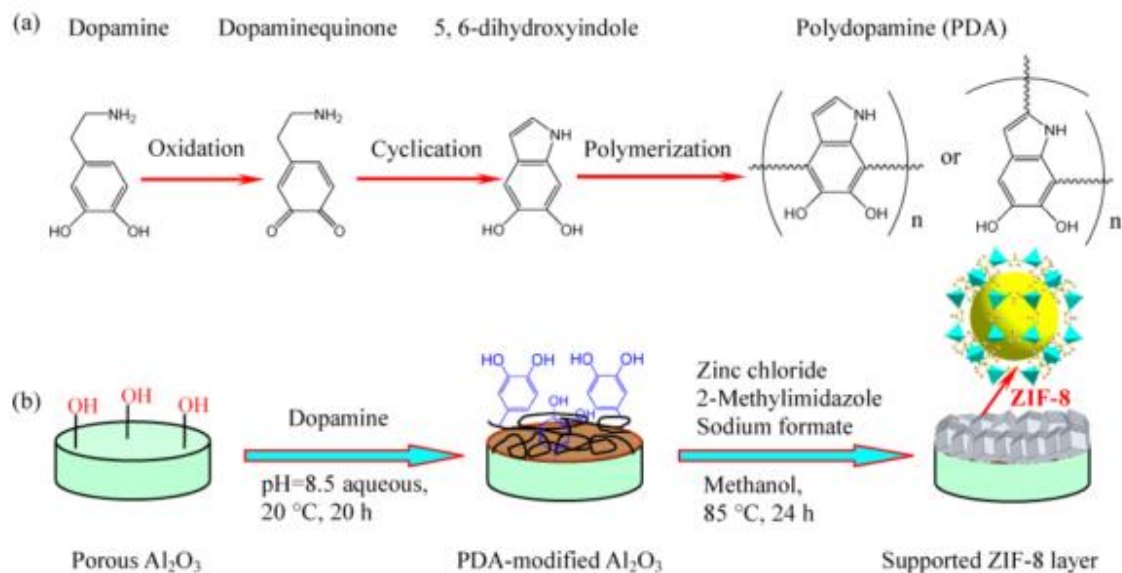
Figure 1.8

Illustrative schematic of (a) the possible reaction mechanism for dopamine polymerization and (b) an overview of ZIF-8 membrane synthesis utilizing dopamine to adhere the ZIF-8 crystals to the support (Q. Liu et al., 2013).

Surface modifications make it possible for other well-established synthesis methods to work, and insomuch they serve a vital role in enhancing the applicability of these trusted and effective methods. Much in the same vein the reactive seeding method emerged, as it does not fall completely under *in situ* synthesis or seeded secondary growth, but rather has components of both. Reactive seeding utilizes porous supports comprised of an oxide of the metal needed for the MOF material to form. In solution with the relevant organic precursors, the free surface atoms on the support lend themselves to MOF formation, and an intimate, well-adhered layer of MOF emerges. The seeds layer, however, requires a secondary growth step to allow for the seeds to grow

23

into a uniform, continuous membrane layer. This synthesis method has been successful for such materials as MIL-53 and MIL-96 on alumina supports, as well as ZIF-71 on ZnO supports (Dong & Lin, 2013; Hu et al., 2011; Nan, Dong, Wang, & Jin, 2012). Reactive seeding is one of the more widely applicable synthesis methods, given the metal needed for MOF synthesis corresponds with an appropriate support material, which is not always the case. There are ways, as Zhang et al. reports, however, of utilizing reactive seeding principles while employing the most appropriate support for the application and not necessarily that which corresponds to the metallic ion needs of the MOF matrix (X. Zhang et al., 2013). ZIF-8 was synthesized on the interior of α-alumina tubes by first creating a layer of ZnO on the inside of the tubular support through sol gel coating and calcination, and then the coated ZnO surface is modified with the appropriate ZIF-8 ligand. Unlike with reactive seeding, however, there is no creation of seeds during activation, the presence of the ligand in the ZnO layer just serves to facilitate nucleation of ZIF-8 during subsequent synthesis (X. Zhang et al., 2013).

In a similar vein as reactive seeding, is direct mixing. Direct mixing goes back to one of the earliest MOF membrane synthesis reports; Huang et al. report on MOF-5 analog MOCP-L (L. Huang et al., 2003). The report outlined the procedure of creating an unsupported membrane wherein the polished side of an anodic alumina template was brought into contact with the needed reaction precursors in a tube, and was then immersed in an amine solution and allowed to react. The following membrane was then immersed in HF for two hours to remove the template and create arrays of MOCP-L nanorods (L. Huang et al., 2003).

The use of nanorods was also reported by Zhang et al. wherein the growth of laterally-oriented ZnO nanorods served as a novel way of structurally adhering ZIF-8 crystals to tubular alumina supports (X. Zhang et al., 2014). The ZnO nanorods grow inward radially from the tubular support's inner radius, and following activation in a solution of methanol and the appropriate imidazole precursor, a homogeneous layer of ZIF seeds are precipitated that, following a secondary growth procedure, create a uniform membrane layer. The ZnO nanorods are an interesting addition to the tubular membrane synthesis procedure, and the researchers hypothesize that the incorporation of the lateral, strut-like nanorods not only served as an inorganic anchoring point for seed precipitation, but also as a neutral barrier to offset differences in thermal expansion that may lead to catastrophic cracking of ZIF-8 membranes at higher temperatures (X. Zhang et al., 2014). The result is a continuous, high quality membrane that is characterized by fascinating microstructure, as shown in Figure 1.9.
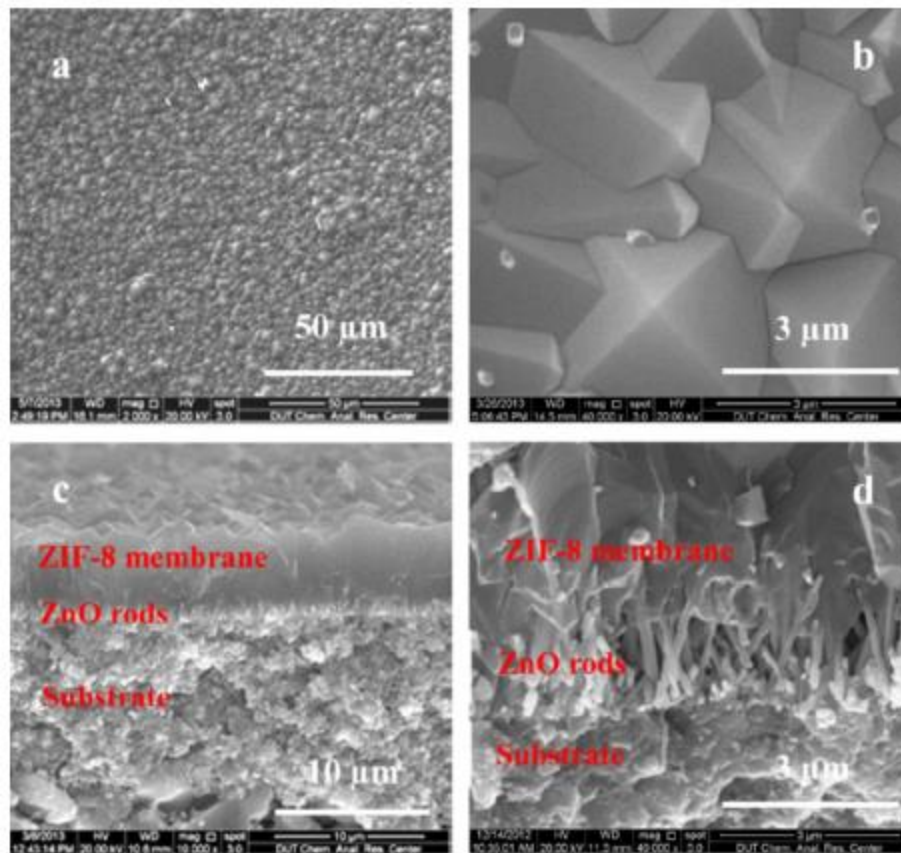
Figure 1.9

SEM images of the ZIF-8 membrane grown on the porous ceramic tube modified by ZnO nanorods after Hmim activation: (a,b) top view, (c,d) cross section, (b,d) a high magnification view of the sample, showing the detailed structure of the support, ZnO nanorods and ZIF-8 layer (X. Zhang et al., 2014).

Further interest has been shown in greatly refining the crystal size of MOF particles synthesized on the tubular supports. After Brown et al. found it very difficult to refine the microstructure of the ZIF-90 membranes they were attempting to synthesize on macroporous Torlon poly(amide-imide) hollow fibers via *in situ* methods, it was found the presence of seeds was necessary to facilitate homogeneous membrane coverage, and a

hybrid *in situ*/secondary growth method was found to be very effective (Brown et al., 2012). Through the separation of the precursors in different organic solvents right up until the time of mixing, the size distribution of crystals synthesized was greatly narrowed. These seeds were then used to seed the polymeric fibers with great success, and subsequent secondary growth resulted in a highly homogeneous, defect-free membrane (Brown et al., 2012).

Perhaps the most interesting synthesis innovations set out to circumvent established hindrances to membrane performance, such as permeability limitations due to membrane thickness. Molecular sieve nanosheet (MSN) membranes have exceptional potential in increasing membrane permeability through dramatically reducing the necessary membrane layer thickness. The process was originally outlined by Tsaptsis et al. for zeolite membranes that exhibited thicknesses on the order of a single unit cell, thus enabling permeability to be exceptionally high (Lee, Choi, & Tsapatsis, 2013). This process has been modified by Peng et al. with ZIF-7 (Peng et al., 2014). The ZIF-7 crystals, following traditional synthesis, are hydrothermally treated for 24 hours in boiling, refluxing water, which rearranges the 6-membered rings characteristic of ZIF-7, and results in 4-membered rings referred to as $Zn_2(bIm)_4$. These $Zn_2(bIm)_4$ clusters can then be exfoliated to create single layer thick, 2D frameworks that are then used to create a stable sol that is then hot dropped onto an Al_2O_3 support (Peng et al., 2014). The resultant membranes of a thickness of ~3 nm and newly refined pore size can provide heretofore unseen abilities to separate via molecular sieving, which will be discussed in greater depth in the sections on gas separation.

1.3 Separation Processes

Gas separation utilizing membrane technologies has become a heavily researched area since the latter half of the 20th century, and there are a number of reasons to justify this trend. Separation via membrane is a passive, continuous process and does not require the energetic input of traditional condensation separation, amine adsorption or cryogenic distillation. Further, membrane separation does not require an overhaul of infrastructure or have a massive footprint that is characteristic of some current technologies, thus rendering membrane separation systems highly amenable to retrofitting (Freemantle, 2005). There is a steadily growing market for membranes for industrially relevant gas separations and this is corroborated by the sizeable underestimate forecasted in 2002 that the total market for membrane gas separation would be upwards of $350 million by the end of 2010, when in fact by the time 2010 ended, the total market for that year was over $500 million (Yampolskii, 2012).

A good deal of growth can also certainly be attributed to global concerns over climate change. The need for cheaper, cleaner energy is undeniable as the population continually grows alongside the parts per million of CO_2 in the atmosphere. Through membrane separation processes it may be possible to overhaul a number of previously higher energy separation processes, as well as safely and efficiently decrease the amount of CO_2 byproducts from these processes. It is worth noting that in the spectrum of dangerous greenhouse gases, the effects of a CO_2 molecule are quite minimal. For example, sulfuryl fluoride can retain 4,800 times as much heat per molecule than CO_2; however, CO_2 is so ubiquitous and widely expelled that its control is of tantamount concern to that of the more deleterious of greenhouse gases (Fox, 2009). It is due to this,

the primary focus of a great many separations at this time deal with the separation of CO_2; be it from a pre- or post-combustion stream, in the process of sweetening natural gas or the tricky separation of CO_2 from CO. The use of membranes in these applications is expected to be very successful, with current estimates indicating that equipping an existing power plant with membranes capable of separating, capturing and storing CO_2 can reduce CO_2 emissions from that plant by 80-90% (J.-R. Li et al., 2011a). Changes such as these, which can be greatly facilitated by membrane technologies, are imperative as society transitions from one that is heavily reliant upon the combustion of hydrocarbons to one characterized by its use of clean and renewable energy resources (J.-R. Li et al., 2011a). It is due to this, the focus herein will on both pre- and post-combustion CO_2 capture and the removal of CO_2 from natural gas streams.

1.3.1 Membrane Separation Principles

Prior to presenting an overview of the current state of MOF materials as they pertain to relevant CO_2 separation processes, an understanding of the mechanisms behind MOF membrane separation must be discussed. Gas separation itself is a straightforward concept, as will be shown in the following paragraphs, however, the nuances of how and why gaseous species permeate as they do is much more complicated and will be discussed on a case by case basis in the following paragraphs.

An understanding of gas separation studies begins with gas permeation. The permeance, F, of molecule, i, through a membrane is measured as shown in Equation 1.1, where Q_i is the flux of molecule i, S is the surface area of the membrane and P_f and P_p are the pressures located on the feed and permeate sides respectively (Y S Lin & Kanezashi, 2007).

$$F_i = \frac{Q_i \cdot X_i}{S(P_f Y_i - P_p X_i)} \tag{1.1}$$

It is possible to estimate the ideal selectivity, or separation factor, of a component, i, in a multi-component feed of i and j, through the ratio of the single-gas permeance of component i, to the single-gas permeance of component j. However, when gas separation is being measured, it is common to utilize a gas chromatograph to quantify the amount of components i and j in the permeate and retentate. This is shown in Equation 1.2, where X_i and X_j are the amount of component i and j in the permeate, and Y_i and Y_j are the amount of components i and j in the retentate stream (Z. Zhao, Ma, Kasik, Li, & Lin, 2013).

$$\alpha_{ij} = \frac{X_i / Y_i}{X_j / Y_j} \tag{1.2}$$

While it is rather straightforward to determine the gas permeation and separation properties of a membrane for a given multi-component system, the mechanism behind the behavior can be more difficult to understand. Metal-organic frameworks, while generally microporous in nature, span an exceptionally wide breadth of pore sizes and conformations. This makes choosing a given MOF for an application exciting since there are countless pore size, cage size and functionality combinations, however, each of these different factors affect the potential separation in different ways. Figure 1.10 shows an overview of four of the most predominant transport mechanisms for membrane materials.
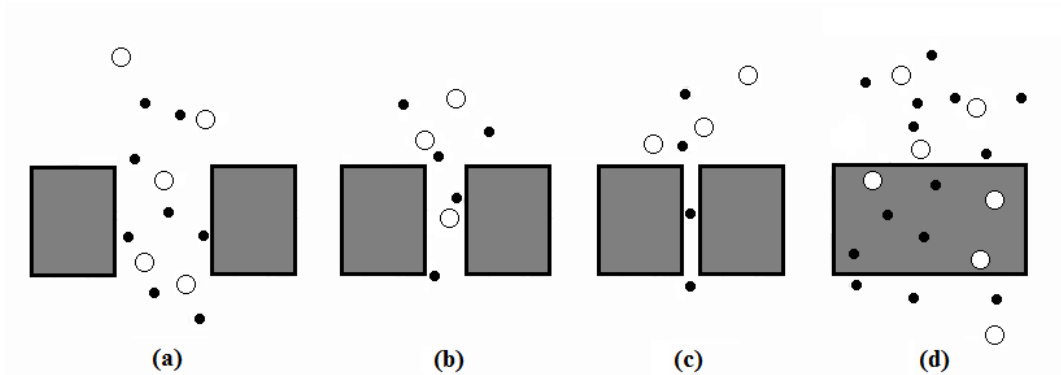
Figure 1.10

Mechanisms of transport in membranes: (a) bulk flow through pores, (b) diffusion through pores, (c) restricted diffusion through pores and (d) solution-diffusion through dense membranes (Seader & Henley, 1998).

Figure 1.10 (a) illustrates non-selective viscous flow through very large membrane pores, or defects. The flow through this region does not contribute to separation or membrane selectivity and depends solely on the transmembrane pressure drop, or hydraulic pressure, to indiscriminately drive permeance of all gaseous components through the membrane layer. Keeping defects of this kind at a minimum will ensure quality membrane performance. Figure 1.10 (b) on the other hand, shows Knudsen diffusion, an intermediate regime, wherein the permeance of larger pore materials (e.g. $d_{pore} > d_{molecule}$) is inversely proportional to the square of its molecular weight. This is shown in Equation 1.3. Where α and z are the diffusion lengths and coordination numbers respectively, RT is the gas constant multiplied by temperature,

MW is molecular weight of the diffusing species and E_d is the activation energy for diffusion.

$$D_c = \frac{\propto}{z}\left(\frac{8RT}{\pi MW}\right)^{1/2} exp^{\left(-E_d/_{RT}\right)} \tag{1.3}$$

From Equation (1.3) the diffusion regime can be determined. For larger pore membranes, when the diffusing species is smaller than the size of the pores, the exponential term goes to one, which renders Knudsen diffusion as the predominant mechanism and diffusion of molecules will vary with $1/\sqrt{MW}$. This is further illustrated in Figure 1.11 where, as the ratio of molecule size to pore size approaches one, the activation energy required for diffusion increases exponentially, marking the transition from the Knudsen diffusion regime to a configurational diffusion regime (J. Xiao, 1992).
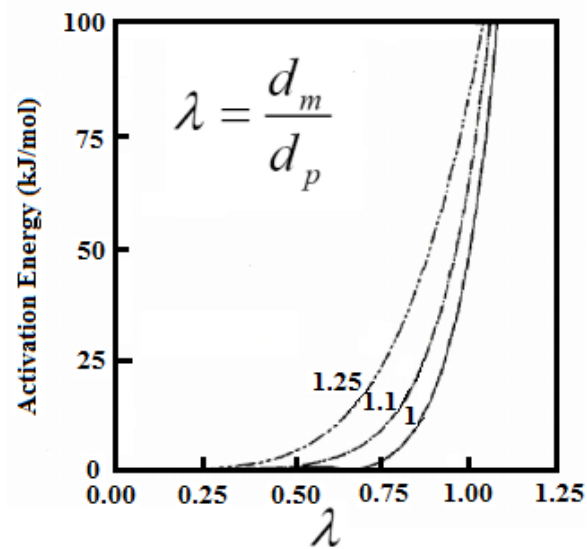
Figure 1.11

Schematic representation of the effect of the molecule size to pore size ratio on activation energy for diffusion (J. Xiao, 1992).

The configurational regime, as shown in Figure 1.10 (c) is where membranes begin to sieve molecules based on size. In this regime the activation energy required for a large molecule ($d_m/d_p \sim 1$) to pass through the pore begins to exponentially increase, and separation is governed by the exclusion of those molecules for which the activation energy for diffusion is too high. The final mode of transport through semipermeable membranes, as illustrated in Figure 1.10 (d), is the solution diffusion mechanism. Solution diffusion, while generally applicable to dense membranes, is also applicable for membranes with pore sizes roughly 10Å or smaller and is very useful in understanding

the desirable preferential adsorption characteristics many MOF materials exhibit (Al-Maythalony et al., 2015).

Solution diffusion provides a model where, in conjunction with other transport mechanisms, the selectivity of certain gaseous species can be attributed to interactions between the gaseous species and the membrane itself. To illustrate this, it helps to consider the permeability of component i (Equation 1.4) as a function of solubility and diffusivity of component i in the membrane (Equation 1.5).

$$P_i = F_i \cdot L \tag{1.4}$$

$$P_i = S_i \cdot D_i \tag{1.5}$$

Where L is the length of the membrane in Equation 1.4 and S_i and D_i are the solubility and diffusivity of component i in Equation 1.5. The permeability of component i is then clearly proportional to the solubility of component i and the diffusivity of component i as they both specifically relate to the interactions of component i within the membrane material.

Having an understanding of the manner in which molecules travel through different porous materials is important when trying to tailor particular membrane materials to separation applications, which is why thoroughly characterizing a membrane material through modeling is an important first step. Experimental data can show, quite quickly, that no matter what confidence level is attached to the modeled data, real life

operating conditions can create completely unforeseen results. These results range for diminishing to increasing exponentially the selectivity and it is with this data further rational design of not only these MOF materials, but the systems in which they can thrive can be utilized.

1.3.2 CO_2/H_2

As the necessity of developing an infrastructure less dependent on nonrenewable resources is continually underscored, the search for an economical, clean and reliable source of energy becomes increasingly imperative. At the forefront of potential is hydrogen. Hydrogen is a clean, efficient source of energy that is poised to make a large dent in our reliance on hydrocarbons, and by virtue of this, the study of CO_2 and H_2 separation has become a hotly researched area. Through the combined processes of hydrocarbon steam reforming and water-gas shift reaction, 95% of currently produced amounts of H_2 for refinery use is produced. This H_2, however, must first be separated from CO_2 prior to its use (Collodi, 2008).

The process of precombustion CO_2 separation from H_2 is outlined in general for a hydrocarbon steam reforming or gasification reaction and is shown in Figure 1.12. Where a fuel, be it coal, methane, gas or biomass is introduced to a stream of high temperature steam held at temperatures between 700-1100°C in the presence of a catalyst to yield carbon monoxide and hydrogen. This is shown chemically (for methane) as follows:

$$CH_4 + H_2O \leftrightarrow CO + 3H_2$$
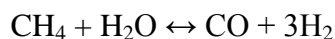
The CO and H_2 are then separated, and the CO can be used to contribute to a lower temperature water-gas shift reaction. In the presence of a catalyst, the water-gas

35

shift reaction produces CO_2 and H_2 when CO is mixed with steam at different temperatures designed to capitalize on the different thermodynamic and kinetic benefits and negate other deficiencies within the process (Smith, Longanathan, & Shantha, 2010). The reaction is show chemically as follows:

$$CO + H_2O \leftrightarrow CO_2 + H_2$$
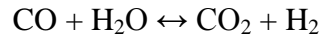
The resultant syngas from the hydrocarbon steam reforming coupled with the water-gas shift reaction is composed primarily of CO_2 and H_2. The separation of CO_2 from this mixture is imperative in order to leave behind a pure stream of H_2, which can then be used as a pollution free fuel and energy carrier. The general process is shown in Figure 1.12 (Ravichandar Babarao & Jiang, 2009).
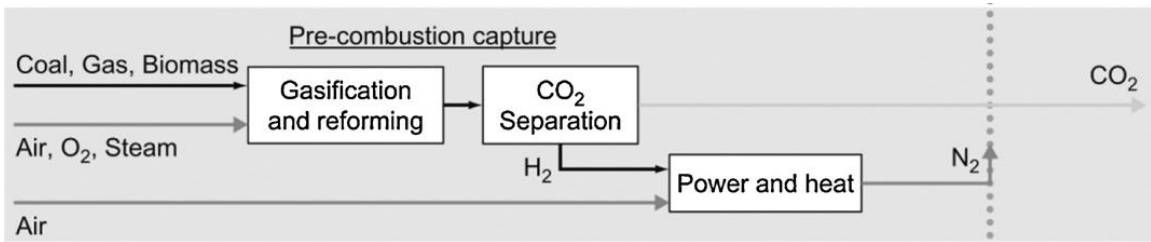
Figure 1.12

Overview of pre-combustion capture in power plants (J.-R. Li et al., 2011a).

To separate the CO_2 from the H_2 stream an existing method known as pressure-swing adsorption (PSA) is commonly used. The process involves the use of a porous material, such as a zeolite or activated carbon, that adsorbs CO_2 at high pressures when the CO_2 is a component mixed with other gases, and then a drop in pressure down to that of ambient allows for regeneration of the adsorbing material (Herm, Krishna, Long, Smit,

& Swisher, 2011). The use of zeolites and activated carbons in PSA separations is a very established process, and due to its maturity, very limited future improvements in selectivity can be assumed. It is in this regard that metal-organic framework membrane materials are at the forefront of interest for precombustion separation process.

It is worth noting that there is virtually no limit to the permutations for which MOF materials can take on. With so much amenability to rational design, it is highly unlikely that every material with potential will be fully explored for each and every separation application, however, through modeling and computational approximation it is possible to explore the suitability of a number of materials simultaneously. This allows for enhanced streamlining of the research process, and only upon finding promising computational data is the effort of membrane synthesis explored. Battisti et al. published work exemplifying the importance of preliminary experimental work in MOF material selection; in their work 9 different ZIF materials and 5 different gas combinations were examined (Battisti, Taioli, & Garberoglio, 2011). This work found CO_2/H_2 zero-pressure adsorption selectivities, as high as 275 and 284 for ZIF-9 and ZIF-7, respectively. The smaller-pore nature of these materials is hypothesized to favor adsorption of smaller species in lieu of larger ones, an effect that decreases with increasing pressure (Battisti et al., 2011). Further modeling by First et al. considered size selective contributions of MOF materials to separation. The findings indicated that, much like, First et al. found, the fore runners in CO_2/H_2 separation were ZIF-7 and ZIF-9, as well as hypothetical MOF material, MOF 23429, all of which showing a shape selectivity of CO_2/H_2 of unity (First, Gounaris, & Floudas, 2013).

Modeling experiments provide invaluable insight into a material's potential; however, experimentation is inevitably needed for substantiation. Experiments with this separation shed light on an interesting duality MOF materials exhibit when separating CO_2 and H_2; even if the pore size indicates that the MOF will molecularly sieve H_2 in the mixture, a number of MOFs exhibit a competing mechanism of transport, and preferentially adsorb CO_2. This combination of effects needs to be considered when choosing a MOF material for CO_2/H_2 separation, because although pore size considerations may make a membrane appear straightforward as a molecular sieve it can be completely marginalized by that materials selective adsorption affinity for CO_2.

Another important consideration when matching a MOF material to an application is the environment in which it will be operating. This was the case for *rht*-MOF, an ionic MOF material known for its unique topology and extraframework NO_3^- ions. When the operating conditions tested neglected the almost negligible amount of H_2O that would be unavoidable, and only considered $CO_2/H_2/CO/CH_4$ at a ratio of 15:75:5:5, the selectivity of CO_2 surpassed 60 at pressures of 50 bar (as seen in Figure 1.13). However, when the experiment was duplicated to incorporate that small portion of H_2O as such, $CO_2/H_2/CO/CH_4/H_2O$ at a ratio of 15:75:5:5:0.1, the CO_2 selectivity over H_2, while still impressive, was substantially decreased to 40, although it too showed a modest increase as the pressure increased to 50 bar (R. Babarao, Eddaoudi, & Jiang, 2010). The high preference for CO_2, even in the system where H_2O was incorporated, was found to be twofold. First, the CO_2 exhibited much stronger electrostatic interactions with the framework itself when compared to H_2, where the electrostatic interactions between the extraframework NO_3^- ions and the CO_2 molecules are especially strong, and second, the

38

temperature studied, 298K, is subcritical for CO_2, but supercritical for H_2, which means that CO_2 is markedly more condensable than H_2 at the temperature considered (R. Babarao et al., 2010).
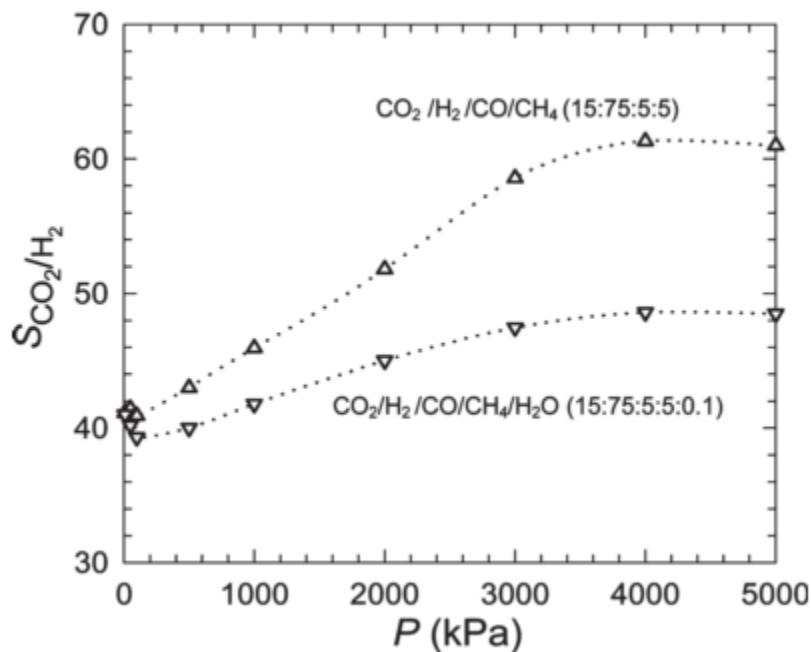
Figure 1.13

Selectivity of CO_2 over H_2 in the $CO_2/H_2/CO/CH_4$ mixture (15:75:5:5) and the $CO_2/H_2/CO/CH_4/H_2O$ mixture (15:75:5:5:0.1) at 298K (R. Babarao et al., 2010).

In a similar vein, novel MOF membrane material $Zn(BDC)(TED)_{0.5}$ has also begun garnering attention for its potential to separate H_2 and CO_2. $Zn(BDC)(TED)_{0.5}$ is a larger pore MOF (0.75 nm along the *c*-axis) with high porosity and has impressive thermal stability and hydrophobicity (A. Huang et al., 2014). The hydrophobicity and thermal stability have promising implications for potential extrapolation to real world applications. In testing the CO_2/H_2 separation, $Zn(BDC)(TED)_{0.5}$ showed strong H_2

selectivity, despite, or rather, because of a strong interactions between CO_2 and the membrane framework (A. Huang et al., 2014). Modeling, as well as single gas and binary gas experiments all confirmed that the interactions between the lattice and CO_2 were so strong they served to decrease the diffusion mobility of CO_2 and by virtue of that, H_2 ideal and experimental selectivities were 16.9 and 12.1, respectively. Further experiments testing the hydrothermal stability of $Zn(BDC)(TED)_{0.5}$ were carried out by introducing water into the system at 180°C and running the test for 48 hours, only a slight decrease in H_2 permeance we seen, and it was attributed to the permeance of H_2O occurring simultaneously. The results indicated that the H_2O did not degrade or embed itself within the framework, and proved the material to be quite hydrothermally stable (A. Huang et al., 2014)

The effect of a strong adsorption affinity to CO_2 creating an enhanced selectivity for H_2 has been evidenced in ZIF-95 as well. ZIF-95, synthesized on an α-alumina support using APTES surface modification, was found to have a H_2 selectivity in the CO_2/H_2 binary system of 25.7 (A. Huang, Chen, et al., 2012). The overt preference within the microstructure for CO_2 is attributed to the quadrupolar moments between the CO_2 molecules with the nitrogen atoms present within the organic linkers. This, as with $Zn(BDC)(TED)_{0.5}$, leads to a diminishment of CO_2 mobility, and an increase in H_2 selectivity (A. Huang, Chen, et al., 2012).

Perhaps one of the more promising materials and innovations for pre-combustion gas separation has been found by Peng et al. (Peng et al., 2014). As discussed previously in the section on novel membrane synthesis methods, Peng et al. performed extensive synthesis optimization to create and refine a means of taking ZIF-7 crystals and

synthesizing $Zn_2(bIm)_4$ single layer sheets known as molecular sieve nanosheets (MSNs) for membrane creation. The resultant membranes are exceptionally thin, (~3 nm) and show unbelievably high H_2 permeance, along with a strict cut off for larger molecules. This combined effect results in separation factors of H_2/CO_2 as high as 291 (Peng et al., 2014).

1.3.2 CO_2/N_2

All separation processes listed herein have the potential to play an important role in creating more sustainable ways to create and store energy, however, the separation of CO_2 from N_2 is especially relevant at this juncture. The incorporation of a membrane that can successfully remove CO_2 from flue gas streams would provide a relatively low-cost, low-energy solution to the CO_2 emissions caused by the combustion of hydrocarbons. Power plants are responsible for more than 1/3 of CO_2 emissions worldwide, so it follows that a crucial intermediate step as societies begin to switch to more efficient and cleaner methods of energy creation, storage and utilization would be to diminish the output of CO_2 associated with established and widely used processes (L. Zhao, Riensche, Menzer, Blum, & Stolten, 2008). A schematic representation of wherein the process CO_2 selective membranes may be utilized is shown in Figure 1.14.
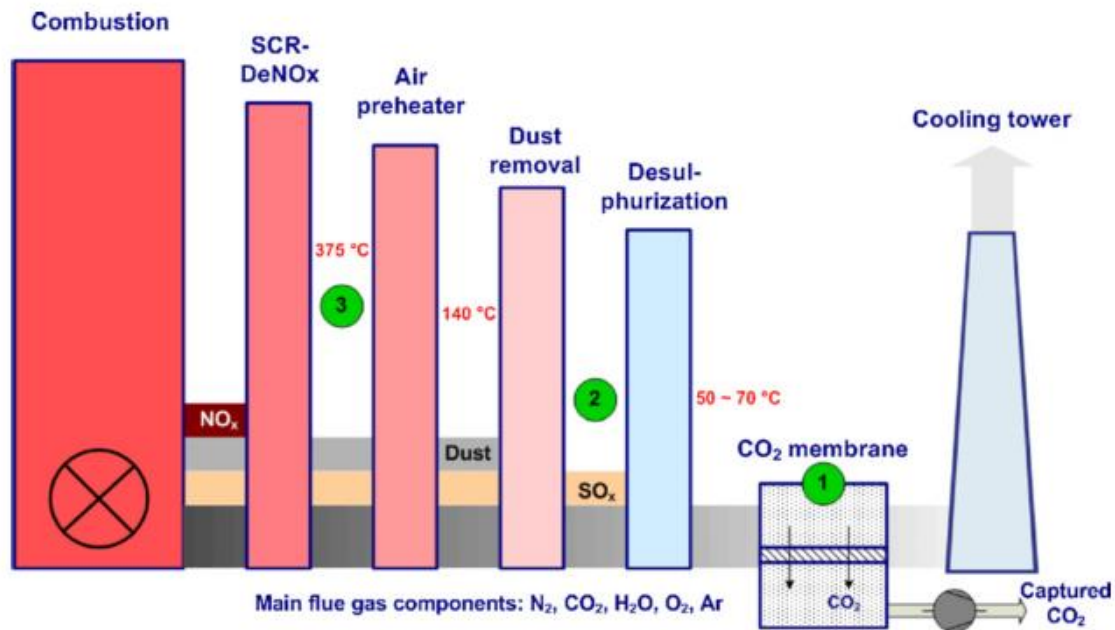
Figure 1.14

Schematic diagram of CO_2 membrane position in a postcomustion flue gas line. The 1, 2 and 3 indicate proposed positions for different membranes in the EnBW power plant (L. Zhao et al., 2008).

The unique and selective adsorption capacities MOF materials can exhibit make them particularly amenable to this separation, a notable example of this being MOF-5. Separation experiments for CO_2/N_2 were carried out by Zhao et al. and tested the effect that chwxsanging composition and feed pressure had on the CO_2 selectivity. The group reported a decrease in CO_2 selectivity with temperature increases, due to the positive effect an increase in temperature has on N_2 permeance and the negative effect it has on CO_2 permeance. The overall CO_2 selectivity decreases from about 64 to 35 as temperatures increase from room temperature to 370 K (Z. Zhao et al., 2013). It was by

no means all bad news, however, the results also indicated that there was a direct correlation between CO_2 selectivities in the CO_2/N_2 system and both CO_2 feed partial pressure and overall feed pressure (Z. Zhao et al., 2013). Increasing the feed pressure showed a marked increase in CO_2 selectivities from around 5 to 65, as did increasing the CO_2 loading, which showed an increase from around 1 at 20% CO_2 to 70 at 88% CO_2 (Z. Zhao et al., 2013). The effect Zhao et al. found for CO_2 mole fraction in feed stream on CO_2 selectivity is presented in Figure 1.15. The values found by Zhao et al. lend important insight into the importance of replicating the potential application environment for the MOF membrane as closely as possible. Previous work by Zhao et al. found that the ideal selectivity of CO_2/N_2 for MOF-5 was a rather unimpressive 0.83, while a review paper by Li et al. found that the MOF-5 membranes reported in literature also all had ideal CO_2/N_2 selectivities around 0.8 (Z. Zhao et al., 2013; Z. Zhao, Ma, Li, & Lin, 2011b). Ideal selectivity, while an important tool to gain insight into membrane behavior, may not always give accurate insight into membrane behavior in the actual binary system.
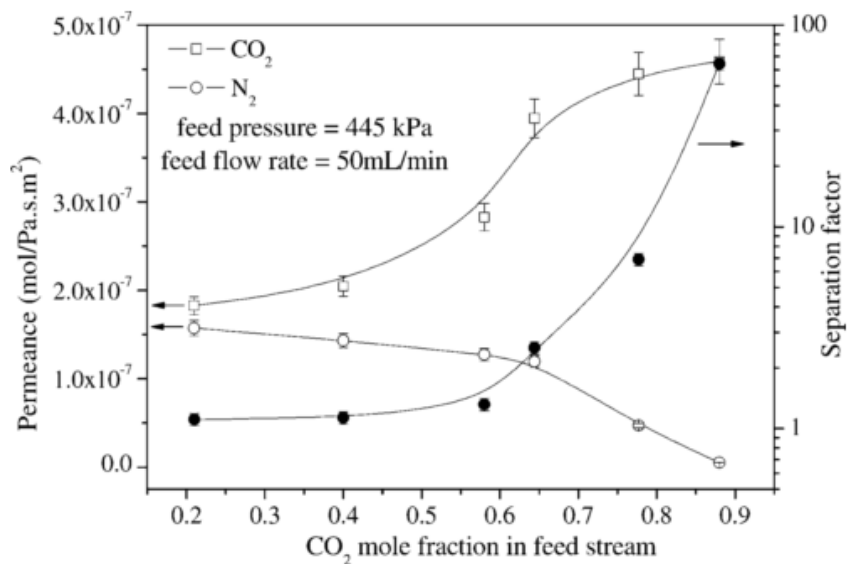
Figure 1.15

Effect of the feed gas composition on the CO_2/N_2 separation factor for the MOF-5

membrane at 298K with a feed pressure of 445 kPa (Z. Zhao et al., 2013).

Not all membranes exhibit a similar disparity in ideal and actual selectivities that span two order of magnitudes, however. This is the case for zeolite-like MOF membrane, sod-ZMOF-1. Sod-ZMOF-1 is characterized by a sodalite zeolite topology and a mid-range pore size, with central channel that measures 0.41 nm across (Al-Maythalony et al., 2015). Pure gas mixtures of CO_2 and N_2 yielded an ideal permeation selectivity of 8.7 for CO_2. Upon testing the system at compositions relevant to flue gas separation ($10CO_2/90N_2$ at 3.4 bar) the sod-ZMOF-1 exhibited a similar affinity for CO_2 over N_2 of 10.5 (Al-Maythalony et al., 2015). The extent to which the ideal selectivity can be used to model the actual selectivity in the binary system is very dependent upon the interactions between the highly soluble CO_2 molecules and the membrane itself. Some MOF materials exhibit enhanced adsorption when the conditions are correct (e.g.

CO_2 loading, feed pressure) whereas other membranes may exhibit more consistent interactions with the CO_2 molecules over a variety of conditions (Yampolskii, 2012).

Operating conditions can have an immense impact on the ability for a MOF membrane to preferentially adsorb a given species. However, with ZIF and MOF membranes, as was alluded to in the section on CO_2 and H_2 separation, there are a number of important microstructural considerations that must be considered; such as ligand functionality, pore size and geometry, and metallic secondary building units. An additional consideration of tantamount concern is that of the propensity for MOF materials to exhibit structural flexibility. ZIF-90, with a pore size 0.35 nm, seems exceptionally well-matched to separate CO_2 from N_2 (kinetic diameters of each being 0.33 and 0.36 nm, respectively) but this was not the case. The ideal selectivity of CO_2/N_2 was found to be only 1.7 (A. Huang, Dou, & Caro, 2010). This low selectivity is counterintuitive when considering that the N_2 molecules should be restricted from entering ZIF-90 pores, but it is a manifestation of the material's inherent framework flexibility. This flexibility is trademark to a number of MOF materials such as, $(Ni_2)(dpce)(bptc)$, ZIF-8 and MIL-53, and while at times it can be advantageous to meeting certain process needs, the inherent nature of framework flexibility can sometimes lead to a diminishment of selectivity (Férey & Serre, 2009; J.-R. Li et al., 2011b).

An additional consideration, as noted by Aguado et al., is that when these separations are modeled or tested, they are often in idealized conditions. The post-combustion flue gas system represented is rarely anything but CO_2 and N_2, in equimolar proportions (Aguado, Canivet, & Farrusseng, 2011). While this can provide very useful

information into membrane performance, it can also be misleading. When discussing

MOF-5 CO_2/N_2 separation previously, the potential seemed very vast; however under

circumstances were H_2O might be present, that potential plummets. Some MOF

materials, typically carboxylate based MOFs such as MOF-5, exhibit overwhelming

aversions to water and similarly polar, H_2-containing molecules (Saha & Deng, 2010).

For example, MOF-5 showed the beginning of degradation from contact with

atmospheric levels of moisture after only 10 minutes, and within 24 hours a solid

structure with the chemical formula of $C_{24}H_{22}O_{18}Zn_4$ was all that remained of the once

porous material (Kaye, Dailly, Yaghi, & Long, 2010). The mechanism of this

degradation is believed to be that the benzene ring of the carboxylate ligand can serve as

a concentration center for these polar molecules, and once securely embedded into the

structure, secondary bonding between the hydrogen atoms and the metallic SBUs can

yield a collapse of the porous structure (Kaye et al., 2010; Saha & Deng, 2010). In lieu

of this, Aguado et al. tested $CO_2/N_2/H_2O$ separation at a ratio of 10:87:3 to more closely

resemble realistic flue gas conditions (Aguado, Canivet, & Farrusseng, 2010; Aguado,

Canivet, et al., 2011). The results found for SIM-1 membrane synthesized on a porous α-

alumina support via an *in situ* synthesis method exhibited CO_2 selectivity that greatly

surpassed Knudsen separation at 4.5 (Aguado et al., 2010). Further experiments with

SIM-1 wherein the group incorporated hydrophobic dodecylamine after SIM-1

membrane synthesis to create SIM-2(C_{12}) membranes showed that the added

hydrophobicity increased the CO_2 selectivity to 5.5 (Aguado, Nicolas, et al., 2011a).

1.3.3 CO_2/CH_4

Removing CO_2 from flue gas created in the combustion of hydrocarbons is important, however, there are marked needs, certainly environmental, but also political in nature, to reduce dependency on oil and coal for energy production in the United States, and in lieu of this there has been a steadily intensifying interest in natural gas. Natural gas consumption in the United States is projected to increase progressively through 2035 as large, natural deposits and an increased efficiency of extraction from shale indicate that a bountiful supply, on the order of 2200 trillion cubic feet, will be available in the lower 48 states and Alaska ("Resources," 2013). In conjunction with the substantial domestic supply, natural gas is also gaining in prevalence because it is significantly cleaner than traditional energy sources. Natural gas, while still a fossil fuel, is much simpler and usually free from a large amount of a contaminants, which results in huge decreases in particulate matter, NOx, CO and SO_2 ("Natural Gas and the Environment," 2013). While those pollutants are also deemed detrimental to the environment, as was mentioned previously, it is the sheer volume of CO_2 in the atmosphere that renders it the cornerstone of environmental concern. Natural gas does not disappoint in that regard either, as it is characterized by 30 and 45% less CO_2 emissions than oil and coal, respectively ("Natural Gas and the Environment," 2013). This reduction in CO_2 output has not gone unnoticed; it has been widely speculated that the 20-year low in United States' CO_2 emissions in the first quarter of 2012 is due in part to enhanced natural gas usage (Nuwer, 2012). Natural gas, which is primarily methane, does not come out of the ground ready for use, however. It is filled with a number of contaminants, most notably of which is CO_2. The CO_2 that is found in natural gas reservoirs can be as high as 8%, which is problematic as the

increased CO_2 substantially decreases the potential energy of the gas, as well as increases the potential for corrosion and severe damage to the processing equipment and pipeline infrastructure ("Natural Gas and the Environment," 2013). There is an eminent need for materials that thoroughly and reproducibly remove the CO_2 from the natural gas mixtures if the projected volume available will ever be able to be utilized efficiently.

There are currently several established processes in place for the removal of CO_2 from natural gas streams; however they are characterized by a number of drawbacks. For example, commonly employed alkanolamines for adsorption are effective, yet they are notoriously expensive, and have a tendency to corrode the units in which they are encased. The corrosion causes foaming and debris which diminishes CO_2 adsorption capacity if left untreated. Further, the regeneration of spent alkanolamines used for CO_2 adsorption is not 100%, which means there is a serious concern regarding conscientious disposal of the harmful amine solvents (Shimekit & Mukhtar, 2012). The difficulties associated with physical adsorbents indicate a need for a simple, semi-permeable layer to allow for continuous gas separation of CO_2 from the natural gas streams. Ideally, the membrane system employed would be characterized by both a high CO_2 permeability and a high CO_2 selectivity, which would result in low methane losses while requiring a smaller surface area of membrane (Shimekit & Mukhtar, 2012).

Modeling work indicates ZIF-8 should have specific functionality that would render it amenable to the separation of CO_2 from binary mixtures of CO_2 and CH_4. Chmelik et al. found that the diffusivity of CH_4 is greatly diminished by the preferential bonding of CO_2 within the ZIF-8 lattice. The CO_2 molecules become bonded to the window regions which serves to dramatically hinder the permeance of CH_4 (Chmelik, van

48

Baten, & Krishna, 2012). As was mentioned previously, Venna et al. created high-quality, tubular ZIF-8 membranes via seeded secondary growth that exhibited exceptionally high CO_2 permeances of $\sim 2.4 \times 10^{-5}$ mol/m^{2}sPa also showed good separation of CO_2/CH_4 with selectivities between 4 and 7 at room temperature (Venna & Carreon, 2010). Another study on a more novel MOF material, bio-MOFs, showed a bit lower CO_2 selectivities in the CO_2/CH_4 system than have been seen for other MOF materials, between 3 and 4, but it is worth noting that bio-MOF-13 and bio-MOF-14 are both exceptionally stable in water. This stability in water renders bio-MOF-13 and bio-MOF-14 functional choices when the presence of water vapor cannot be eliminated (Xie, Li, Rosi, & Carreon, 2014).

Highly *c*-oriented ZIF-69 membranes have exhibited an increasing selectivity of CO_2 over CH_4 with increasing transmembrane pressure drops. As the pressure increased from 1 to 3 bars, the selectivity for CO_2 increased from roughly 2.25 to 4.5, this enhanced preference for CO_2 as the pressure increases is consistent with the modeling data Liu and Smit found (B. Liu & Smit, 2010; Yunyang Liu, Zeng, Pan, & Lai, 2011a). Aside from selectivity, another important consideration when choosing a MOF for an application is stability or propensity to foul. This was not a concern for ZIF-69 in the CO_2/CH_4 system, as these membranes were found to be very stable; exhibiting virtually no changes in CO_2 selectivity after 35 hours on stream separating CO_2/CH_4 (Yunyang Liu et al., 2011a).

As was seen with CO_2/N_2 separation, these novel materials can exhibit a wide array of unforeseen and competing mechanisms of transport. This was evidenced again with ZIF-90, when it was suspected to have a large preference for the 0.33 nm CO_2 molecule over the 0.38 nm CH_4 molecule due to its sharp pore size cut off at 0.35 nm,

49

however, this was not found to be the case (A. Huang, Dou, et al., 2010). Lattice flexibility diminished any sharp molecular sieving separation that was expected, and resulted in a comparatively small CO_2 selectivity of 1.6 (A. Huang, Liu, Wang, & Caro, 2013). This effect was also evidenced in ZIF-90 membranes synthesized on polymeric hollow fibers wherein the CO_2 selectivity is in good agreement at 1.5 (Brown et al., 2012; A. Huang, Dou, et al., 2010; A. Huang et al., 2013). The same group worked to remedy the selectivity diminishing flexibility through APTES functionalization. The APTES served to covalently bond the aldehyde groups of the ZIF-90 structure to the APTES, and thus narrow the effective pore opening (A. Huang et al., 2013). Through this narrowing, the selectivity increased substantially to a very competitive 4.7 CO_2 selectivity over CH_4 (A. Huang et al., 2013).

1.3.4 CO_2/CO

The separation of CO_2 is far less widely studied than the previously discussed separations, but it has potential to be of tantamount concern. The separation of CO_2 from CO is a current concern in a number of established processes discussed previously, such as the sweetening of natural gas and the purification of H_2 following steam reforming, although there is a compelling and very unique reason why the separation of CO from CO_2 will likely become more widely studied (Krishna, 2012). If long-term settling on Mars is going to ever be a reality, there needs to be an immensely efficient, self-sufficiency plan enacted to extract as much necessary fuel, oxygen and water as possible from Mars' hostile environment (Walton & LeVan, 2004). One resourceful means of converting the CO_2 rich Martian atmosphere into CO fuel and O_2 is through a four-step adsorption process, as shown in Figure 1.16 (Walton & LeVan, 2004). This adsorption

process requires a two-bed set up, however, due to the unavoidable requirement of desorbing the adsorbed CO_2 in the sorbents. This process could potentially be streamlined by a CO_2 selective membrane which could separate the feed components without the need for regeneration-induced downtime.
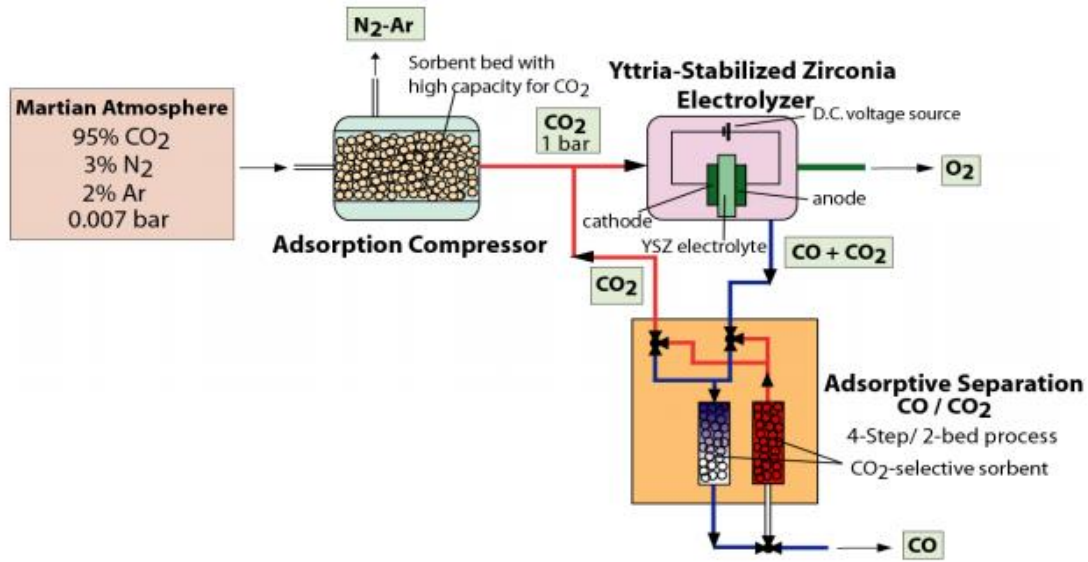
Figure 1.16

Flow diagram of a system for conversion of Martian atmosphere to O_2 and CO at

moderate pressures using sorbents for separation (Walton & LeVan, 2004).

Another compelling, potential CO_2/CO separation process that could be used to create the needed oxygen for any future human inhabitants of Mars is the reverse water-gas shift reaction (Rapp, 2013). As discussed previously, the traditional water-gas shift reaction takes the less useful and relatively bountiful CO and combines it with H_2O to make H_2. Whereas, in Mars, this reverse action could create CO and H_2O to create the O_2

needed by any human inhabitants (Rapp, 2013). The reaction would proceed as follows (Rapp, 2013):

$$CO_2 + H_2 \rightarrow CO + H_2O$$

$$2H_2O + \text{electricity} \rightarrow 2H_2 + O_2$$
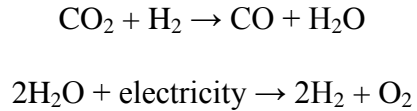
Although there is currently limited research, the difficulty and potential importance of this separation led Lai *et al.* to examine the first successfully synthesized ZIF-69 membrane for use in CO_2/CO separations (Yunyang Liu et al., 2010). As shown in Figure 1.17, the CO_2 permeance differs substantially from Knudsen diffusion due to preferential CO_2 adsorption in the lattice. This effect was exacerbated in the two component CO_2/CO binary system, wherein CO_2/CO at a ratio of 1:1 at room temperature showed not only enhanced permeation, but increased CO_2 selectivity over single component measurements. Instead of an ideal CO_2 selectivity of 2.5, binary gas experiments showed a preference for CO_2 of 3.5, the group postulated these enhanced effects were the result of the preferential adsorption serving to increase the CO_2 mobility (Yunyang Liu et al., 2010).
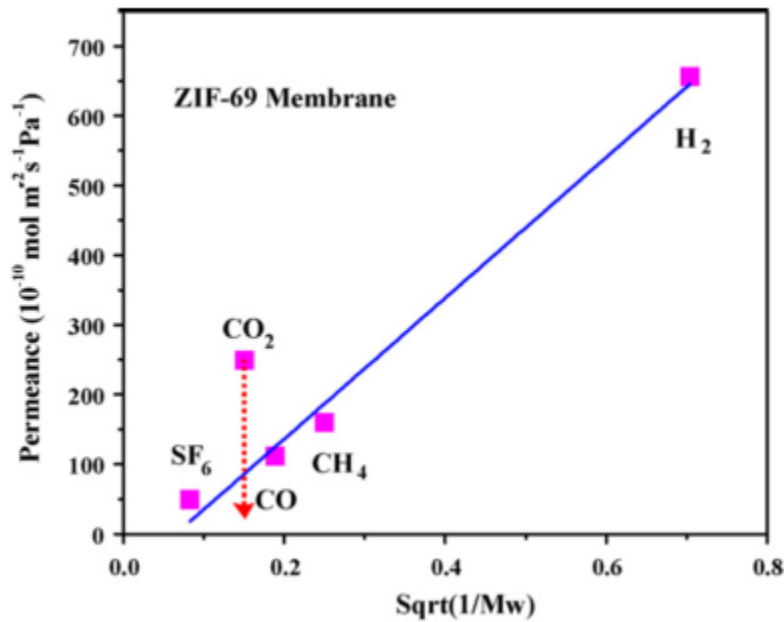
Figure 1.17

 Single-component gas permeation results through ZIF-69 membrane under 1 bar
(Yunyang Liu et al., 2010).

Despite the limited MOF membrane CO_2/CO separations reported in literature currently, there have been a handful of studies on a wide breadth of MOF materials, such as ZIF-68, ZIF-69, ZIF-70, Cu-BTC, ZIF-95, ZIF-100, Mg-MOF-74 (Banerjee et al., 2008; J.-R. Li et al., 2011a; Morris, Doonan, Furukawa, Banerjee, & Yaghi, 2008).   Of those, the most promising thus far is Cu-BTC, where CO_2 selectivities were found to be as high as 25 for pressures of up to 5 atm (Mccarthy et al., 2010).   These preliminary studies do show that there is potential for MOF membranes to successfully be implemented in this separation, and it is likely as the interest in this separation grows, so too shall the interest in MOF membranes for this separation.

1.4 Pervaporation

Pervaporation, as its name would indicate, is a cross between permeation and evaporation, and in a number of ways, pervaporation is quite analogous to gas permeation (Bowen, Noble, & Falconer, 2004). As opposed to a gas feed upstream, pervaporation involves a liquid feed on the membrane side and the subsequent driving force for permeation is the low vapor pressure on the permeate side of the membrane that is obtained through the pulling of a continuous vacuum. The process of membrane pervaporation is very simply illustrated in Figure 1.18. The permeate side is shown, in Figure 1.18, to be full of the preferentially permeating species, which can then be further purified or condensed for future use and the retentate side is conversely saturated with the non-selectively permeating species, which can also be subject to further purification or used as is (Bowen et al., 2004). Given the driving force for pervaporation is vapor pressure differences, pervaporation is ideal for liquid systems that have otherwise proven challenging by traditional separation methods, such as azeotropic mixtures, those with close-boiling points and mixtures that are sensitive to heat (Shao & Huang, 2007).
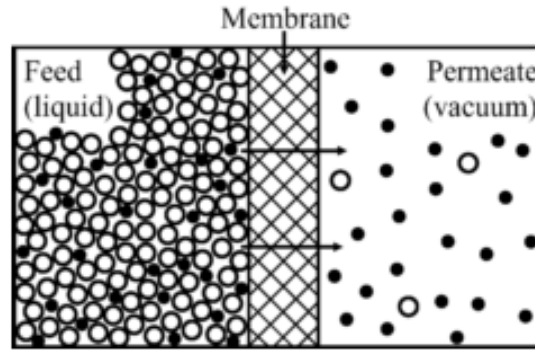
Figure 1.18

Simple schematic showing the process of liquid pervaporation across a membrane

(Bowen et al., 2004).

As with gas separation, the preferential permeation of a species is widely determined using the separation factor. The separation factor is determined through comparison of the pervaporation flux. The flux of component i, Q_i, is calculated as follows.

$$Q_i = \frac{[Y_i(W_f - W_o)]}{[(MW_i) \cdot \Delta t \cdot S]} \tag{1.6}$$

Where Y_i, is the percentage of component i in the feed stream, W_f and W_o are the final and initial weight of the cold trap respectively, MW_i is the molecular weight of component i, Δt is the elapsed time (usually in seconds or hours) and S is the effective area of the membrane through which molecules can pass. Two widely used units of pervaporation flux are mol/m^{2}s or kg/m^{2}hr. From there, it is possible to determine the separation factor as either a ratio of the percentages of i and j in the feed, as shown in Equation 1.7.

$$\alpha_{ij} = \frac{\left(X_i / X_j\right)}{\left(Y / Y_j\right)} \qquad (1.7)$$

Where α_{ij} is the real separation factor and X and Y are the molar fractions in the permeate and feed streams respectively for each component, i and j (Z. Zhao et al., 2013). An additional method of calculating the separation factor is through direct comparison of the fluxes of each permeating species, as shown below.

$$\alpha_{ij} = \frac{(Q_i)}{(Q_j)} \qquad (1.8)$$

Where α_{ij} is the real separation factor, Q is the flux for each component, i and j, and X is the molar fractions in the permeate stream for each component, i and j (Smitha, 2004).

Currently in literature there are limited reports of MOF pervaporation data, however the number is increasing as the relevance and effectiveness of this process becomes more evident. Despite how comparatively few reports of pervaporation may be compared to those published for other membrane processes, the research body indicates that pervaporation through MOF membranes can show interesting and sometimes counterintuitive behaviors through the mainly smaller pore MOF membranes, such as ZIF-8 and ZIF-71, that have been studied thus far. ZIF-8, with a pore size of only 3.4 Å, theoretically would exhibit a sharp cut off that would exclude aromatic molecules larger than the pore size; however Diestel et al. found that this was not the case (Diestel, Bux, Wachsmuth, & Caro, 2012). During pervaporation experiments using benzene and n-hexane, probing molecules with effective diameters that exceed the pore size of ZIF-8 by twenty to forty percent, significant fluxes of approximately 0.6 x 10^{-4} and 14 x 10^{-4}

mol/m^{2}s, respectively, were reported. Only when pervaporation using a binary solution of n-hexane and mesitylene, a molecule with a kinetic diameter just over 2.5 times the size of the ZIF-8 pores, did ZIF-8 behave as a molecular sieve (Diestel et al., 2012). Another study on a small-pored MOF, ZIF-71, by Dong et al. found ZIF-71 to show good permselectivity for dimethyl carbonate (DMC) over methanol despite DMC having a larger kinetic diameter than methanol. This was attributed to the hydrophobicity of ZIF-71, and its preference to the weaker polarity of the DMC molecules (Dong & Lin, 2013).

Pervaporation runs the gamut, from diagnostic tool used to determine membrane quality and behavior to an integral part of many firmly established industrial processes. But it is also an emerging technology that can be used to lower the environmental burden of a number of increasingly relevant separation processes. A prime example of the latter point is in the separation of bioalcohols from the fermentation broths in which they were produced.

As bioalcohols like bioethanol and biobutanol are gaining interest as potential alternatives and additives to traditional gasoline, the ability to separate them efficiently and cleanly is becoming a pressing concern. The low concentrations of alcohol produced in the broth, coupled with the aqueous nature of the broth itself, makes it ill-suited for traditional distillation methods, and any adsorbing material would need to be highly selective and stable in the aqueous broth (Saint Remi et al., 2011). Preliminary testing of hydrophobic ZIF-8 crystals as an adsorbent showed a remarkably high uptake of biobutanol from aqueous solutions containing acetone, biobutanol and bioethanol. The uptake of the alcohols were shown to follow a sigmoidal, step-wise curve, attributable to a tilting of the imidazole ligands that occurs at a given pressure, thus enabling this small-

pored material to exhibit substantial accommodation of these molecules that are comparable in size to the pore openings (Saint Remi et al., 2011). This was further investigated by Liu et al. when they placed ZIF-8 nanoparticles in a polymer matrix of polymethylpheylsiloxane. The findings indicated that at all loadings of flexible ZIF-8 nanoparticles in the polymer matrix the separation factor of biobutanol in water was between 35 and 40, which would result in an estimated energetic savings of half when compared to that required for distillation (X. Liu et al., 2013). Research indicated that permeability and selectivity continued to increase with the degree of ZIF-8 in the polymeric matrix, leading the group to hypothesize that an entirely polycrystalline ZIF-8 membrane would be the most effective separator of bioalcohols from fermentation broths (X. Liu et al., 2013).

Further experiments extrapolating the role hydrophobicity and hydrophilicity play in the separation of bioalcohols from predominantly aqueous broths were carried out with hydrophilic Na-*rho*-ZMOF and hydrophobic $Zn_4(bdc)(bpz)_2$ (Nalaparaju, Zhao, & Jiang, 2011). The Na-*rho*-ZMOF membrane was shown to be quite water selective due to its hydrophilic nature, however, this effect decreased with increasing water concentration. On the other hand, the $Zn_4(bdc)(bpz)_2$ membrane was found to have a distinct preference for ethanol over water, and this effect was only exacerbated by increasing the percentage of water in the water/ethanol system. Given permselectivity of $Zn_4O(bdc)(bpz)_2$ continued to increase with decreasing levels of ethanol up to 75, these membranes are potential candidates for use in the separation of bioalcohols from fermentation broths where the percentage of bioalcohols is quite low in comparison to the amount of water present (Nalaparaju et al., 2011).

1.5 Research Objectives and Significance

This dissertation aims to present a comprehensive look at two analogous large-pore metal-organic framework membranes in terms of stability, pervaporation and permeation. The main objectives of this work are to 1) study MOF-5 membranes in an environment where exposure to atmosphere can be limited, such as during organic solvent pervaporation, 2) synthesize, optimize and characterize a heretofore never synthesized MOF membrane, ZIF-68 and 3) linearly study the CO_2/N_2 and CO_2/CH_4 binary gas separation behavior of these MOF materials at pressures that have not been tested as of yet.

Objective 1

The first objective of this work is to study environments in which MOF-5 membranes can be successfully utilized wherein H_2O exposure can be negated or dramatically minimized. The reasoning behind this being MOF-5 membranes materials exhibit rapid and substantial degradation upon contact of atmospheric levels of H_2O. This effect has been widely reported and has proven to a bit of a hindrance in the more widespread utilization of this remarkable material. To test this, the work in Chapter 2 will be to study the pervaporation behavior of MOF-5 membranes, as well as the stability of MOF-5 membranes throughout pervaporation in different organic solvents. This objective will serve to elucidate other, perhaps less prevalent, processes and applications in which the unique size and functionality of the MOF-5 structure can be coupled with virtually complete avoidance of atmospheric contact.

Objective 2

Next, still as a direct result of the instability of MOF-5 membranes, a second, linear MOF membrane that is known instead for its stability will be synthesized and studied. ZIF-68 will be utilized for this activity. With similar pore sizes to MOF-5, the synthesis of ZIF-68 should allow for a study in tandem of both membrane materials. ZIF-68 synthesis shall be modeled after those reported for similar dual-ligand ZIF membranes in literature. Chapters 3 and 4 are directly related to this object and will outline synthesis trials and subsequent optimization for strength. There will also be a thorough characterization of the ZIF-68 membrane for its stability in atmosphere for extended periods of time, water, boiling water and a variety of organic solvents. The ZIF-68 membrane will be characterized as thoroughly as possible to determine if the membrane is as stable as initial literary reports seem to indicate.

Objective 3

The third objective of this work will be to tie together ZIF-68 and MOF-5 studies through a comprehensive binary gas separation study. The gas mixtures considered shall be CO_2/N_2 and CO_2/CH_4 given initial data on CO_2/N_2 separation from previous group members indicated exceptional potential for MOF-5. Herein the pressures tested for both MOF-5 and ZIF-68 will surpass those previously reported in literature for MOF-5. This will be done due to selective adsorption of MOF-5 which is expected to increase substantially as pressure increases. This work will be presented in Chapter 5 and will also contain stability data to indicate the on-stream stability of these materials during longer testing. This should give indication of the applicability and foreseeable use of these materials in industrial applications wherein continuous loading and separation demands may occur.

These outlined objectives present a comprehensive look at not only the impressive properties of MOF-5 membranes, but also a variety of other options that could potentially extend the functionality of this material through ascertaining particular environments where the effects of atmosphere are eliminated. This work will also serve to provide a complete and thorough optimization of synthesis for a never-before synthesized MOF membrane, ZIF-68, as well as provide a wide breadth of characterization data for this material's permeation, pervaporation and inherent stability in a variety of substances and environments. Finally, this work will present a linear study of two large-pore MOF membranes. There are limited reports on larger-pore MOF membranes, and virtually none, at this time, on large-pore ZIF membranes. This work will provide significant insight into the separation behavior of similar, large-pore MOF membranes.

1.6 Structure of the Dissertation

This dissertation, while divided into three objectives, will be in the form of 6 individual chapters. The first chapter, Chapter 1 aims to provide sufficient background to underscore where research is currently with MOF membranes. Chapter 2 directly supports Objective 1, through outlining the comprehensive organic solvent pervaporation studies that were carried out for MOF-5. Chapters 3 and 4 both fulfill the second objective of synthesizing, optimizing and characterizing ZIF-68 membranes. And Chapter 5 will present the study of CO_2/N_2 and CO_2/CH_4 binary gas separation at a range of temperatures and pressures and feed compositions to thoroughly characterize the binary gas separation behavior of both of these MOF materials. And Chapter 7 summarizes the work done and outlines suggestions for future research avenues for which MOF-5 and ZIF-68 are well-suited.

CHAPTER 2

ORGANIC SOLVENT PERVAPORATION OF MOF-5

2.1 Introduction

Throughout the course of researching and studying the ubiquitous and widely studied MOF-5, it became clear that there are severe issues with the stability of MOF-5 in atmospheric conditions. This instability of MOF-5 may serve as a hindrance to the future integration of MOF-5 in real world applications, such as hydrogen storage, CO_2 sequestration, and a wide array of separation processes wherein contact with atmospheric conditions cannot be negated (Yunyang Liu et al., 2009; Meek, Greathouse, & Allendorf, 2011; Panella, Hirscher, Pütter, & Müller, 2006; Z. Zhao et al., 2011a).

The crippling aversion to small amounts of atmospheric moisture that ultimately results in irreversible destruction of the structure of MOF-5 has not only been evidenced during the research carried out for this dissertation, but also has been substantiated in literature as well. Kaye et al. reported a systematic degradation of MOF-5, monitored by obtaining XRD patterns at different time intervals. The XRD patterns began showing a significant phase shift that began after only 10 minutes in air, and ultimately rendered the porous material a solid with the chemical formula $C_{24}H_{22}O_{18}Zn_4$ after a 24 hour period (Kaye et al., 2010). The mechanism of this extreme degradation was researched by Huang et al. who noticed that water rather insidiously replaced portions of the BDC ligand and fully ingratiated itself into the structure, leading to hydrolysis of Zn atoms from adjacent Zn_4O tetrahedra (L. Huang et al., 2003). The effect is not limited to just water vapor, as further reports tout the ability of any polar, hydrogen-containing molecule to alter the structure of MOF-5 by secondarily bonding to the zinc-oxygen tetrahedra

causing a collapse or shift of the structure (Schrock, Schroder, Heyden, Fischer, & Havenith, 2008). This premise is further substantiated by Saha and Deng who showed a structural degradation of MOF-5 tangibly via measuring a substantial surface area reduction from 2449 to 10 m^2/g following exposure to ammonia (Saha & Deng, 2010). By virtue of this widely reported instability of MOF-5 in humid atmospheric conditions, the potential to utilize MOF-5 membranes for applications in which the contact with atmosphere is negated, such as pervaporation, is gaining interest.

As was mentioned in the previous chapter pervaporation through smaller pore MOF membranes such as ZIF-8 and ZIF-71, has given initial indication of the interesting and sometimes unpredictable nature of pervaporation through MOFs. ZIF-8, with a pore size of only 3.4 Å, would most likely exhibit a sharp cut off that would exclude aromatic molecules larger than the pore size; however Diestel et al. found that this was not the case (Diestel et al., 2012). During pervaporation experiments using benzene and *n*-hexane, probing molecules with effective diameters that exceed the pore size of ZIF-8 by twenty to forty percent, significant fluxes of approximately 0.6×10^{-4} and 14×10^{-4} mol/m^2s mol, respectively, were reported. Only when pervaporation using a binary solution of *n*-hexane and mesitylene, a molecule with a kinetic diameter just over 2.5 times the size of the ZIF-8 pores, did ZIF-8 behave as a molecular sieve (Diestel et al., 2012). As the concentration of mesitylene increased, it hindered the flux of *n*-hexane through the membrane, as the bulky molecule was unable to pass [16]. Another study on a small-pore MOF, ZIF-71, reported successful separation of organic-inorganic and organic-organic solvents. Dong et al. found ZIF-71 to show good permselectivity for dimethyl carbonate (DMC) over methanol despite DMC having a larger kinetic diameter than

methanol. This was attributed by the hydrophobicity of ZIF-71, and its preference to the weaker polarity of the DMC molecules (Dong & Lin, 2013).

Virtually all reports of MOF pervaporation behavior is of smaller pore MOFs, with limited research into the pervaporation behavior of larger pore membranes, such as MOF-5. Previously, Zhao et al. reported xylene isomer and large probing molecule pervaporation as a means of deducing the quality of the MOF-5 membranes; however sustained stability upon exposure to organic solvents has not been investigated (Z. Zhao et al., 2011a). Because of the large pore size of MOF-5, MOF-5 membranes offer potential for liquid phase separation of organic molecules. The focus of the work presented herein is to determine the ability of MOF-5 membranes to withstand immersion in organic solvents while maintaining structural stability, which may allow for the novel properties of this membrane to be utilized for organic separation without the risk of degradation in humid atmosphere.

2.2 Experimental

2.2.1 Synthesis of MOF-5 Seeds and Suspension

MOF-5 powders were synthesized via solvothermal synthesis as reported previously (Z. Zhao, Li, & Lin, 2009; Z. Zhao et al., 2013). Given amounts of zinc nitrate hexahydrate ($Zn(NO)_3$, 1.664g, 99%, Sigma Aldrich) and terephthalic acid (BDC, 0.352g, 99+%, Acros Organics) were added to a vial containing 2,2-dimethylformamide (DMF, 40 mL, 99.8+%, Alfa Aesar) that had been previously degassed for 60 minutes in argon. Once the precursors were fully dissolved, the vial was capped and immersed in an oil bath held at 403K for three hours. After removal from the oil bath, the vial, now containing macroscopic, colorless crystals, was allowed to naturally return to room

temperature. Once cooled, the solvent was decanted and the crystals were washed three times with DMF in order to remove any unreacted precursors. After the final washing, the crystals were immersed in chloroform, held at 343K for three days to allow for solvent exchange to occur and dried under vacuum overnight at 323K. The resultant crystals were quite large, between 20 and 40 μm, and further mechanical processing was necessary to reduce the size of the crystals to that needed for creating a suspension for membrane synthesis.

In previous work the powders were ground by a mortar and pestle to reduce the particle size (Z. Zhao et al., 2011a). In this work, the powders were ball milled in a Teflon container, the MOF-5 crystals were immersed in 50 mL of chloroform and the grinding media, in this case alumina balls, were added at a ball to powder mass ratio of 25:1. The container was then sealed and securely placed in an Across International PQ-N04 Planetary Ball Mill set to 150 rpms for 24 hours. An rpm of 150 was chosen because it is high enough to ensure an adequate reduction in crystal size, while preserving the nanoscopic crystalline structure. After ball milling, the seeds were dried under vacuum overnight to remove any excess chloroform. The ball milled seeds, now between 1 and 3 μm in sizes, were added at a concentration of 2 wt% to DMF and ultrasonically agitated for four hours to create a stable MOF-5 suspension.

2.2.2 MOF-5 Membrane Synthesis

Once a stable MOF-5 suspension was obtained, the membrane synthesis via dipcoating and secondary growth proceeded. Macroporous α-Al$_2$O$_3$ supports were synthesized in-house, from a 10:1 ratio of alumina powders (A16, Alcoa) to distilled water by the press-sintering method. After being intimately ground, 2.1g of the mixture

was used to form pellets, using a Carver pellet press slowly raised to 20,000 pounds for 5 minutes. The supports were then sintered and polished with progressively finer grit sandpaper (#500, #800 and #1200). Once well-polished, the supports were placed, polished side up, in a solution of ethanol and distilled water and ultrasonically agitated for 15 minutes to remove any debris that may remain from polishing. The supports, once dried at 373K for twelve hours, were then ready for use in dipcoating. To dipcoat, the supports were immersed, polished side down, in the MOF-5 suspension for 5 seconds, then removed and left to dry at 323K for 24 hours. This process was repeated three times to achieve a thorough covering of the seed layers.

Following MOF-5 seed deposition, secondary growth was carried out to achieve a continuous membrane. As with MOF-5 crystal synthesis, a given amount of zinc nitrate hexahydrate (0.416g) and BDC (0.88g) are mixed with 40 mL of degassed DMF in a sealable vial. The solution was then stirred vigorously to allow for the precursors to completely dissolve while a given amount of N-ethyldiisopropylamine (EDIA, 0.069g, +99.5%, Acros Organic) was slowly added drop-wise. The EDIA was incorporated to allow less competition between ligands and available metal sites (Z. Zhao et al., 2011a). Once the solution was thoroughly stirred two seeded supports, held vertically by Teflon holders, were placed in the solution. The vial was then tightly capped and placed in an oil bath heated to 303K for three hours. After three hours, the vial was removed from the oil bath and left to cool. Upon returning to room temperature, the membranes were removed and washed three times with DMF to remove any unreacted precursors. The membranes were then placed in chloroform for two days to allow for solvent exchange and, following solvent exchange, were dried overnight under vacuum.

2.2.3 MOF-5 Membrane Characterization

Using the membrane synthesis method outlined, multiple membranes were synthesized concurrently under the same processing conditions. This created theoretically identical MOF-5 membranes, which allowed for destructive characterization using scanning electron microscopy to illuminate membrane microstructure prior to any pervaporation stability testing. The membrane used for pervaporation was stored in a desiccator at all times between testing to minimize contact with atmospheric moisture. Membranes were imaged using a Philips FEI XL-30 scanning electron microscope at a 12 kV accelerating voltage following a thorough coating of Pd-Au to reduce sample charging. The crystallinity of the MOF-5 membrane was determined before and after pervaporation using a Panalytical X'Pert Pro X-ray Diffractometer at 40 kV and 40 mA at a scan speed of 5°/min using CuKα radiation. Helium permeation measurements were taken using a steady state permeation setup as shown in Figure 3.1. The membrane was activated in a vacuum oven at 100°C for five hours prior to placement in a stainless steel membrane cell. For permeance testing, the membrane was sealed, with MOF-5 layer on the feed side, with silicone O-rings.
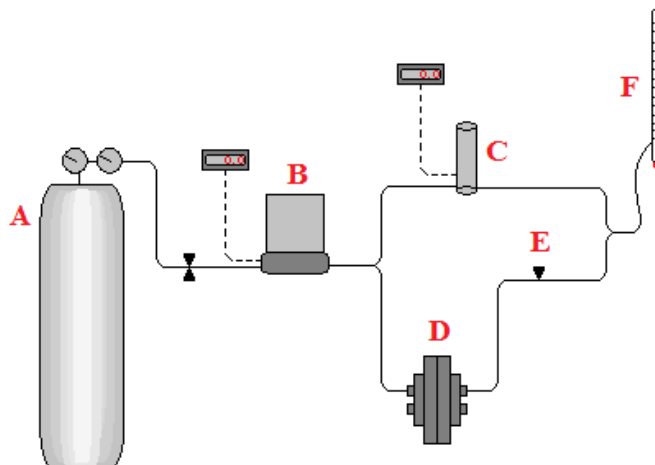
Figure 2.1

Schematic representation of the steady-state permeation setup. Legend: (a) helium cylinder, (b) mass flow controller, (c) pressure sensor, (d) membrane cell, (e) needle valve, (f) bubble flow meter

Fourier Transform Infrared Spectroscopy (FTIR) was carried out before and after pervaporation using a Nicolet 6700 FT-IR Spectrometer and the Smart Orbit Diamond accessory. In obtaining an absorbance spectrum for a pristine MOF-5 membrane and using it as a baseline for a spectrum obtained for the membrane following pervaporation, it is possible to use any notable changes in absorbance to determine if any xylenes remained trapped in the pores following pervaporation and activation. The membrane was activated prior to obtaining the FTIR spectrum as outlined for helium permeance testing.

2.2.4 MOF-5 Pervaporation

Pervaporation of various organics through MOF-5 membranes were performed on a setup shown in Figure 2.2 to elucidate molecular sieving properties and determine the stability of MOF-5 membranes in various organic solvents.
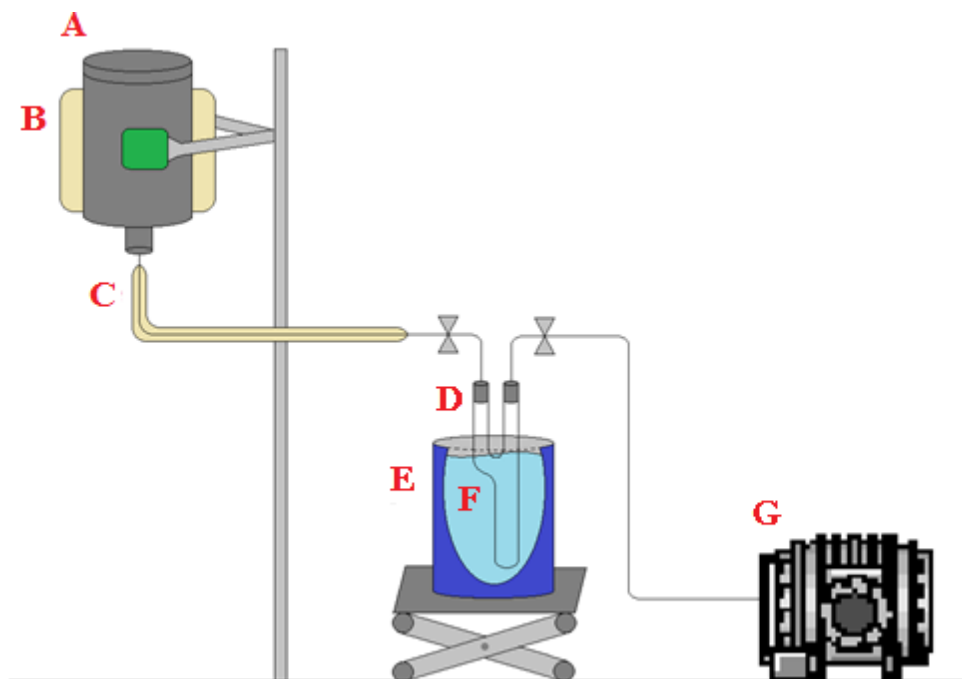
Figure 2.2

Schematic representation of the pervaporation setup. Legend: (a) membrane cell, (b) heating jacket, (c) heating coil, (d) cold trap, (e) liquid nitrogen dewar, (f) liquid nitrogen, (g) vacuum pump.

The probing molecules used for pervaporation were chosen based primarily on their effective size. Table 2.1 contains a summary of the liquids and molecules used and their properties. In using molecules close in size to each other and the MOF-5 pores it is possible to obtain information about the efficacy of molecular sieving through the MOF-5

pores, while in using larger probing molecules, it is possible to determine if the membrane is free of large defects and intercrystalline gaps.

Table 2.1 *Summary of probing molecule properties.*

Molecule	Molecular Weight (g/mol)	Viscosity (cP)[1]	Kinetic Diameter (nm)[3]
p-xylene (PX)	106.1	0.605	0.58
o-xylene (OX)	106.1	0.756	0.68
m-xylene (MX)	106.1	0.581	0.68
1,3,5-triisopropylbenzene (TIPB)	204.4	3.53	0.84
1,3-di-tert-butylbenzene (DTBB)	190.3	0.69[2]	1.1
2-di-cyclohexyl-phosphino-2'-(N,N-dimethylamino)-biphenyl (DCPD)	393.6	~3[2]	1.2

[1]Viscosity information for *p*-xylene, *o*-xylene, TIPB, DTBB and DCPD, from reference (Z. Zhao et al., 2011a) and viscosity information for *m*-xylene from reference (Bhatia, Rani, & Bhatia, 2011).
[2]Tested at temperatures above room temperature to accommodate higher melting points.
[3]Kinetic diameter information for *p*-xylene, *o*-xylene, TIPB, DTBB and DCPD, from reference (Z. Zhao et al., 2011a) and kinetic diameter information for *m*-xylene from reference (O'Brien-Abraham, Kanezashi, & Lin, 2008).

When the molecules used were liquid at room temperature, the procedure is as follows. The membrane was activated under vacuum for a given amount of time at 100°C; following activation the membrane was immediately placed, with the MOF-5 membrane layer exposed to the open containment portion, into the pervaporation cell. Once the membrane was secured in place with chemically resistant Viton O-rings, the membrane end of the cell was sealed tightly. The cell was then filled with liquid in the remaining open end, and sealed tightly. Once the cold trap was cleaned, dried and weighed, the pervaporation cell and the cold trap were affixed to the set up and the

vacuum pump was turned on and left to evacuate the set up for 30 minutes. Following adequate evacuation, the heating coil was turned on and the cold trap was immersed in liquid nitrogen, signifying the beginning of the run. Following the pervaporation run, the weight of the cold trap was taken.

When the pervaporation molecules are solid at ambient temperatures, the pervaporation procedure was different only in the application of the heating jacket. To melt the solid molecules, the heating jacket was applied and set to slightly above the melting point of the molecules. The heat was applied and held there for an hour prior to beginning the testing, to ensure the heat reached all the way through the thick-walled membrane cell and that the solid was given enough time to completely melt.

For the 24 hour pervaporation run, the vacuum was continually drawn, but the surrounding valves were closed around the cold trap every approximately two hours. Any ice and condensation that had accumulated on the cold trap was removed prior to obtaining the post-pervaporation cold trap weight. The cold trap was then washed and dried and its empty weight was taken prior to placement back in the pervaporation setup. Once in place, the valves were opened and the cold trap was replaced in the liquid nitrogen to obtain the next pervaporation measurements.

2.3 Results and Discussion

The initial MOF-5 crystals synthesized for the seed layer measure an approximate 20 to 50 µm in sizes. These crystals, being far too large to use to effectively seed a support, were ball milled as outlined to result in MOF-5 particles between 1 and 3 µm. MOF-5 seed layer was obtained from the suspension containing these micron-sized MOF-5 crystals, and then grown into the continuous membrane. The resultant MOF-5

membranes, as can be seen in Figure 2.3, were comprised of MOF-5 crystals mostly in 5 to 10 μm, with a few large crystals between 10 and 20 μm in size. The MOF-5 membrane has a cross-sectional thickness of 10 μm. These compare nicely with those synthesized by Zhao et al., where the slightly larger seeds, 2 to 4 μm, obtained through manual grinding, yielded membranes with defined MOF-5 crystals measuring less than 20 μm in size with a cross sectional thickness of 14 μm (Z. Zhao et al., 2011a). However, the size reduction of MOF-5 crystals by ball-milling gave a much better control in reproducible coating of MOF-5 seed layers.

SEM images showing a homogeneous, highly crystalline microstructure are not enough to fully assume the membrane is continuous, and relatively defect-free. The quality of the MOF-5 membrane is tested further using helium permeance.
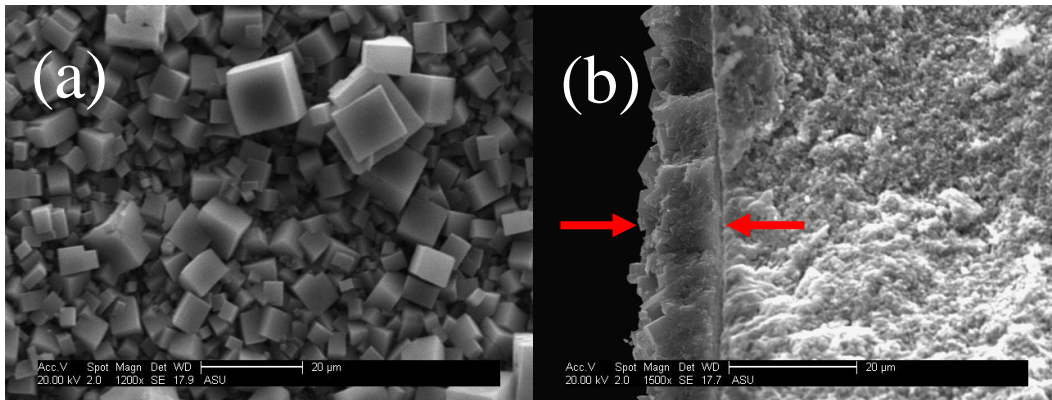
Figure 2.3

SEM micrographs of a (a) MOF-5 membrane surface morphology and (b) cross-sectional view

The helium permeance of the MOF-5 membranes used in this work was found to be about 1 x 10^{-7} mol/m^{2}sPa, as compared to 2 x 10^{-6} mol/m^{2}sPa for the alumina support. The MOF-5 membrane prepared in this work exhibit 1,3,5-triisopropylbenzene (TIPB) and 2-di-cyclohexyl-phosphino-2'-(N,N-dimethylamino)-biphenyl (DCPD) pervaporation flux of 0.24 x 10^{-3} and 0.47 x 10^{-5} mol/m^2.s, similar to those for the MOF-5 membrane prepared by Zhao et al. (0.21 x 10^{-3} and 0.14 x 10^{-5} mol/m^2.s) (Z. Zhao et al., 2011a). These indicate that the MOF-5 membranes synthesized in these two studies have comparable quality.

The as-synthesized MOF-5 exhibits *p*-xylene pervaporation flux of 18 x 10^{-4} mol/m^{2}s. While on-stream during pervaporation test with *p*-xylene for 24 hours, the *p*-xylene pervaporation flux decreases continuously to roughly 11 x 10^{-4} mol/m^{2}s, about 40% reduction compared to the initial flux, after 18 hours of *p*-xylene pervaporation, as shown in Figure 3.4. The result clearly shows initial fouling effects of passing *p*-xylene through the MOF-5 membrane on xylene pervaporation flux. The pervaporation flux reaches steady state value after the initial decline. Wegner et al. reported a similar decrease in *p*-xylene flux through a polycrystalline MFI (ZSM-5) membrane as a function of time. This decrease in flux was attributed to a chemical adsorption of xylene molecules into the lattice that increased with time until flux normalization occurred (Wegner, Dong, & Lin, 1999). From Figure 2.4 it can be seen that a similar stabilization of the flux occurs in MOF-5 membranes as a function of time. If the chemisorption of xylenes into the lattice is occurring with the MOF-5 lattice, as it was hypothesized in Wegner's work on ZSM-5 membrane, the leveling off that is observed after 12 hours indicates that a saturation of sites to which the xylene molecules can adhere occurs

(Wegner et al., 1999). It was proposed that in the zeolite microstructure the electrons in the benzene rings of xylene molecules find themselves attracted to the metallic cations and oxygen atoms of the lattice and π-complexes form between them leading to fouling (Faibish & Cohen, 2001). In the MOF-5 structure, the formation of π-complexes due to reactions with the benzene rings may be responsible for the fouling, however the mechanism would be different (Amirjalayer & Schmid, 2009; Amirjalayer, Tafipolsky, & Schmid, 2007).
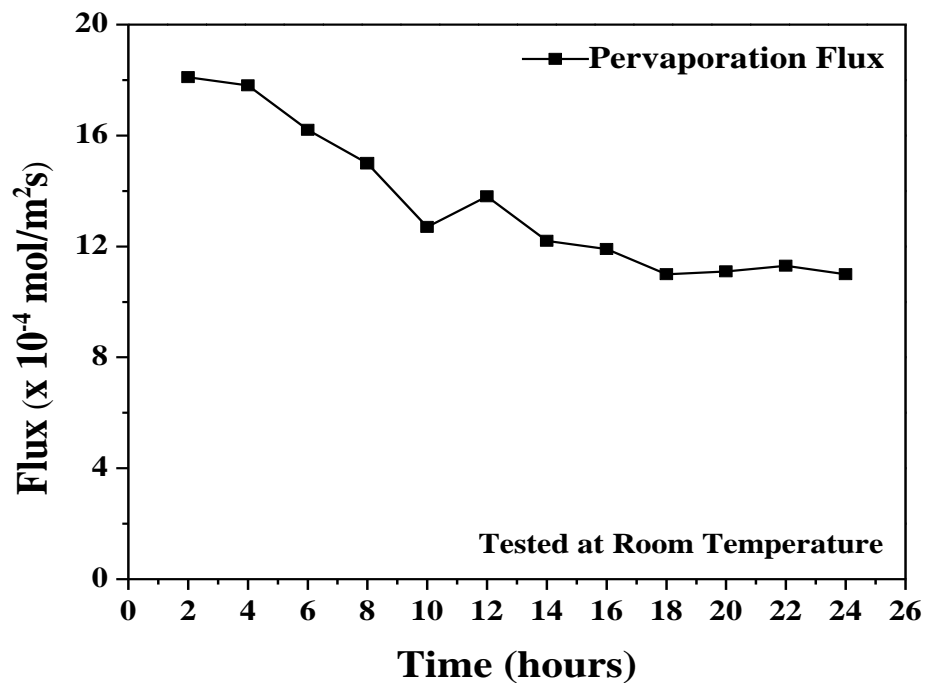
Figure 2.4

Pervaporation flux of p-xylene through MOF-5 membrane

Within the MOF-5 structure there are a few potential sources of fouling from π-complex formation. The first is the inherent nature of MOF-5 powder and membrane

synthesis. Following initial powder synthesis and secondary growth, the MOF-5 powders and seeded supports are washed three times with DMF to remove any excess precursors. This step is incorporated necessarily as the occurrence of any retained unreacted precursors in the matrix would contribute to additional lone electrons. A second potential source for charge disparity leading to fouling is from any defects within the MOF-5 lattice such as unsaturated atoms and point defects within the zinc-oxide tetrahedra. The final source for potential fouling is the benzene ring contained in the organic ligand. The possibility of guest-guest interactions between benzene rings is high, so it follows that the potential for interactions between the benzene rings in the structure and the guest species should be high (Amirjalayer & Schmid, 2009; Amirjalayer et al., 2007).

In many studies, it is reported that activation of the membrane allowed for a removal of all retained molecules and a return to original states of flux, indicating the mechanism governing the decreased flux was not an irreversible structural degradation, but the result of interactions between the guest pervaporation molecule and the lattice, however this was not observed in the MOF-5 membrane (Faibish & Cohen, 2001). Following the 24 hour pervaporation run using only *p*-xylene, subsequent measurements were taken with three of the xylene isomers, *p*-, *o*- and *m*-xylene, with activation in a vacuum oven at 100°C for duration ranging from 5 to 48 hours between permeation tests, as summarized in Table 2.2. As shown, steady state permeation flux of *o*-xylene and *m*-xylene is in the range of 5.0-5.5 and 5.8-7.4 (10^{-4} mol/m^{2}s) respectively depending on the duration of activation prior to the pervaporation measurement. The next two *p*-xylene trials after 34 and 36 total hours of xylene pervaporation followed by 24 hour activation each showed a reproducible decline in pervaporation flux down to 7 to 8 x 10^{-4} mol/m^{2}s.

To test the permanence of this decline, the membrane was activated for 48 hours, and the resultant *p*-xylene flux returned to the values previously found, although it was never returned to the flux that was seen for the as-synthesized membrane.

For permeation of larger molecules (TIPB, DCPD and DTBB) through MOF-5 membrane, only TIPB exhibited fouling similar to *p*-xylene. TIPB showed a large decrease of over an order of magnitude, from 24 x 10^{-5} to 0.13 x 10^{-5} mol/m^{2}s following the initial fouling of the MOF-5 membrane. This indicates that the intercrytalline gaps large enough to accommodate DCPD and DTBB are not hindered by the adherence of xylene molecules; that these defects either do not facilitate fouling inherently, or they are just spacious enough to allow for all molecules to move through. TIPB, however, must travel via different routes through the membrane, and these routes showed severe decline following xylene pervaporation.

Table 2.2

Summation of activation time and pervaporation data for pervaporation of xylene

isomers through MOF-5 membranes

Hours in Xylene	Hours Activated at 100°C Prior	Xylene Isomer	Flux (10^{-4} mol/m^{2}s)
2	5	*p-*	18.0
24	5	*p-*	11.7
26	12	*o-*	5.0
28	48	*o-*	5.5
30	5	*m-*	5.8
32	48	*m-*	6.2
34	24	*p-*	7.4
36	24	*p-*	7.0
38	48	*p-*	11.9

The results given in Figure 2.4 and Table 2.2 show that the MOF-5 membrane, after exposure to the pervaporation flux of xylene, experiences a permanent reduction in pervaporation flux (from 18.0 x 10^{-4} to 11.9 x 10^{-4} mol/m^{2}s). Phase structure and morphology of the MOF-5 membrane after many pervaporation/activation cycles in xylene are compared with that of the as-synthesized MOF-5 membrane in Figures 2.5 and 2.6. The XRD spectra shows no discernible difference in peak location indicating that whatever mechanism is responsible for the non-recoverable decrease in pervaporation flux with time is not a manifestation of any crystallographic degradation or alteration. The SEM images also show a remarkably consistent morphology and microstructure between the as-synthesized MOF-5 membrane and a MOF-5 membrane that had

undergone many pervaporation/activation cycles in xylenes. These show that the effect of the fouling with xylene on pervaporation flux does not cause a change in the crystal structure and morphology of the MOF-5 membrane.
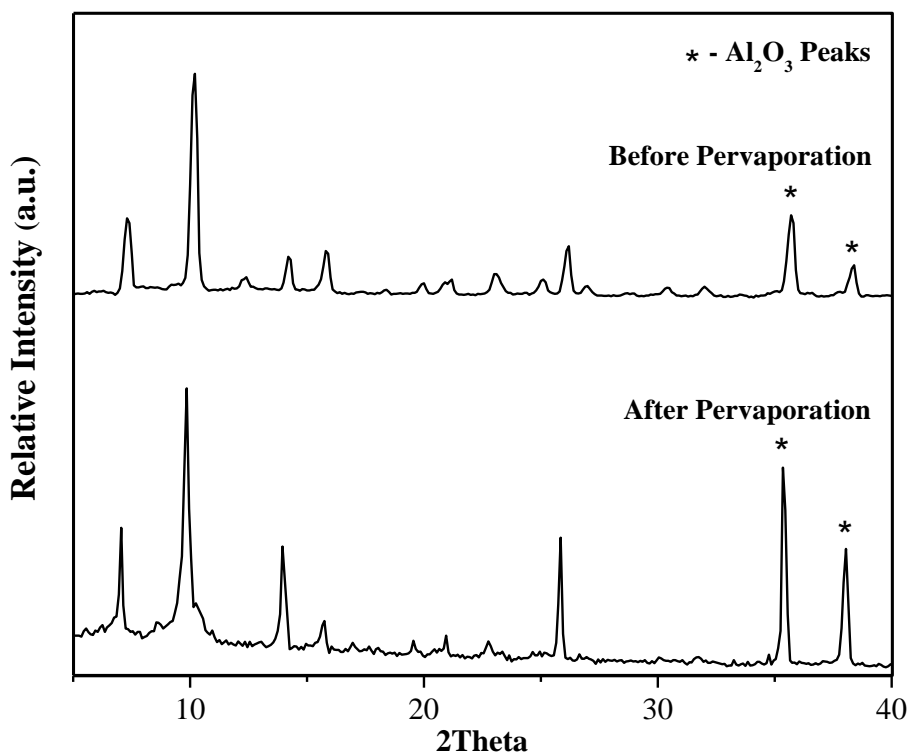
Figure 2.5

XRD spectra of a MOF-5 membrane before and after xylene pervaporation for 24 hours

To confirm the effects of fouling causing permanent reduction in flow permeability through the MOF-5 membrane, helium permeance for a MOF-5 membrane following the pervaporation testing with xylene was measured and is compared in Figure 2.7 with that of the as-synthesized membrane. As shown, there is a slight decrease (about 10%) in permeance from exposure to the xylenes, which indicates that there is

something contained within the pores that does not manifest itself in notable changes to structure or microstructure of MOF-5 membrane.
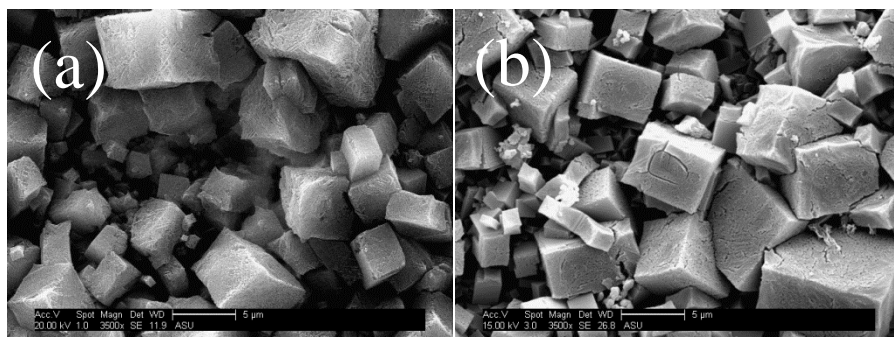
Figure 2.6

SEM photomicrographs showing (a) an as-synthesized MOF-5 membrane and (b) a MOF-5 membrane following pervaporation

The IR spectra of the as-synthesized MOF-5 membrane and the one following xylene pervaporation and subsequent regeneration are given in Figure 2.8. Both spectra are similar except that the transmittance for the fouled sample is lower than that for the as-synthesized one. Using the as-synthesized membrane as background, an IR spectrum showing only the net changes to MOF-5 following pervaporation was obtained and given in Figure 2.8 (c). The differences between the as-synthesized and post-pervaporation membrane IR spectra are subtle. The main manifestation is the fouled membrane exhibits enhanced peaks in IR spectrum, notably, the peaks around and just after 1500 cm^{-1}. These peaks, 1600.2 and 1389.9 cm^{-1}, are present in both Figure 3.8 (a) and (b), and are consistent with characteristic peaks of MOF-5 IR spectra from literature (Frunza et al., 2010). While the decrease in flux occurred during pervaporation in *p*-xylene, it is not

known for certain that the entirety of the adhered *p*-xylene remains intact once ingratiated into the structure.
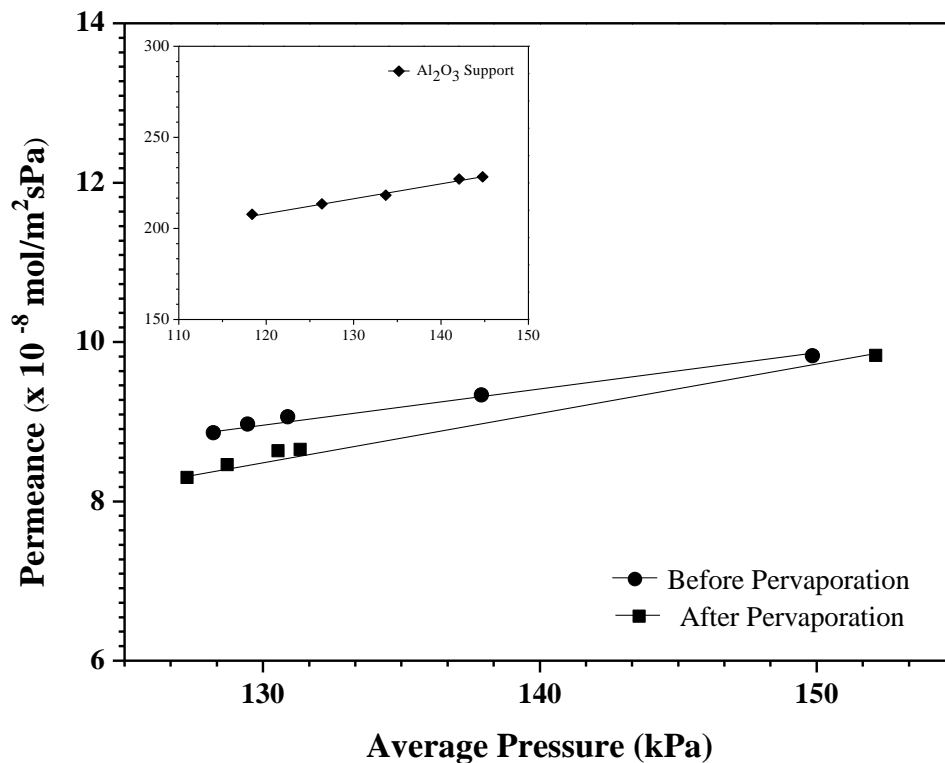
Figure 2.7

Helium permeance as a function of average pressure for MOF-5 membranes before and after pervaporation and a bare alumina support (inset).

Being mindful of this, the FTIR spectra were looked at to determine a presence of C=C-C ring-related vibrations as well as C-H bonds in- and out-of-plane that would indicate the presence of extra aromatic rings (Coates 2000).   The primary C=C-C vibrations occur between 1615-1580 cm^{-1} and 1510-1450 cm^{-1} which coincides well with the larger peaks of the sample following pervaporation, which occur at 1600.2 and 1508.2

cm^{-1} (Frunza et al., 2010). The peak at 1600.2 cm^{-1} is a peak inherent to MOF-5, however, it is about 12% larger in the sample following pervaporation, which allots for the incorporation of any extraneous C=C-C bonds that may be artifacts of the xylene fouling process. There are also several smaller peaks that fall into the 1225-950 cm^{-1} range for in-plane C-H bending, as well as between 900 and 670 cm^{-1} for out-of-plane bending of the C-H bonds, all of which can indicate the presence of aromatic rings (Frunza et al., 2010).
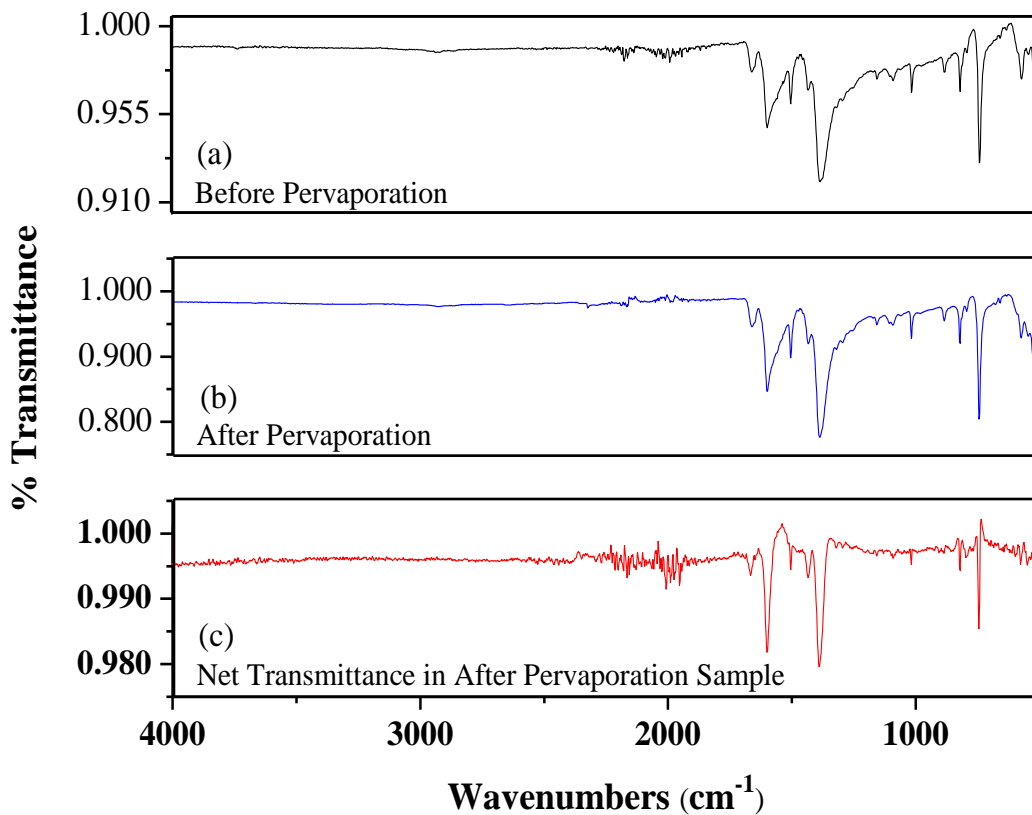
Figure 2.8

IR spectra of a MOF-5 membrane before (a) and after (b) p-xylene pervaporation for 24

hour. The bottom spectrum (c) shows the differences in peaks between the before and

after pervaporation spectra.

From the characterization results of the membrane before and after pervaporation

it can be concluded that the mechanism responsible for the decreased xylene flux through

MOF-5 membrane as a function of time is not the result of any alteration or degradation

of the MOF-5 crystal structure, nor is it an indicator of phase change within the

membrane. Given the decrease in flux as well as helium permeance, it can be concluded

there are retained xylenes in the pores of the membrane that cannot be fully removed through traditional activation of the membrane. The stabilizing of the flux with time indicates there are a finite number of accessible sites to which xylene molecules can bond within the MOF-5 microstructure, and once they are filled, it continues that way until the secondary interactions between retained xylene molecules and those passing through the membrane compound into further decreases in the flux through the membrane. To activate the sample is an effective means of keeping the amount of retained xylene isomers present within the sample to a minimum, however, once saturation of the sites available for xylene bonding occurs, and secondary xylene-xylene interactions occur, it quickly requires an increasing amount of time spent activating to return to an expected pervaporation flux.

Table 2.3 compares stable pervaporation fluxes of the organic compounds listed in Table 2.1 for the MOF-5 membrane prepared in this work with those for the MOF-5 membrane reported by Zhao et al. (Z. Zhao et al., 2011a). The fluxes for the two membranes agree quite well with each. Considering the fact that these membranes were prepared by different researchers at different times, the results show that the experimental procedure developed in this laboratory is quite reproducible in synthesis of MOF-5 membranes.

Table 2.3

Pervaporation fluxes of xylene isomers and large molecules for MOF-5 membranes.

Molecule	Flux in 10^{-5} mol/m^{2}s	
	Zhao et al. (Z. Zhao et al., 2011b)	This work
p-xylene	90.0	117.0
o-xylene	72.5	52.5
m-xylene	-	60.0
TIPB	20.8	24.0
DTBB	17.1	2.58
DCPD	0.14	0.47

The major difference in the data between the two membranes is that the new MOF-5 membrane gives much smaller pervaporation flux for the DTBB molecule than the MOF-5 membrane reported earlier. Since the aperture of the MOF-5 cage is about 0.8 nm, the molecule cut-off between the TIPB (0.8 nm) and DTBB (1.1 nm) as found in the present MOF-5 membrane is more reasonable. This may suggest that the MOF-5 membrane reported previously may contain intercrystalline gaps sufficiently large to allow DTBB to permeate through. The MOF-5 membrane synthesized in this work contains less intercrystalline gaps showing molecular sieving effects determined by the MOF-5 pore structure. The difference in the pervaporation fluxes for the smaller molecules (*p*-, *o*- and *m*-xylenes and TIPB) through the MOF-5 membranes can be caused by the differences in the viscosity and size of these molecules. The pervaporation

fluxes listed in Table 3.3 clearly show the potential to use MOF-5 membranes for separation of organic molecules in liquid phase.

2.4 Conclusions

High quality MOF-5 membranes can be reproducibly synthesized by the secondary growth method from MOF-5 crystals with size reduced by ball-milling for the seed layer. The on-stream xylene permeation flux of as-synthesized MOF-5 membrane decreases and reaches a steady-state value about 70% of the initial flux value. Such a reduction in pervaporation flux is permanent, and is not accompanied with any discernible change in crystal structure and morphology. The MOF-5 membranes, after the initial permanent fouling effect due possibly to the trapping of the xylene in the pores of MOF-5 crystals and given adequate activation, offer stable pervaporation fluxes for organic molecules sized smaller than the aperture of the MOF-5 structure. While MOF-5 membranes exclude the organic molecules sized larger than the MOF-5 aperture. The results show that MOF-5 membranes, offer stable operation in organic solvents and have potential for uses in separation of organic molecules in liquid phase.

CHAPTER 3

SYNTHESIS AND STABILITY OF ZEOLITIC IMIDAZOLATE FRAMEWORK-68

MEMBRANES

3.1 Introduction

Due to the previous issues outlined in Chapter 2 regarding MOF-5 and its aversion to atmospheric levels of moisture, a slight deviation, albeit a rather linear one, was decided on partway through this dissertation work. Zeolitic imidazolate frameworks (ZIFs), as outlined in Chapter 1, are a subset of metal-organic frameworks (MOFs) that are gaining substantial interest. ZIFs, much like MOFs, are characterized by highly crystalline, microporous structures constructed from three-dimensionally repeating arrays of tetrahedrally coordinated metallic ions connected by rigid organic ligands (Banerjee et al., 2008; Park, 2006; Phan et al., 2010). The distinguishing feature of ZIFs is the use of imidazole linkers which create bond angles, that when coordinated with inorganic constituents, mimic those of the bonds intrinsically created between silicon and oxygen atoms in the formation of zeolites. To this end, it is possible to synthesize ZIFs in any number of topological conformations previously only found in aluminosilicate zeolites while still retaining the customizability of metal-organic frameworks (Banerjee et al., 2008; Park, 2006; Phan et al., 2010; Tavolaro & Drioli, 1999b). The duality of the organic and inorganic components, coupled with the self-assembling nature of the crystals renders them highly amenable to rational design. Through altering synthesis conditions, organic linkers and metallic ions, it is conceivable that a ZIF material can be tailored to address with better acuity established zeolite applications, such as membrane

reactor processes and gas and liquid separations (McLeary et al., 2006; J. Tan, Bennett, & Cheetham, 2010; Tavolaro & Drioli, 1999b).

Of the known ZIF materials, there have been many synthesized and studied in crystalline form, while a few have been mainly relegated to theoretical research methods and fewer still have been synthesized and studied as continuous membranes. There are currently reports on no more than a handful of ZIF membranes; most notably are ZIF-7 (Y.-S. Li et al., 2010), ZIF-8 (Bux, Liang, Li, Cravillon, & Wiebcke, 2009; Mccarthy et al., 2010; Shah, Kwon, Tran, Sachdeva, & Jeong, 2013; Venna, Zhu, Li, & Carreon, 2013), ZIF-22 (A. Huang, Bux, Steinbach, & Caro, 2010), ZIF-69 (Yunyang Liu et al., 2010, 2011a), ZIF-71 (Dong & Lin, 2013), ZIF-78 (Ban, Li, Liu, Peng, & Yang, 2013), ZIF-90 (A. Huang et al., 2013; A. Huang, Wang, Kong, & Caro, 2012) and ZIF-95 (A. Huang et al., 2014). All of which are characterized by smaller pore openings, with pore sizes ranging from 2.9Å for ZIF-7 and ZIF-22 to 4.4Å for ZIF-69 (Banerjee et al., 2008). Given the relative saturation of smaller-pore ZIF membrane materials being studied, it would be advantageous to begin exploring membrane synthesis of larger-pore ZIF materials. The characteristic desirability of ZIFs (enhanced stability, zeolite topologies, etc.) would remain intact, but studying a larger-pore ZIF membrane would allow for a different set of potential gas and liquid separation applications to be explored, and a linearity between research of the similar, non-zeolitic MOF-5 could provide substantial insights into the effects of functionality and structural disparity on membrane performance. These applications include separation of gas molecules with perm-selectivity determined by the adsorption properties, such as those offered by the large pore FAU type zeolite membranes and large liquid molecules by molecular sieving (Y. S.

87

Lin et al., 2007). It is in this regard, the interest in studying ZIF-68 in membrane form has emerged. ZIF-68, a ZIF material characterized by a 7.4Å pore diameter and 10.5Å cage diameter, has been lauded for its crystalline integrity in harsh conditions, as well as its predicted preferential adsorption of CO_2, and could serve well as a stable membrane for gas and liquid separation processes (Banerjee et al., 2008; Y. S. Lin et al., 2007).

To synthesize continuous ZIF-68 membranes a novel reactive seeding approach was utilized. Reactive seeding is a membrane synthesis method that has been reported for MIL-53 (Hu et al., 2011), MIL-96 (Nan et al., 2012) and ZIF-71 (Pan, Wang, & Lai, 2012) which centralizes around a surface modification step wherein the seeds are created from an in situ solvothermal reaction between the imidazole linkers and the inorganic support itself. In this manner an intimately adhered and homogeneous seeds layer can be directly created from the support itself, and following secondary growth, a defect free membrane layer can be obtained. The objective of this work is to reproducibly synthesize continuous and defect-free ZIF-68 membranes by the reactive seeding method, and to study the stability of ZIF-68 membranes to help determine for which potential applications this larger-pore ZIF material is suited.

3.2 Experimental

3.2.1 Zinc Oxide Supports

ZIF-68 synthesis via reactive seeding was carried out using homemade zinc oxide supports. To prepare the supports, a 3wt% solution of polyvinyl alcohol (Sigma Aldrich, PVA, 99+%) in deionized water was added to 76g of zinc oxide powder (Sigma Aldrich, ZnO, 99.9+%) and intimately mixed. Once mixed, 3.2g of the powder was placed in the support mold and pressed in a Carver hydraulic pellet press to an applied load of roughly

12,500 pounds for a minute. The green bodies were sintered for 5 hours at 570°C to produce the disks with the diameter of 22 mm, thickness of 2 mm, and normal pore size of ca. 100 nm. The sintered supports (one side) were then gently polished using 800 and 1200 grit sandpaper, rinsed in deionized water and ethanol for 15 minutes under ultrasonic agitation, and dried at 100°C for three hours.

3.2.2 ZIF-68 Seed Layer Synthesis

To create the seeds synthesis solution, 0.25 mmol each of 2-nitroimidazole (Bosche Scientific, nIm, +98%) and benzimidazole (Sigma Aldrich, bIm, 99%) were added to 30 mL of dimethylformamide (Alfa Aesar, DMF, +98%) and thoroughly stirred until all precursors were dissolved. The solution was then added to a Teflon autoclave containing a cleaned and dried ZnO support suspended polished side down. Due to the nature of reactive seeding, all exposed surfaces of the ZnO support are susceptible to the growth of ZIF-68 seeds. To avoid complications due to seed and membrane growth on both sides of the ZnO support, an unreactive alumina support was placed flush to the unpolished side of the ZnO support to serve as a hindrance to seed growth. Once both supports were in place in the solution, the autoclave was sealed shut and left to react in an oven at 120°C for 8 hours. At the end of 8 hours, the autoclave was allowed to return to room temperature naturally. Once cooled, the seeded support was removed and gently cleaned with a cotton ball wet in DMF to remove any unreacted imidazole precursors. The membrane was then soaked for three hours in DMF and dried for 3 hours under vacuum.

3.2.3 ZIF-68 Secondary Growth

Once the support containing the ZIF-68 seeds layer was washed and dried, secondary growth began. The secondary growth step differed from the synthesis of the seeds layer mainly as it incorporated the addition of a zinc source, as the free surface zincs were largely depleted in the seeds layer creation. To prepare the secondary growth solution, 1 mmol of each precursor, bIm, nIm and zinc nitrate hexahydrate (Sigma Aldrich, $Zn(NO_2)_3 \cdot 6H_2O$, 98+%) were measured out. The zinc nitrate hexahydrate was added to 10 mL of DMF and stirred thoroughly until completely dissolved. Concurrently, the imidazole precursors were added to a separate vial containing 20 mL of DMF and were also allowed to stir until completely dissolved. After the precursors were completely dissolved in their respective solutions, the 10 mL of DMF in which the zinc source was dissolved was added dropwise to the still-stirring solution of imidazole precursors in 20 mL of DMF. Once the mixtures were both completely combined and thoroughly stirred, the solution was poured into a Teflon lined autoclave wherein the seeded support was suspended horizontally, with the seeded side down. As with before, an unreactive alumina support was placed flush with the unpolished side of the support. The autoclave was then sealed shut and placed in an oven at 120°C for 8 hours and allowed to return to room temperature naturally. Once the autoclave was cooled, the membrane was removed, washed thoroughly in DMF and brushed gently with a cotton ball to remove any unreacted precursors. The membrane was then immersed in methanol overnight to allow for solvent exchange and dried under vacuum at ambient temperature.

3.2.4 Characterization of ZIF-68 Crystals and Membranes

The crystallinity of the ZIF-68 membranes was determined through X-ray diffraction (XRD) on a Panalytical X'Pert Pro X-ray Diffractometer at 40 kV and 40 mA at a scan speed of 5°/min using Cu Kα radiation. Further characterization of ZIF-68 membranes included permeation measurements using a simple permeation set up as described previously (Kasik & Lin, 2013). The permeation testing using helium, nitrogen, oxygen and carbon dioxide was carried out following thorough membrane activation. The ZIF-68 membrane was held under vacuum in an oven at 100°C for 5 hours to remove trapped impurities within the pores, and following activation the membrane was placed in a stainless steel permeation cell, with the ZIF-68 layer on the feed side, and sealed on both sides with Viton O-rings.   Following permeance measurements, ZIF-68 membranes were further characterized through pervaporation, as it allows for further insight into the membrane continuity and quality. Pervaporation was carried out as shown in previous works (Kasik & Lin, 2013). Prior to pervaporation, the membrane was activated under vacuum at 100°C for 5 hours, then immediately transported to a stainless steel pervaporation cell, where it was sealed securely on both sides by chemical resistant O-rings.

The final step was to carry out the destructive characterization of these membranes using a scanning electron microscope (SEM). Micrographs of ZIF-68 membranes were obtained using a Philips FEI XL-30 scanning electron microscope set at a 12 kV accelerating voltage. The membranes were sputtered thoroughly with a coating of Pd-Au prior to imaging to decrease the likelihood of surface charging during imaging.

3.2.5 ZIF-68 Stability Tests

To test the stability of ZIF-68 membranes in atmospheric conditions, the structure of the as-synthesized ZIF-68 membranes were first examined by XRD, then the membranes were placed in a petri dish (loosely covered) in the air and left undisturbed for 12 months. At the end of the twelve months the crystal structure was analyzed again to determine any alterations to crystallinity.

Much in the same manner, testing the stability of ZIF-68 in water, hexane, *p*-xylene and DMF at room temperature began with obtaining an initial XRD pattern for a fresh ZIF-68 membrane. The membranes were then each placed in a vial containing 50 mL of the relevant liquid, capped and left undisturbed for the entirety of the week. Upon removal and drying, their crystal structures were analyzed again. The boiling water stability testing was carried out in a similar manner, with the exception of the testing apparatus. The membrane was placed in a vial of deionized water that was left uncapped and almost fully immersed in a beaker containing refluxing water kept at 100°C. As the water evaporated more deionized water was added to keep the membrane continuously covered with water held at its boiling point. In shielding the membrane from the violent bubbling of the refluxing water and any resultant deleterious effects due to the dynamic boiling process, it was possible to isolate the stability of the ZIF-68 membrane as a function of boiling temperature water. The membrane was taken out every 24 hours in the 7 day duration of the test to obtain an XRD pattern.

3.3. Results and Discussion

Well-intergrown, ZIF-68 membranes on ZnO supports were reproducibly synthesized via the reactive seeding method. Initially, synthesis parameters such as the

holding times and amounts of precursors used were systematically altered in an attempt to optimize the synthesis procedure. The resultant membranes remained remarkably consistent regardless of the parameters altered, so the synthesis procedure requiring the least amount of energetic input and precursors was chosen, exclusively utilized and outlined herein.

Figure 3.1 shows micrographs of the surface of ZnO support covered with ZIF-68 seeds after the seeding step of synthesis. As shown, a seed layer that covers roughly 90 percent of the support with small randomly dispersed crystals around 3 μm in diameter is formed.
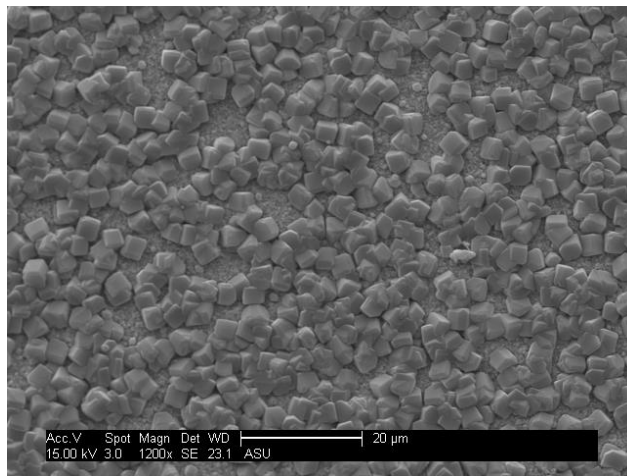
Figure 3.1

SEM micrographs of the top view of the ZIF-68 seeds layer on a ZnO support following a reactive seeding step at 1200x.

The XRD pattern shown in Figure 3.2 (a) confirms the seeds are in fact ZIF-68. Although the peaks are very weak relative to the intensity of the underlying ZnO support,

the XRD data shows the initial emergence of characteristic ZIF-68 peaks that remain present following secondary growth (Banerjee et al., 2008).
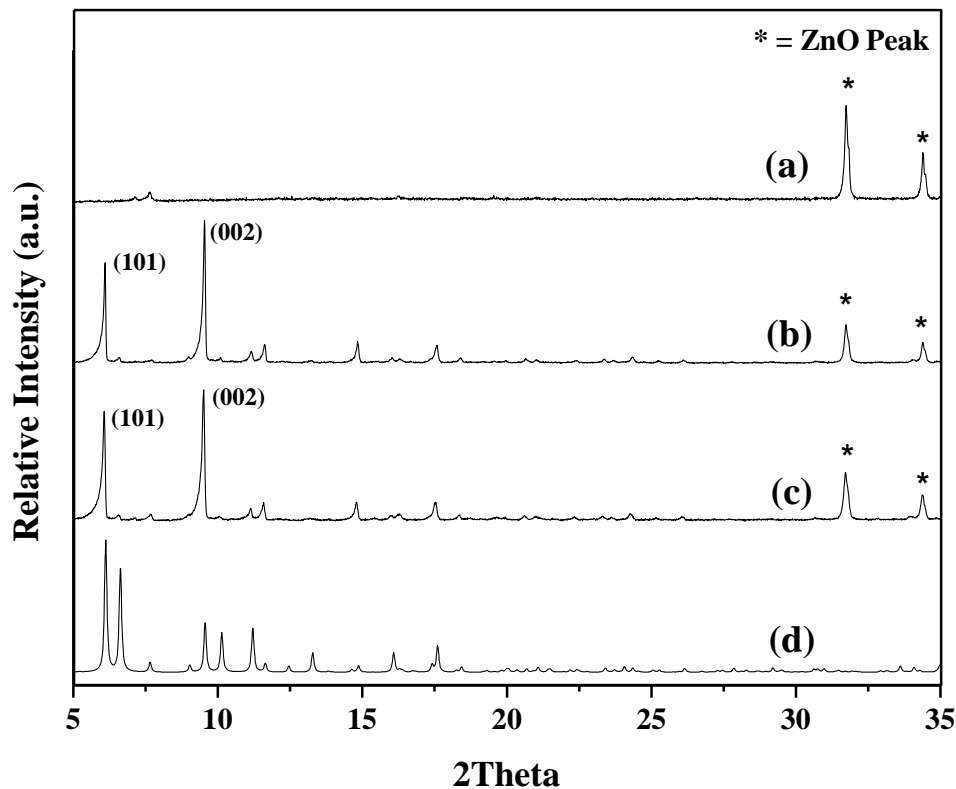
Figure 3.2

XRD spectra: (a) *showing the support following reactive seeding and the initial emergence of ZIF-68 peaks,* (b) *showing the ZIF-68 membrane following secondary growth,* (c) *the same membrane following a year in atmospheric conditions and* (d) *theoretical data showing all potential peaks associated with ZIF-68.*

The XRD data, coupled with the SEM micrographs, indicates the reactive seeding step allowed for the intimate growth of ZIF-68 seeds homogeneously across the support surface through the utilization of surface zinc atoms.

94

While the seeds layer was relatively evenly dispersed across the surface of the support, it was not entirely continuous initially. The discontinuity was remedied during secondary growth, as shown in Figure 3.3 (a) and (b). The surface of the resultant membrane is homogeneous, free of cracks and covered by truncated hexagonal prismatic grains with the size of 10-20 μm. A high degree of intergrowth of the grains within the membrane is observed. Figure 3.4 illustrates that the membrane layer is well-bonded with the ZnO support, and the thickness of the membrane is about 40 μm.

(a) (b)
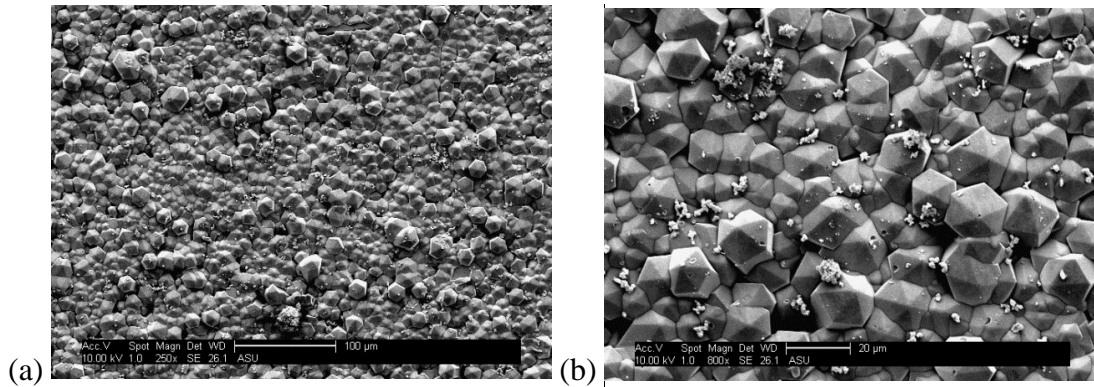
Figure 3.3

SEM micrographs of the top view of a ZIF-68 membrane at (a) *250x and* (b) *800x.*
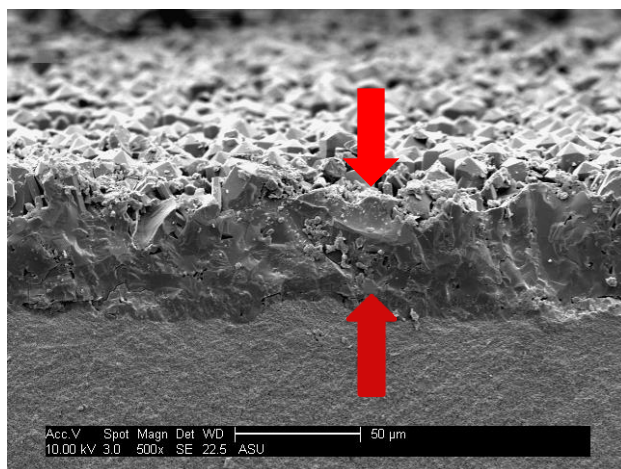
Figure 3.4

Cross-sectional image of ZIF-68 membrane showing a thickness of roughly 40 microns.

The XRD pattern of a ZIF-68 membrane after secondary growth is given in Figure 3.2 (b). The XRD pattern for the as-synthesized ZIF-68 membrane shows good crystallinity, especially the clear characteristic peaks at around 6.12^o (101) and 9.56^o (002), however the intensities of other peaks, as well as the peak visible in Figure 3.2 (a), are relatively low when compared to the theoretical XRD spectrum for randomly oriented ZIF-68 crystals as presented in the work of Banerjee et al. and shown in Figure 3.2 (d) (Banerjee et al., 2008). A possible explanation is that during the initial reactive seeding step the ZIF-68 seeds orient themselves along the *a*- and *b*-axis and as secondary growth occurs the ZIF-68 membrane begins to grow preferentially along the (002) direction (*c*-axis) on the ZnO support. This explains the very strong presence of peaks associated with the basal (*c*-axis) and pyramidal (*c*- and *a*-axis) planes following secondary growth. A similar result was also observed by Liu et al. (Yunyang Liu et al., 2011a) when they found that the ZIF-69 membrane showed preferred growth along the (002) direction even

without a structure orienting agent. Therefore, this may be a special property of the ZIFs with GME topology. Furthermore, ZIF-68 has a known hexagonal $P6_3$/mmc structure, and the surface of the membrane shown in Figure 3.3 (a) and (b) is dominated by 120° facets characteristic to the *a*- and *b*- directions in hexagonal single crystals, indicating the direction orthogonal to the support is predominantly *c*-oriented (Banerjee et al., 2008; Park, 2006; Phan et al., 2010). Similar morphology was observed on other ZIF membranes with GME topology, such as ZIF-69 (Yunyang Liu et al., 2010, 2011a) and ZIF-78 (Dong et al., 2012) membranes.

In our experiment, ZIF-68 membranes synthesized via reactive seeding were found to be relatively thick (between 30 and 60 μm). The thick cross-sections of the membranes synthesized were not found to be correlated to high precursor concentration, as increases and decreases in precursor concentration all yielded relatively consistent thicknesses. The reproducibly large thicknesses are likely associated with the general tendency for these membranes to grow preferentially along the *c*-axis. During secondary growth the randomly dispersed seeds grow predominantly with the *c*-axis oriented orthogonally to the surface of the ZnO support, while the *a*- and *b*-axis grow steadily outward until complete impingement of neighboring seeds hinders further growth. Therefore the length along the *c*-axis does not face such staunch hindrance to growth. Although, the relatively thick membrane layer is not necessarily desirable, the tendency toward *c*-orientation is preferable for molecular diffusion through the membrane because ZIF-68 has a one-dimensional channel along the *c*-axis (Banerjee et al., 2008). Modeling work has associated an increased mobility of CO_2 with *c*-orientation of ZIF-68 crystals, as well as a considerable attraction between the protruding phenyl groups of the

97

benzimidazole linkers that line the largest channel oriented along the *c*-axis (Banerjee et al., 2009; Hou & Li, 2010; Yang Liu, Liu, Chang, & Zheng, 2012; Rankin, Liu, Kulkarni, & Johnson, 2009). In Figure 3.5 the ZIF-68 unit cell is shown along the *c*-axis, where the prominent phenyl rings are evident through the main channel.
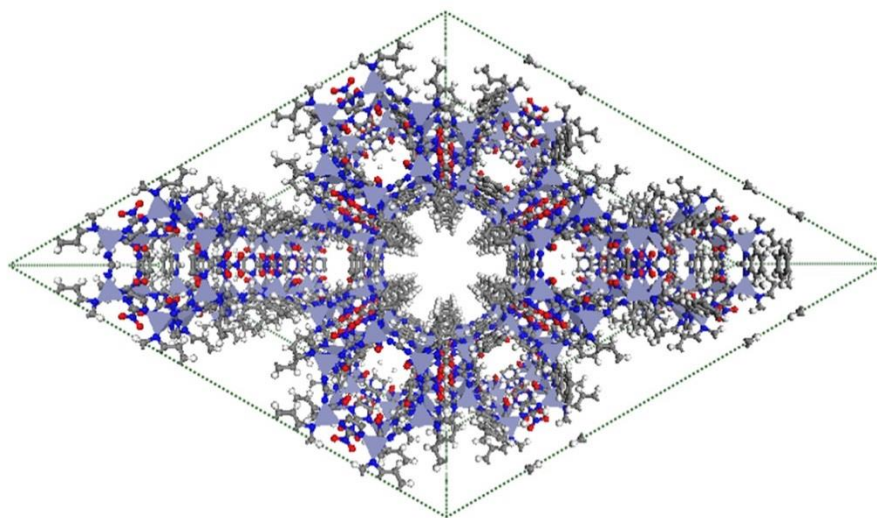
Figure 3.5

C-oriented ZIF-68 unit cell showing the protruding phenyl groups along the main channel.

In Figure 3.6, the helium, nitrogen, argon and carbon dioxide single gas permeation results are plotted. For a larger-pore MOF, such as ZIF-68, with pore and cage sizes of 7.5 and 10.3Å respectively, the single gas permeation should follow the Knudsen diffusion mechanism and vary with the inverse of the square root of the molecular weight of the permeating molecules (Koros & Fleming, 1993). Although a smaller pore-sized MOF membrane, ZIF-8, has shown adherence to Knudsen diffusion, in that case it was largely indicative of a dominance of permeation flow through non-ZIF

pores, amorphous regions and crystalline boundaries (Venna et al., 2013). The adherence to Knudsen diffusion of the ZIF-68 membranes outlined in this work is illustrated in Figure 3.6, as the line fitted for Knudsen diffusion is shown going through the origin, and the squares are the single gas permeance measurements for a given transmembrane pressure drop. The fitness of data was determined to be quite close, with a R^2 value of 0.99837, and indicates the membrane has limited nonselective defects. A slight deviation in adherence to the straight line does exist at the point that corresponds to CO_2 single gas permeance. The higher than predicted CO_2 permeance is not a manifestation of a sizeable defect in the membrane but rather an artifact that is exhibited when the CO_2 permeance is tested in microporous materials that exhibit discrete levels of preferential CO_2 loading sites (Sirjoosingh, Alavi, & Woo, 2010).
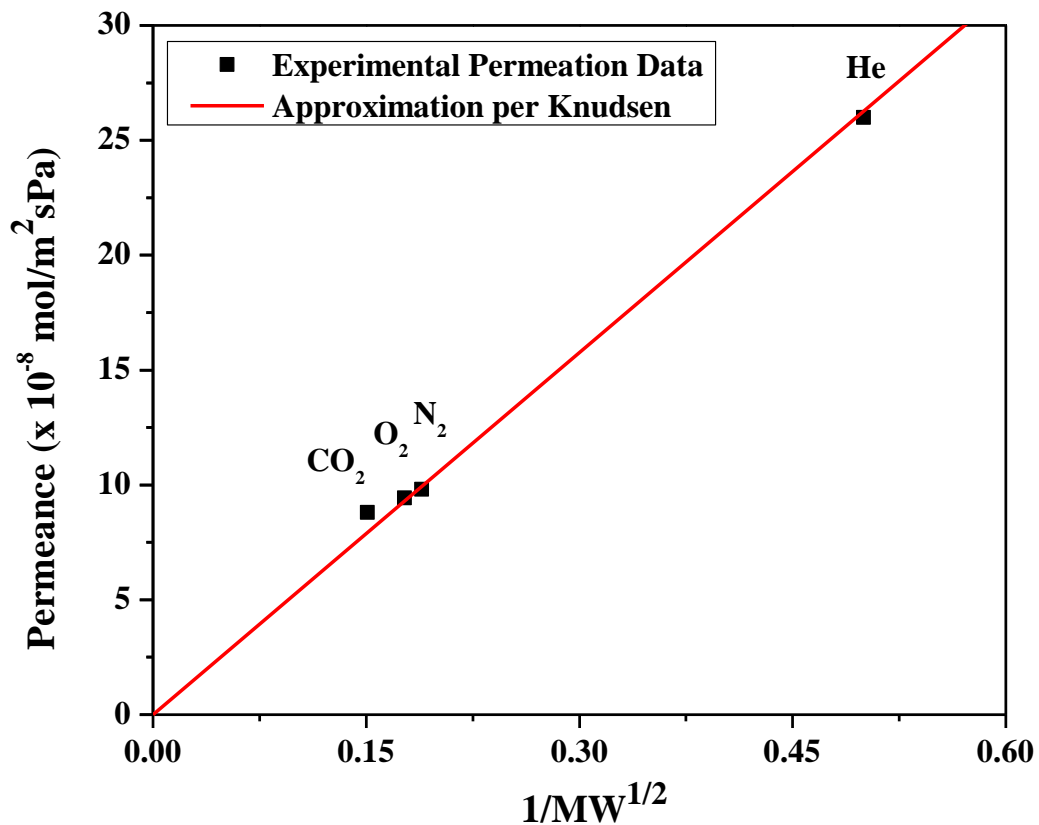
Figure 3.6

Plot of permeance as a function of the inverse square of molecular weight for various gases through ZIF-68.

In Table 3.1 permeance data for various microporous MOF membrane materials are presented. Membranes such as MOF-5, HKUST-1 and MIL-53 have similar pore size, and the disparity in cross-sections does not account for the differences in permeance values indicating differences in porosity may be largely responsible (Guerrero, Yoo, McCarthy, & Jeong, 2010a; Nan, Dong, Wang, Jin, & Xu, 2011; Z. Zhao et al., 2011a).

The helium and nitrogen permeance for the 40μm thick ZIF-68 membrane at room temperature is respectively about 26 and 9×10^{-8} mol/m^2.s.Pa, slightly smaller than the values of 30 and 12×10^{-8} mol/m^2.s.Pa, respectively for the 14 μm MOF-5 membrane (Z. Zhao et al., 2011a). Considering the difference in thickness, these results shows that ZIF-68 membranes have higher permeability than MOF-5 membranes. MOF-5 and ZIF-68 have a similar, large pore size (8 Å for MOF-5 and 7.5 Å for ZIF-68), and similar porosity. The percentage of the MOF-5 structure accessible to gaseous species is approximately 55%, while for ZIF-68 the percentage is approximately 59% (Eddaoudi et al., 2000; J. Tan et al., 2010). The slightly higher porosity of ZIF-68 reasonably accounts for the increase in permeability that the ZIF-68 membranes exhibit. Another possible reason for the higher permeability of ZIF-68 membrane is that the growth of the membrane layer along c-orientation (the direction of the one-dimensional channel in ZIF-68) facilitates the diffusion of molecules through the membrane

Table 3.1 *Membrane and permeance data for similar pore-size MOF membranes.*

Material	Pore Size (Å)	Surface Area (m^2/g)	Membrane Thickness (μm)	Helium Permeance (x 10^{-8} mol/m^{2}sPa)	Nitrogen Permeance (x10^{-8} mol/m^{2}sPa)	Reference
ZIF-68	7.5	1090[1]	40	26	9	This Work
MOF-5	8	2304[2]	14	30	12	(Z. Zhao et al., 2011a)
MIL-53	7.3&7.7	1180[3]	8	-	13.9	(Hu et al., 2011)
HKUST-1	9	2200[4]	25	-	53	(Guerrero et al., 2010a)
HKUST-1	9	2200[4]	25	-	20	(Nan et al., 2011)

1 (Phan et al., 2010) 2 (Z. Zhao et al., 2009) 3 (Y. Zhang et al., 2014) 4 (Wong-foy, Matzger, & Yaghi, 2010)

In Figure 3.2 (c), the XRD pattern of a ZIF-68 membrane after one year of exposure to air in the laboratory is shown and compared with the XRD pattern of the as-synthesized membrane shown in Figure 3.2 (b). The XRD spectra show very limited deviations, indicating the material did not undergo any phase shifts, or losses of crystallinity due to the contact with atmospheric levels of moisture. The SEM image of the same sample is also shown in Figure 3.7. The sample although, differing slightly morphologically from the sample shown in Figure 3.3 (a) and (b), shows no degradation or loss in crystallinity. This finding is very contrary to the behavior of MOF-5, which has shown irreversible degradation after only 10 minutes in atmospheric levels of moisture (Kaye et al., 2010). Given water has a way of adhering, permanently and deleteriously, to the microstructure of MOF-5, it is likely that, despite activation, there

are retained water molecules within the microstructure resulting in a slight decrease in permeability (Eddaoudi et al., 2000; Kaye et al., 2010; Saha & Deng, 2010).
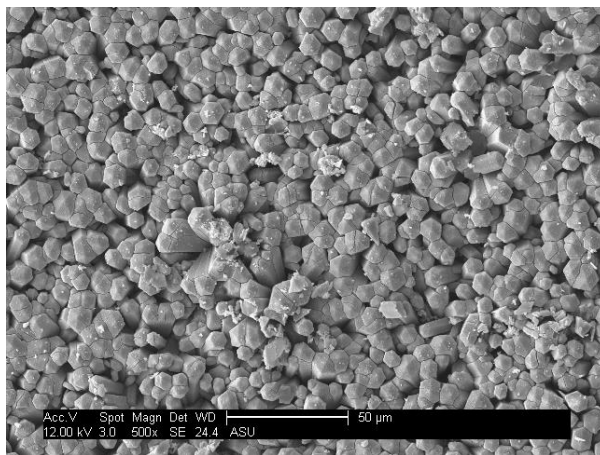
Figure 3.7

SEM micrograph of the top view of a ZIF-68 membrane following one year in atmospheric conditions at 500x.

Once it was determined that ZIF-68 membranes exhibit exceptional stability in ambient conditions, further stability of the membranes in more adverse conditions and, by extension their suitability for a number of applications, was examined. Figure 3.8 compares the as-synthesized microstructure of a ZIF-68 membrane to that obtained following complete submersion in room temperature water for seven days. The XRD data show that while the membrane was not completely degraded, as characteristic peaks were not shifted or eradicated entirely, crystallinity was severely diminished. As was touched on earlier, reports of MOF instability are widely centralized around non-zeolitic metal-organic frameworks, such as MOF-5 and MOF-177, wherein the hypothesized

mechanism of degradation is polar, hydrogen containing molecules, such as water and ammonia, insidiously ingratiating themselves into portions of the organic ligand and secondarily bonding to the oxygen in the zinc-oxygen tetrahedra (Eddaoudi et al., 2000; Kaye et al., 2010; Saha & Deng, 2010). ZIF materials tend to avoid this devastating degree of degradation due to the hydrophobic nature of the pores; the pores themselves repel water thus protecting the Zn_4N tetrahedra from any structural collapse due to secondary bonding (Park, 2006). Due to this pore protecting hydrophobicity, the ZIF-68 membranes show incredible stability in atmospheric conditions, and only mild degradation in room temperature water.

Figure 3.9 shows the XRD spectra obtained from a ZIF-68 membrane throughout the course of a weeklong immersion in boiling water. Within the first 24 hours of immersion in boiling water, any trace of a ZIF-68 characteristic peak disappeared and an entirely separate set of peaks emerged. The XRD spectra remained mostly constant from the second day forward, indicating that whatever new crystalline byproduct emerged was stable upon immersion in boiling water. The new peaks characteristic to the destroyed membrane were not identifiable as any currently categorized crystalline compounds containing the same atomic constituents of the ZIF-68 membrane. Due to the unexpected degradation to the membrane, the experiment was duplicated exactly with ZIF-68 crystals synthesized per methods outlined in literature to determine whether or not the extreme degradation was specific to the crystals synthesized in the membrane layer on the ZnO support via reactive seeding (Banerjee et al., 2008). The same lack of stability and shift in XRD peaks were observed when a small amount of crystals synthesized as outlined in literature were also immersed in boiling water for a week (Banerjee et al., 2008).
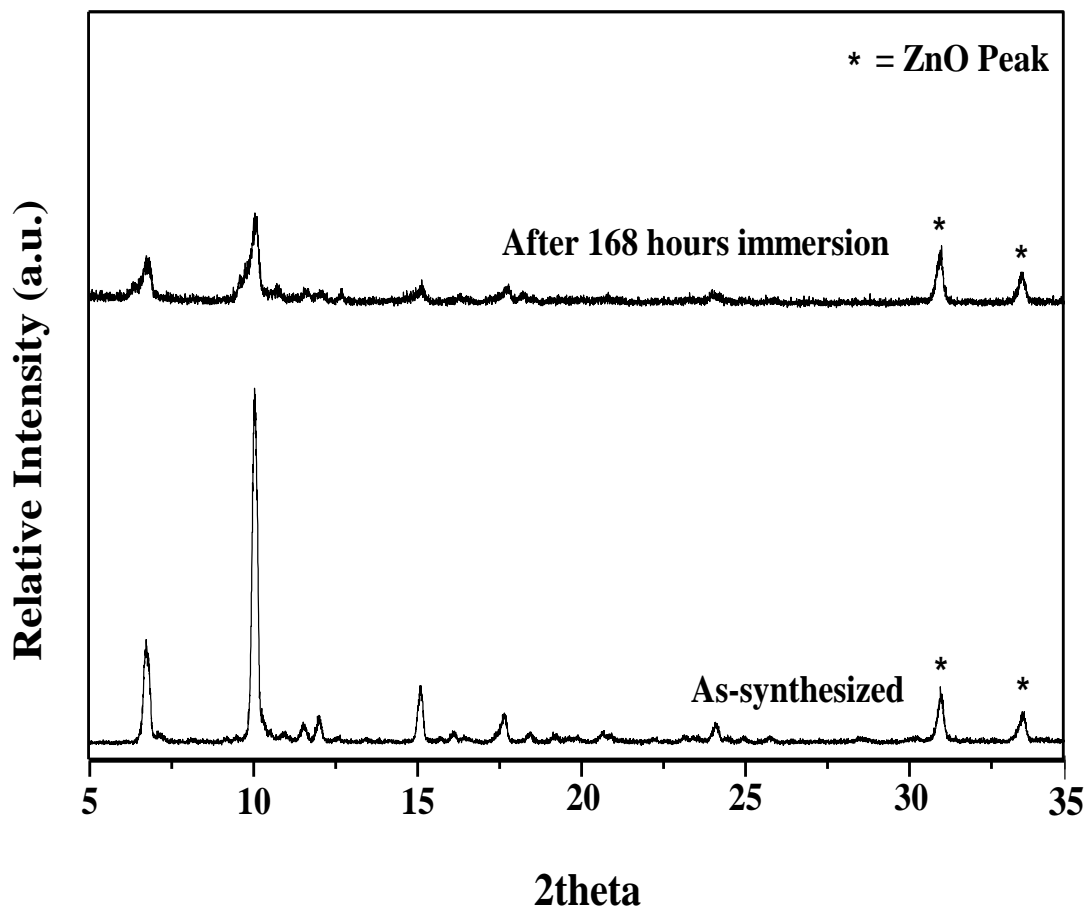
Figure 3.8

Comparative XRD spectra of an as-synthesized ZIF-68 membrane before and after 168 hours continuous immersion in room temperature water.
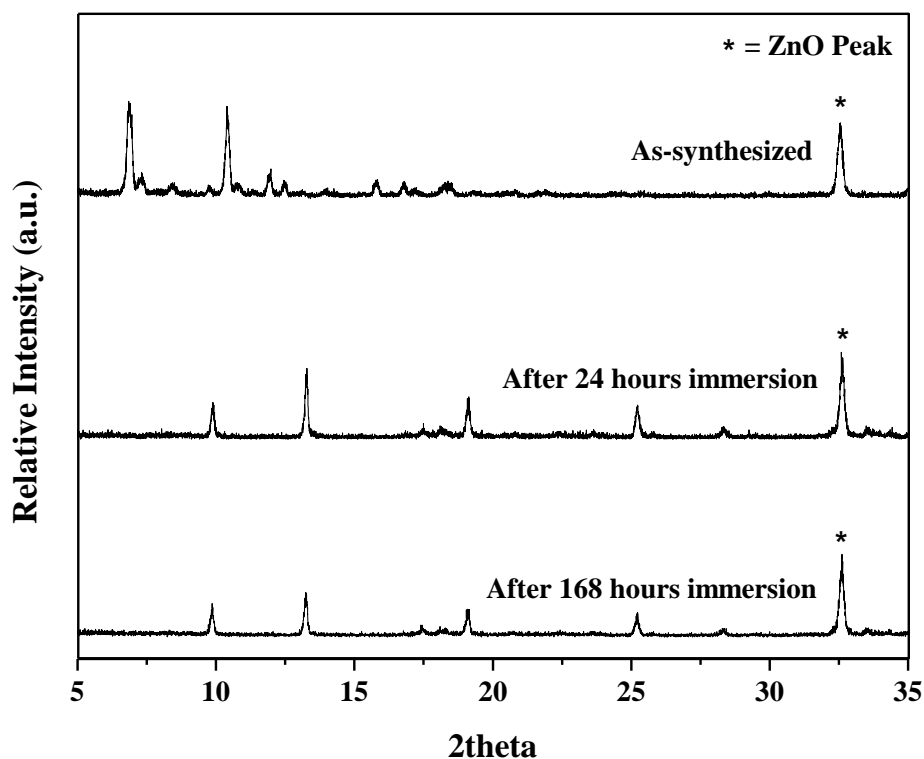
Figure 3.9

XRD spectra for an as-synthesized ZIF-68 membrane compared to those obtained following 24 hours and 168 hours submerged in boiling water.

The perplexing nature of the degradation of the ZIF-68 crystals was only exacerbated upon examining the membrane surface and single crystals with scanning electron microscopy, as shown in Figure 3.10. The morphology of the crystals (shown in Figure 3.10 (a) on a background of carbon tape) and the crystals on the ZIF-68 membrane (shown in Figure 3.10 (b) on the ZnO support on which they were synthesized) after one week immersion in boiling water show no resemblance to their previous form and only show an intricate network of shearing and cleavage planes. The crystal degradation is the

direct result of instability of ZIF-68 crystals and ZIF-68 membranes in water held at high temperatures. Since the violent bubbling effects of the boiling process were minimized and essentially negated through the apparatus used to test stability, it is clear that the ZIF-68 structure is especially intolerant to high temperature water. These findings are quite contrary to the results of similar studies. Banerjee et al. reported that ZIF-68 crystals showed no decrease in crystallinity after a week of immersion in boiling water, while Liu et al., reporting on the stability of a ZIF-69 membrane (a Zn-based ZIF with the same GME topology and similar organic linkers) during a weeklong immersion in boiling water, found that ZIF-69 showed only a slight loss in crystallinity and no shifts in peak location (Banerjee et al., 2008; Yunyang Liu et al., 2010). It is worthy of note that Park et al. found the same structural degradation was evidenced in crystals of ZIF-7 and ZIF-11 after one day and three days of immersion in boiling water, respectively (Park, 2006). The results for ZIF-7 and ZIF-11 that show degradation akin to that seen with ZIF-68 were for a week in boiling water kept refluxing at 100°C, while the reports of ZIF-68 crystal synthesis that indicated weeklong stability in boiling water were kept refluxing at 65°C (Banerjee et al., 2008; Park, 2006). This temperature difference must be accountable for the stark contrast in stability reported. ZIF-68 is not stable for any extended period of time in membrane or single-crystalline form in refluxing boiling water at 100°C.

(a)   (b)
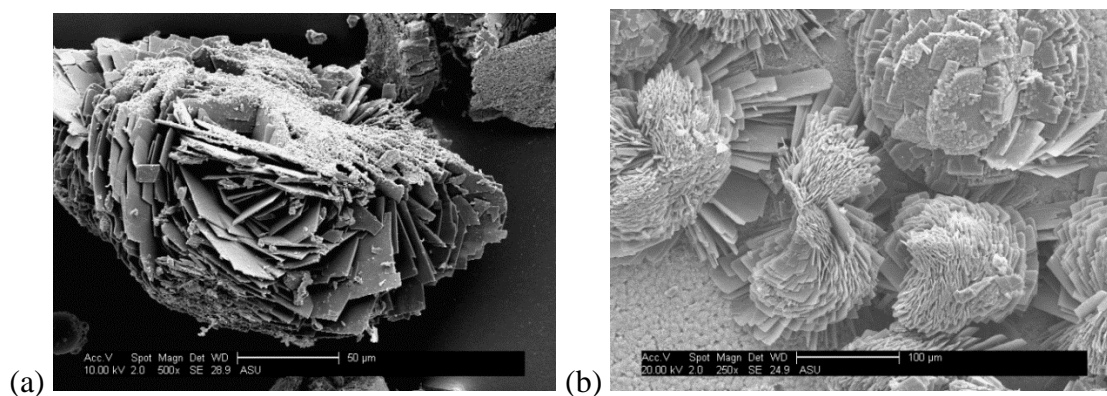
Figure 3.10

SEM micrographs showing the (a) *deterioration of ZIF-68 crystals following a weeklong immersion in boiling water* (b) *and the resultant membrane morphology following a weeklong immersion in boiling water*

Figure 3.11 compares the XRD pattern of a ZIF-68 membrane as-synthesized to those of the membrane after weeklong immersions in hexane, DMF and *p*-xylene. As shown, the XRD patterns of the fresh membrane and those after a weeklong immersion in the solvents are identical in terms of peak location and sharpness. This shows that the membrane is robust and stable when submerged in representative solvents. There are reversals of peak intensity evidenced for certain spectra, but these are attributable to the inconsistencies in obtaining diffraction spectra from the varying shaped portions of the membrane. Overall, the membranes showed a good stability in hexane, DMF and *p*-xylene. Although immersion of the ZIF-68 membrane in room temperature and boiling water both caused different degrees of irreversible destruction of the ZIF-68 structure, the ZIF-68 membrane is suitably stable and thereby viable for applications wherein

108

interaction with atmospheric conditions are present or immersion in organic solvents, such as xylene isomers, occurs.
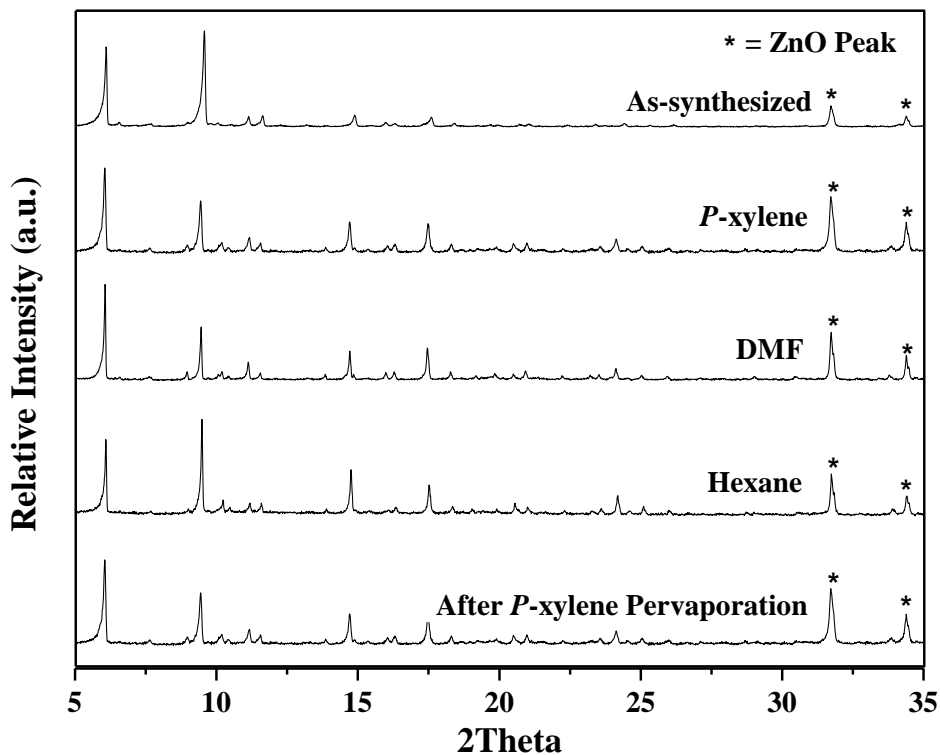
Figure 3.11

XRD spectra for an as-synthesized ZIF-68 membrane compared to those obtained following weeklong immersion in p-xylene, DMF, hexane and following p-xylene pervaporation.

The ZIF-68 membrane was further characterized through an extended pervaporation run in *p*-xylene. The results after 20 hours of continuous testing are shown in Figure 3.12. The initial data point was obtained after two hours of pervaporation and showed a pervaporation flux of approximately 4.4×10^{-3} mol/m^{2}s. The second data point

was taken two hours later and showed a decrease in pervaporation flux by approximately 55%, to 2×10^{-3} mol/m^{2}s. The remainder of the test showed remarkably consistent pervaporation fluxes, indicating there was an immediate saturation of potential fouling sites. Wegner et al. reported fouling as a decrease in *p*-xylene flux through a polycrystalline MFI (ZSM-5) membrane as a function of time wherein the decrease in flux was attributed to a chemical adsorption of xylene molecules into the lattice that increased with time until flux normalization occurred (Wegner et al., 1999). This same effect was also evidenced in *p*-xylene pervaporation through MOF-5 membranes, wherein the *p*-xylene flux decreased by approximately 38% within the first 20 hours on-stream (Kasik & Lin, 2013). The chemisorption of xylenes into the lattice occurring in the ZSM-5 and MOF-5 membranes was hypothesized to be the result of an attraction between the electrons in the benzene rings of the xylene molecules and the metallic cations and oxygen atoms of the zeolite lattice, thus causing π-complexes to form between them and ultimately leading to fouling (Breck, 1974; Faibish & Cohen, 2001; Kasik & Lin, 2013; Wegner et al., 1999).
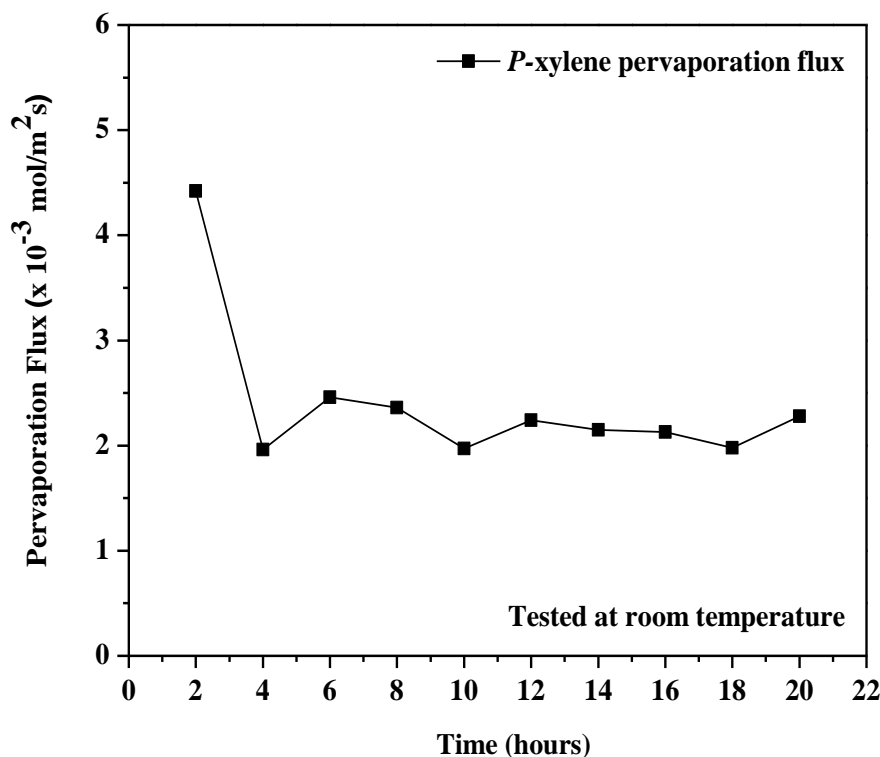
Figure 3.12

Pervaporation flux of p-xylene through a ZIF-68 membrane as a function of time.

The almost instantaneous decrease followed by stabilization in the pervaporation flux of *p*-xylene through ZIF-68 structure indicates that immediate fouling occurs, and once every available site for *p*-xylene to secondarily bond to within the ZIF-68 structure is saturated, the flux levels off and remains virtually constant. There are a number of sources within the ZIF-68 microstructure that have the potential to form π-complexes. Potential sources of fouling include the presence of unreacted precursors that may contribute unsatiated electrons, point defects within the Zn_4N tetrahedra and the protruding phenyl groups of the benzimidazole linkers (Amirjalayer & Schmid, 2009;

111

Amirjalayer et al., 2007).   An XRD pattern of the ZIF-68 membrane after the pervaporation of p-xylene is compared with that of as-synthesized ZIF-68 membrane in Figure 3.11. The consistency of the peaks shows that despite the fouling, the crystallinity of the membrane itself remains unaltered by immersion and the process of pervaporation in *p*-xylene. This further confirms the robustness of the ZIF-68 membrane in organic solvents.

3.4 Conclusions

Continuous ZIF-68 membranes can be reproducibly synthesized when using the reactive seeding method followed by secondary growth. The membranes synthesized exhibit gas permeation behavior that obeys the Knudsen diffusion mechanism, indicating they are free from non-selective defects when utilizing this synthesis approach. ZIF-68 membranes show good stability in air and organic solvents, but immersion in water of any temperature will result in different degrees of irreversible damage to the membranes. The membranes are susceptible to fouling during organic solvent pervaporation, however once complete saturation of available fouling sites occurs the flux stabilizes. Pervaporation of organic solvents does not degrade the membrane morphology.

CHAPTER 4

SYNTHESIS OF ZIF-68 MEMBRANE ON A ZNO MODIFIED α-ALUMINA SUPPORT BY A MODIFIED REACTIVE SEEDING METHOD

4.1 Introduction

As was discussed in Chapter 3, zeolitic imidazolate frameworks (ZIFs) are a relatively new extension of the widely studied metal organic frameworks (MOFs). ZIFs are characterized by an extensive cross-section of traditional aluminosilicate zeolite topologies and high chemical and thermal stability(Banerjee et al., 2009; Choi et al., 2006; Yao & Wang, 2014). At this time, the research on ZIF membranes is saturated with smaller pore ZIF materials. Those reported on are ZIF-7 (3.0 Å), ZIF-9-67 (< 3.4 Å), ZIF-8 (3.4 Å), ZIF-90 (3.5 Å), ZIF-78 (3.8 Å), ZIF-71 (4.2 Å) and ZIF-69 (4.4 Å) (Banerjee et al., n.d., 2008; Dong & Lin, 2013; Yao & Wang, 2013). The pore size and functionality of these membrane materials has rendered them front running candidates for many applications involving the separation of smaller molecules, such as H_2 purification and CO_2 sequestration (Yao & Wang, 2013). Further, some small-pore ZIFs have shown potential in smaller molecule pervaporation separation and vapor sensing (Yao & Wang, 2013). There are, however, marked differences between the smaller, more widely researched ZIFs, and those with larger pores. Larger pore ZIFs, while still retaining the characteristic desirability afforded to ZIF materials, exhibit perm-selectivity that is driven by adsorption properties of the material. The isolation of solely adsorption based separation has been used to effectively separate a number of mixtures in other large pore MOF and zeolite materials (Y. S. Lin et al., 2007; Z. Zhao et al., 2013). To isolate the inherent adsorption properties of the ZIF membrane material, without having to suffer

113

any losses in selectivity due to secondary sieving effects, could prove invaluable for a number of industrially relevant separation processes. Further, another motivation behind studying large pore ZIF membranes is the potential they offer for large molecule gas and liquid separation. It is by virtue of this, the work outlined in Chapter 3 was carried out to synthesize the 7.5Å pore size ZIF-68 in useable membrane form (Kasik, Dong, & Lin, 2014).

Given no other large-pore ZIFs have been synthesized in membrane form as of yet, initial synthesis attempts for ZIF-68 were modeled after a smaller pore ZIF, ZIF-69, that was chosen due to its similar dual ligand nature and P6$_3$/*mmc* structure (Sirjoosingh et al., 2010). The two reports on ZIF-69 membrane synthesis outline a seeded secondary growth method and an *in situ* method utilizing porous alumina supports (Yunyang Liu et al., 2010; Yunyang Liu, Zeng, Pan, & Lai, 2011b). In initial synthesis attempts of ZIF-68, these methods were used as a general rubric, and modifications were made as necessary. The findings, however, were that regardless of the parameters altered, heterogeneous nucleation of ZIF-68 was not attainable through *in situ* synthesis, nor was seeding effective. Images obtained using scanning electron microscopy showed exceptionally poor coverage of the alumina support, and it was hypothesized that the rate at which ZIF-68 grows along the *c*-axis yields crystals that are far too large for effective seeding without the addition of a surface modification or anchor. In lieu of this, reactive seeding on a ZnO support was attempted.

The reactive seeding method, which has been reported in literature previously for MIL-53 (Hu et al., 2011), MIL-96 (Nan et al., 2012) and ZIF-71 (Dong & Lin, 2013), utilizes the unsatiated terminal metallic atoms at the surface of the oxide support to then

react with the organic precursors in solution to create a closely bound seeds layer. Following a secondary growth step with the relevant organic precursors and an external source of the needed metallic ion, a continuous, well-intergrown membrane layer can be obtained. It was found, however, during the characterization of the ZnO supported ZIF-68 membranes synthesized via reactive seeding that great care was needed to maintain a transmembrane pressure drop of no more than 0.68 atm, or catastrophic cracking of the support would occur (Kasik et al., 2014). Given the weaker nature of the ZnO support, and its potential hindrance to the applications for which ZIF-68 membranes synthesized upon it are suited, developing a new manner of synthesis on an alumina support was necessary. The objective of this work is to synthesize ZIF-68 membranes on more robust alumina supports by a method that utilizes the principles behind reactive seeding.

4.2 Experimental

4.2.1 Surface Modification of Alumina Support with ZnO

The alumina (Al_2O_3) supports used in the synthesis of ZIF-68 via the modified reactive seeding method were made in house from a press-sintering method reported elsewhere (Kasik & Lin, 2013). Once sintered, the supports were polished with progressively finer grit sandpaper (#500, #800 and #1200) using an MTI Unipol-320 polisher. Following an ultrasonic cleaning in ethanol and distilled water and an overnight drying at 100°C, the supports were then ready for use.

4.2.2 Surface Modification via Dip Coating and Sintering

The first method of surface modification attempted was dip coating. A solution of 2 wt% zinc oxide (ZnO, 99.9%, Sigma Aldrich) in dimethylformamide (DMF, 98%, Alfa Aesar) was agitated until the <5 µm ZnO particles were homogeneously dispersed. An

Al$_2$O$_3$ support was then placed, polished side down, on the surface of the solution for 5 seconds and left in an oven at 50°C for 3 hours to dry. This was repeated two more times. Following the last dip coating and drying cycle, the support was then heated to 570°C for five hours at a ramp rate of 2°C/min.

4.2.3 Surface Modification via In Situ Deposition of ZnO

The second method of surface modification attempted was derived from a method outlined previously by Jeong et al. wherein a solvothermal reaction results in a well adhered layer of ZnO along the surface of an Al$_2$O$_3$ support (Shah et al., 2013). To create the synthesis solution, 1.43 g of sodium formate (HCOONa, ≥99%, Sigma Aldrich) and 0.55 g of zinc chloride (ZnCl$_2$, ≥98%, Sigma Aldrich) were mixed in 35 mL of methanol (MeOH, 99.8%, BDH). The mixture was left to stir for 20 minutes to allow for the precursors to adequately dissolve within the methanol. The solution was then poured into a Teflon-lined autoclave where two alumina supports were placed vertically, polished sides facing out. The benefit of arranging the two alumina supports in this manner is twofold; first, this allows for multiple supports to be modified simultaneously, and second, with the backs of the supports flush with one another, the growth of ZnO is hindered on that side, which means that further seeding and secondary growth steps will not result in ZIF-68 seeds and layers on both sides of the support. The autoclave was then sealed and placed in an oven set to 120°C for 4 hours. Following surface modification, the autoclave was allowed to return to room temperature naturally. The modified support was then removed, gently washed in fresh methanol and dried overnight under room temperature vacuum.

116

4.2.4 Reactive Seeding of ZIF-68

Once the supports were adequately coated in ZnO, be it by dip coating or an *in situ* reaction, reactive seeding occurred. To create the reactive seeding solution, 0.25 mmol each of 2-nitroimidazole (0.28 g, 2-nIm, 98%, Bosche Scientific) and benzimidazole (0.29 g, bIm, ≥98%, Sigma Aldrich) were added to 30 mL of DMF and thoroughly stirred. The solution was then poured into a Teflon-lined autoclave where the ZnO coated alumina support was suspended vertically, ZnO coating face down, using a Teflon holder. The autoclave was then sealed and placed in a low-temperature oven held at 120°C for six hours. The autoclave was not allowed to return to room temperature naturally following synthesis, but instead was quenched with cool running water until cooled, usually 5-10 minutes. Once cooled, the supports were removed, rinsed gently in fresh DMF and dried under vacuum at room temperature overnight.

4.2.5 Secondary Growth of ZIF-68 Membranes

Following reactive seeding, a final secondary growth step was carried out. The secondary growth solution was created in steps. First 1 mmol of each precursor, bIm (0.117 g), 2-nIm (0.113 g), sodium formate (0.063 g) and zinc nitrate hexahydrate (0.297 g, $Zn(NO_2)_3 \cdot 6H_2O$, 98+%, Sigma Aldrich) was measured out. The zinc nitrate hexahydrate and sodium formate were added to 10 mL of DMF and stirred thoroughly until completely dissolved. In a separate vial, the imidazole precursors were added to 20 mL of DMF and allowed to completely dissolve. Once both solutions were well mixed, the 10 mL solution containing the zinc nitrate hexahydrate and sodium formate was added dropwise to the still-stirring solution of imidazole precursors in 20 mL of DMF. Once the mixtures were both completely combined and thoroughly stirred, the solution

was poured into a Teflon-lined autoclave wherein the seeded support was suspended horizontally, with the seeded side down. The autoclave was then sealed shut and placed in an oven at 120°C for 6 hours. At the end of the 6 hours, the autoclave was promptly removed and cooled under running water as before. Once the autoclave was cooled, the membrane was removed and washed gently in DMF. The membrane was then immersed in methanol overnight to allow for solvent exchange and dried under vacuum at ambient temperature.

4.2.6 Characterization

Non-destructive testing of the supports, seeds layers and membranes encompassed X-ray diffraction (XRD), gas permeance and liquid pervaporation. X-ray diffraction was carried out on a Panalytical X'Pert Pro X-ray Diffractometer at 40 kV and 40 mA at a scan speed of 5°/min using Cu Kα radiation. The gas permeance behavior of the membranes was obtained using a single gas permeation set up as described in previous publications (Kasik & Lin, 2013). The membrane is first activated under vacuum for five hours at 100°C to ensure any trapped gaseous species are removed prior to testing. Once thoroughly activated, the membrane was placed in a stainless steel membrane cell, and sealed with Viton O-rings. The ZIF-68 membrane layer was placed facing the feed side and the membrane was not activated further between different gas measurements given it was not exposed to atmospheric conditions at any point during testing. Further non-destructive characterization of ZIF-68 membranes included pervaporation. The pervaporation set up was described in previous work as well (Kasik & Lin, 2013). Prior to the initial pervaporation test, and following each pervaporation test, it was necessary to evacuate the membranes of any trapped impurities through further activation under

vacuum at 100°C for five hours. The activated membrane was then placed, membrane layer toward the feed side, in a stainless steel pervaporation cell and sealed with Viton O-rings.

Imaging of the supports, seeds layers and membranes was carried out destructively using a Phillips FEI XL-30 scanning electron microscope (SEM). The microscope was set at a 12 kV accelerating voltage and the samples were sputtered thoroughly with Pd-Au to minimize the amount of surface charging and increase the quality of the images.

4.3 Results and Discussion

4.3.1 ZnO Coating on Al$_2$O$_3$

Initially membrane formation was modeled after *in situ* methods outlined by Jeong et al. to synthesize ZIF-7 and ZIF-8 and Lai et al. to synthesize ZIF-69 (Yunyang Liu et al., 2011a; Shah et al., 2013). The attempts to create ZIF-68 membranes on Al$_2$O$_3$ supports based off of these established synthesis methods, despite tailoring to known specific needs of ZIF-68 crystal and membrane growth, did not yield continuous membranes. When attempts at altering time and temperature proved unsuccessful and costly, the procedure outlined in this work was established to create a generally applicable synthesis method that used greatly reduced quantities of the costly 2-nitroimidazole precursor.

In order for ZIF-68 membranes to be viable for use in applications where transmembrane pressure drops can increase above 0.68 atm, the strength of Al$_2$O$_3$ needed to be coupled with the intimate seed growth afforded through reactive seeding on ZnO. Following the initial attempts at *in situ* synthesis, the strength of Al$_2$O$_3$ was merged with

119

the reactive seeding capabilities of ZnO through the mechanical, and later, chemical, adhesion of ZnO on the surface of a polished Al_2O_3 support. Both methods of ZnO deposition proved successful. The SEM images shown in Figure 4.1 (a) and (b) indicate that the dip coating of ZnO on the surface of the Al_2O_3 support was a successful means of attaining a surface largely covered in ZnO, with a cross-sectional thickness of roughly 4 μm.

(a)   (b)
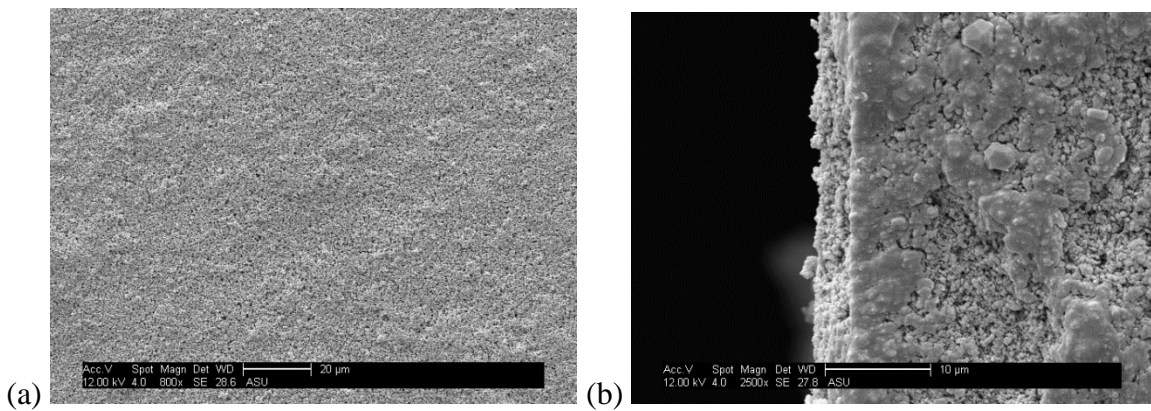
Figure 4.1

SEM micrographs of Al_2O_3 support following dip coating of ZnO and sintering at (a) *1000X and* (b) *a cross sectional view at 2500X.*

SEM images shown in Figure 4.2 (a) and (b) indicate that the *in situ* method of ZnO deposition also yielded a large, albeit morphologically quite different, covering of ZnO.

(a)   (b)
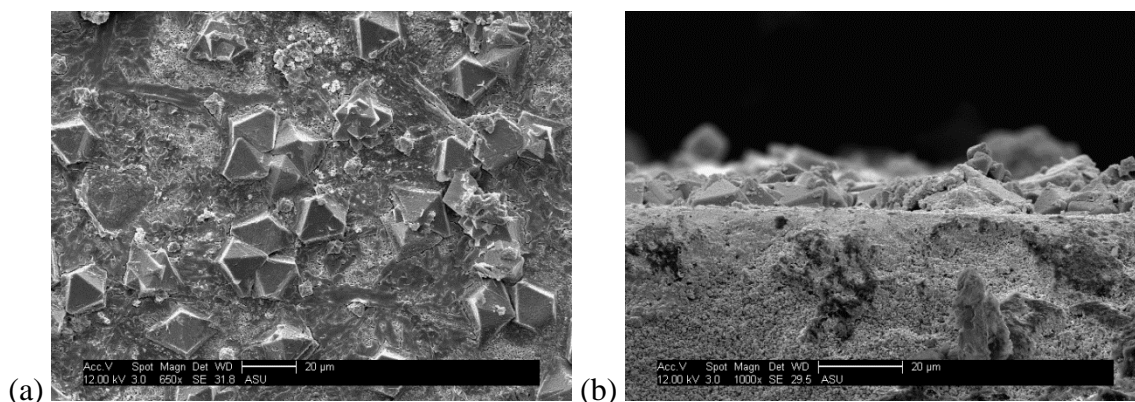
Figure 4.2

SEM micrographs of a ZnO layer covering α-alumina support following surface

modification at (a) *650X and* (b) *a cross-section of the modified support at 1000X.*

The SEM image in Figure 4.2 (a) show a ZnO layer covering between 80 and

90% of the support, and the SEM image in Figure 4.2 (b) indicates this layer was roughly

15µm thick. The XRD pattern in Figure 4.3 (a) further corroborates the presence and

thickness of the ZnO layer created via dip coating and sintering, while Figure 4.4 (b)

corroborates the presence and thickness of the ZnO layer created utilizing the *in situ*

synthesis method.
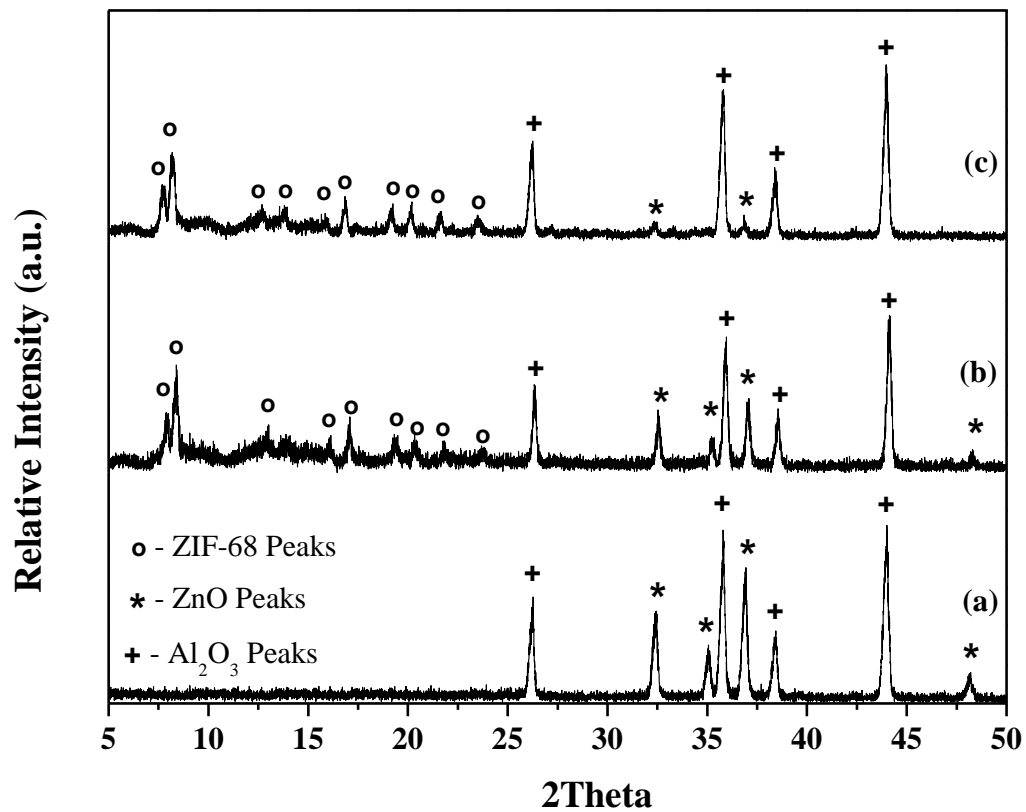
Figure 4.3

XRD patterns for (a) *an Al₂O₃ support dip coated in ZnO,* (b) *the dip coated support following reactive seeding and* (c) *the membrane layer following secondary growth in the presence of sodium formate.*
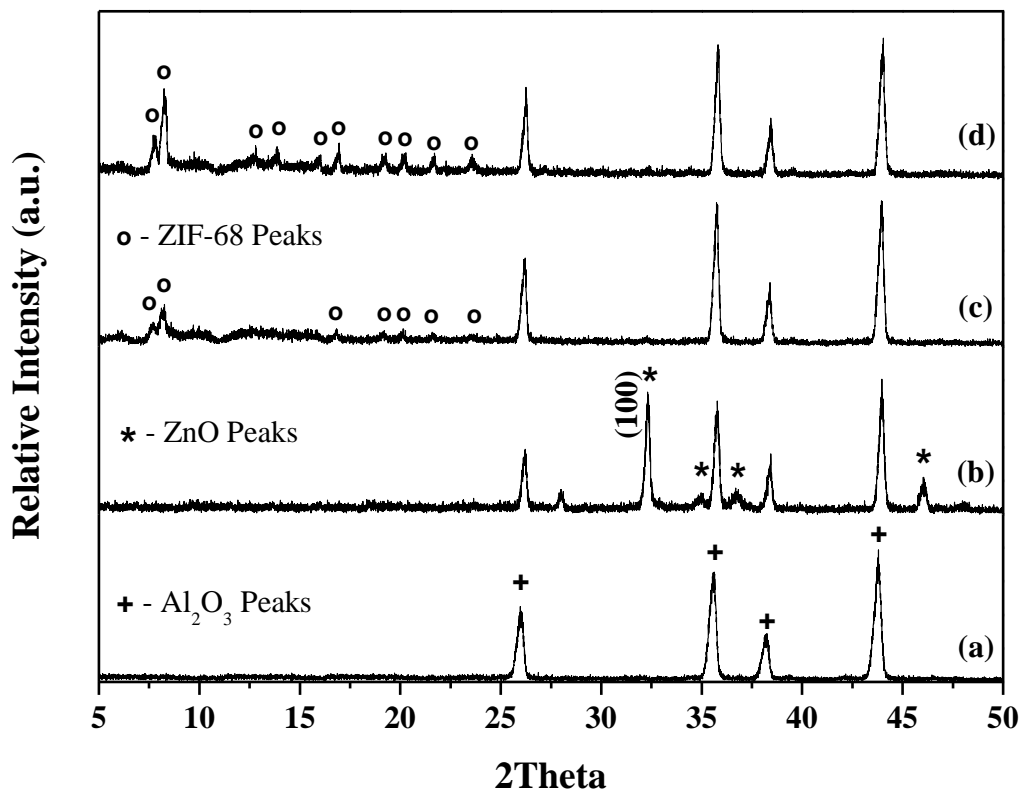
Figure 4.4

XRD patterns for (a) *a bare alumina support,* (b) *a support modified with* $ZnCl_2$ *and sodium formate,* (c) *a modified support following reactive seeding and* (d) *the membrane layer following secondary growth in the presence of sodium formate.*

The second method of support modification, referred to herein as an *in situ* modification, is based on a chemical reaction reported previously by Shah et al. in the synthesis of ZIF-8 (Shah et al., 2013). The method, which utilizes a solution of $ZnCl_2$ and sodium formate in methanol to create an attached layer of ZnO on the surface of the support, proved to be remarkably successful at creating reproducibly prominent,

intimately adhered layers of ZnO on Al_2O_3 supports. A representative XRD pattern can be seen in Figure 4.4 (b), with a spectrum of an unmodified Al_2O_3 support shown in Figure 4.4 (a) for comparative purposes. It is worth noting that the ZnO formulated on the surface of the support is overwhelmingly *a*-oriented, as evidenced by the intensity of the (100) peak, denoted on the XRD spectrum shown in Figure 4.4 (b), as compared to those for the other ZnO peaks. This is further proven to be a consequence of the *in situ* synthesis method when compared to the dip coated layer of ZnO, shown previously in Figure 4.3 (a), where the ZnO peaks indicate the layer is far more equiaxed.

4.3.2 Seeding and Membrane Synthesis

Once it was verified that both methods of ZnO adhesion produced relatively homogeneous layers of ZnO on the Al_2O_3 supports, reactive seeding was carried out. The reactive seeding step was successful in utilizing the ZnO on the Al_2O_3, regardless of the method used to obtain the ZnO coating, and this is shown by the presence of ZIF-68 peaks shown in Figure 4.3 (b), for the dip coated ZnO layer, and Figure 4.4 (c), for the *in situ* layer of ZnO. SEM images showed that the seeds layers that resulted from both were very different, however. The seeds that resulted from dip coating of ZnO onto the support, shown in Figure 4.5 (a) and (b), are far denser and dramatically shorter than those yielded on the *in situ* modified support shown in Figure 4.6 (a) and (b).

(a)

(b)

Figure 4.5

SEM micrographs of ZIF-68 seeds layer on Al$_2$O$_3$ support following dip coating of ZnO, reactive seeding and secondary growth at (a) *1000X and* (b) *at 6500X.*

(a)

(b)
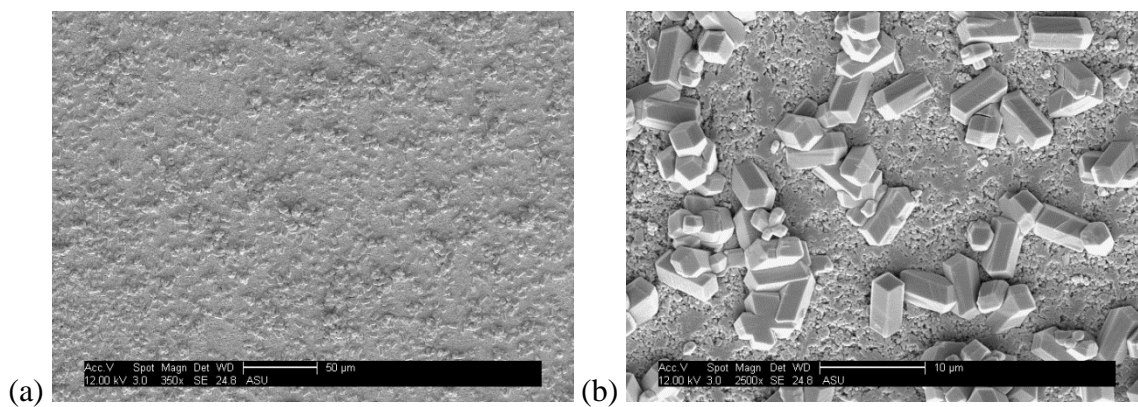
Figure 4.6

SEM micrographs of seeds on an α-alumina support following reactive seeding at (a) *1500X and* (b) *at 2500X.*

Both support modifications yielded highly *a-* and *b*-oriented seeds layers, as determined by the conspicuous absence of the prominent peak at around 9.56° that corresponds to the *c*-axis in the XRD spectra shown. The SEM micrographs of the seeds

layer on the support modified by dip coating indicate that seeds nucleated easily and homogeneously along the support surface. The dip coated ZnO likely created such a dense seeds coating due to the very high surface area of the small particles of ZnO that were used to create the layer. The high surface area that resulted from dip coating with <5 μm ZnO powders means there are many terminal zinc ions available to react to the imidazoles in solution and create seeds.

So effective was this dip coated layer at nucleating seeds during reactive seeding, that the resultant seeds were only between 3-5 μm in length along the *c*-axis and are characterized by a morphology that is not immediately recognizable as ZIF-68. ZIF-68 crystal are characterized by substantial length along the *c*-axis, with previous work by this group finding an average length of 90 μm (Yang Liu, Kasik, Linneen, Liu, & Lin, 2014). The short ZIF-68 seeds are only recognizable upon closer inspection when it becomes possible to make out some of the characteristic 120° angles associated with the *a*- and *b*- axis of the hexagonal ZIF-68 structure, as visible in Figure 4.5 (b). On the whole, however, the structure looks almost cubic due to how severely stunted the seeds are; with so many successfully nucleated seeds sites, there was no room for the ZIF-68 structure to develop prior to complete impingement from all sides by neighboring seeds. Due to the high density of nucleation sites along the ZnO coated layer, the surface of the support was almost completely filled with seeds. From Figure 4.3 (a) it appears that upwards of 99% of the support is coated in seeds, which is especially impressive when considering that the seeding of ZIF-68 on a ZnO support did not exceed 90% (Kasik et al., 2014). Further, the XRD pattern presented in Figure 4.3 (b) shows that not all of the ZnO was utilized, as some ZnO peaks are still present alongside the newly formed ZIF-

68 peaks and the Al_2O_3 peaks. The continued presence of ZnO peaks on the XRD spectra following reactive seeding initially seemed to give indication of a firmly adhered layer of ZnO, and thereby a firmly adhered seeds layer.

Reactive seeding of the supports modified via the *in situ* method resulted in a strikingly different morphology. Instead of a high density of unrecognizably ZIF-68 crystals, the support was covered in a sparse layer of larger, more-developed ZIF-68 crystals. One similarity is that, along with reactive seeding on the dip coated support, the crystals synthesized during seeding are almost entirely *a*- and *b*-oriented. This was determined, again, by a complete lack of the (002) peak in the XRD spectrum for the seeds layer shown in Figure 4.5 (c).

Despite the differences in seeds that resulted following reactive seeding on the supports modified by each method, secondary growth was similarly carried out for the each. It is here that the differences between the two methods are underscored, as a continuous ZIF-68 membrane was successfully synthesized on the support modified via an *in situ* method, but the procedure outlined herein did not yield a successful membrane layer on the support modified by the mechanical application of ZnO via dip coating.

While XRD patterns (shown in Figure 4.3 (c)) indicate strong characteristic ZIF-68 peak presence, testing the membrane's gas permeance showed that single gases flowed through the membrane as they would through a bare alumina support. Further examination in the SEM showed the membrane was riddled with deep cracks; see Figure 4.7 (a). Along with the cracks, the cross-sectional area showed many areas where the ZnO and membrane layers were delaminating from the support, as shown in Figure 4.7 (b). Two common mechanisms for crack formation in membrane synthesis are

differences in coefficients of thermal expansion between the supports and the MOF materials, exacerbated by quick heating or cooling of the membrane, and solvent removal following synthesis (Aceituno Melgar, Kwon, & Kim, 2014; Guerrero, Yoo, McCarthy, & Jeong, 2010b; Y. S. Lin et al., 2007). The membranes synthesized herein were controlled so no rapid cooling of the membranes occurred and in this synthesis method, PVA in adequate quantities has already been incorporated. Given two proven methods of circumventing crack formation have already been implemented, it is likely the reason for such widespread cracking is a weakness between the mechanical bond formed between the alumina support and the dip coated ZnO layer. From Figure 4.7 (b) a close up of the pulling away of ZnO layer and support is shown, and it likely that this effect, widespread beneath the ZnO and membrane layer, caused stresses that lead to the severe cracking across the membrane.
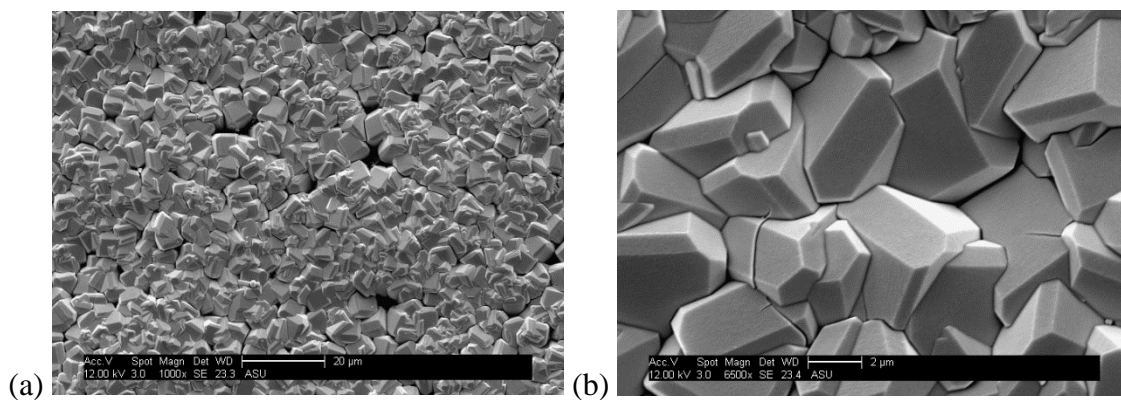

(a)   (b)
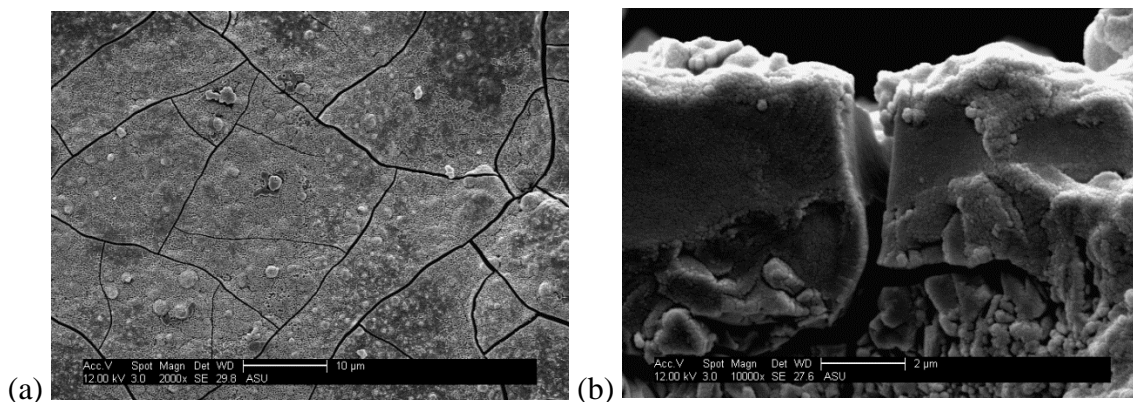
Figure 4.7

SEM micrographs of ZIF-68 membrane layer on Al$_2$O$_3$ support following dip coating of ZnO, reactive seeding and secondary growth at (a) *2000X and* (b) *a cross sectional view at 10000X.*

To further pinpoint to exact step at which cracking occurs, the synthesis was repeated a number of times and SEM images were obtained at different steps. From this it was found that there is absolutely no crack formation during the dip coating/drying/sintering step, but the reactive seeding step always shows the beginning of cracking (as is visible upon close inspection in Figure 4.5 (b)) and following secondary growth the cracking was uniformly widespread. Initial speculation was that the mechanical bond between the dip coated ZnO layer and the support was not strong enough to support a well-developed membrane layer. In order to test this, everything in the synthesis was carried out as outlined, however the dip coated support was placed in DMF without any additional precursors and then held at the reaction time and temperature. From these experiments it was found that even in a complete lack of ZIF-68 precursors, the ZnO layer still showed cracking following heating and holding in DMF. Due to this, it is likely that the cracking occurs due to the weakness of the bond between the dip coated ZnO layer and the Al_2O_3 support as it is dried and DMF is removed.

Thankfully this effect has not been seen with the support modified via an *in situ* application of ZnO. Secondary growth in the presence of sodium formate of the seeded support modified via an *in situ* application of ZnO successfully synthesized ZIF-68 membranes that are continuous and approximately 30 μm in thickness, as shown in Figure 4.8 (a) and (b). The membrane layer morphology is, however, strikingly different from membranes previously synthesized via the reactive seeding method on a ZnO support. Instead of being characterized by the visible *a-* and *b*-planes due to a *c*-axis being oriented predominantly orthogonal to the support, these membranes are characterized by an overgrown and stunted microstructure that is due to the *a-* and *b*-axis

129

lying perpendicular to the support. From unpublished work on the synthesis of ZIF-68 crystals for previous membrane synthesis attempts it became clear that the growth along the *c*-axis occurs more readily, which has been reported for other hexagonal MOF materials as well (Yunyang Liu et al., 2010). A favored growing direction would account for the smaller cross-sectional thickness yielded during this synthesis method, as well as the almost unrecognizable microstructure of the membrane layer.
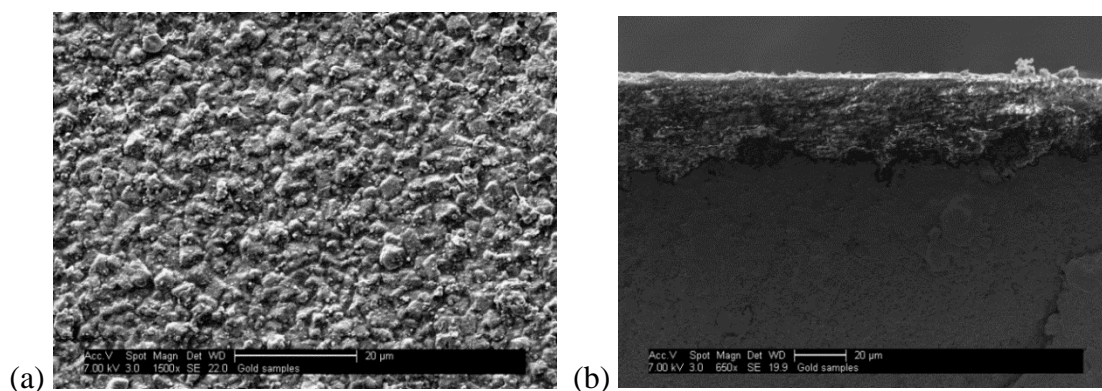
Figure 4.8

SEM micrographs showing ZIF-68 membrane layer formed following secondary growth at (a) *1500X and* (b) *a cross sectional picture at 660X.*

A substantial difference between the method of secondary growth used for these modified supports and that previously reported for reactive seeding on a ZnO support is the need for sodium formate in the secondary growth solution (Kasik et al., 2014). During secondary growth of the seeds layer on a pure ZnO support, any crystal growth that occurs can naturally anchor itself to the support as it grows through utilizing the available Zn^{2+} ions at the surface. However, when carrying out secondary growth of the

membrane layer on an alumina support, any area not already covered with seeds does not have that sort of anchoring site. In adding the sodium formate, not only is membrane growth supported, but there is the simultaneous addition of anchoring surface zincs that work to create a homogenous, well supported membrane (Shah et al., 2013). This bimodal mechanism by which sodium formate aids in membrane formation was elucidated by Jeong et al. when the progress of a formate modulated *in situ* synthesis of ZIF-8 was monitored by obtaining periodic XRD patterns during synthesis (Shah et al., 2013). It was found that sodium formate aids not only in the creation of the ZnO layer on the surface, but serves as deprotonator to propel membrane development forward as well (Shah et al., 2013).

The first manner in which sodium formate allows for the successful secondary growth of ZIF-68 seeds on Al_2O_3 supports is its ability to react with a zinc source in solution to create an intimately adhered layer of ZnO. In this modified reactive seeding synthesis approach, the amount of ZnO created during *in situ* surface modification gets exhausted during seeding. This is seen in Figure 4.4 (c) by the complete lack of any remaining ZnO peaks in the XRD spectrum. From Figure 4.6 (a) and (b) it is clear that although there is a strong showing of seeds, the seeds layer is not dense enough to allow for a complete membrane to be anchored by intimately adhered seeds created from the ZnO layer. This was remedied through the incorporation of sodium formate into the secondary growth solution. The sodium formate reacts with the zinc nitrate hexahydrate to create the same ZnO coating, which is simultaneously used to create anchoring points for either new crystals to develop or for existing crystals to expand and grow. Jeong et al. explain this phenomenon as temperature dependent (Shah et al., 2013). Upon placing

131

the autoclave in the oven, it is initially at a lower temperature and takes time to ramp up to the 120°C at which synthesis occurs. During this period of ramping temperature, the sodium formate serves as a competitive ligand for Zn^{2+} and this, coupled with the already basic nature of the solution due to the saturation of unused imidazole linkers, allows for ZnO formation (Shah et al., 2013). As temperatures rise, however, the role of sodium formate is changed to that of deprotonator.

As deprotonator, sodium formate works to decrease the solution hydrogen activity and decrease the amount of protons in the solution, which swings the driving force to deprotonate the organic linkers to maintain equilibrium (Mccarthy et al., 2010). The benefits of adding sodium formate as a deprotonating agent has already been proven for ZIF-8 (Mccarthy et al., 2010). While other MOF materials, such as MOF-5, have also shown the incorporation of other deprotonators, such as ethyldiisopropylamine, allows for complete deprotonation of the appropriate terminal portions of the ligand, as opposed to the random and partial deprotonation that can occur in a less basic solution (Mccarthy et al., 2010; Z. Zhao et al., 2011a). The refinement and control of deprotonation allows for crystal growth to proceed naturally in all directions. Jeong et al. illustrates this mechanism through carrying out secondary growth of ZIF-7 and ZIF-8 films both with and without sodium formate; the findings indicated that without sodium formate the film growth was sporadic and characterized by random crystal branching and overall discontinuity, but with sodium formate, healthy crystal growth occurred and well-intergrown, continuous membrane layers were attainable (Mccarthy et al., 2010).

4.3.3 Membrane Characterization

Utilizing the modified reactive seeding method allowed for the synthesis of ZIF-68 membranes on strong Al_2O_3 supports that exhibit gas permeance behavior that obeys Knudsen diffusion. With smaller pore ZIF membranes, such as ZIF-7 and ZIF-8, an adherence to Knudsen diffusion usually indicates there is a substantial contribution to permeation from amorphous regions and non-zeolitic pores while in larger pore membranes (e.g. $d_{pore} > d_{molecule}$), an adherence to Knudsen diffusion indicates there are limited non-selective defects (Y. Li, Liang, Bux, Yang, & Caro, 2010; Venna et al., 2013; Karger, 1992). This can be illustrated through Equation (4.1) (Y S Lin & Kanezashi, 2007; J. Xiao, 1992).

$$D = \frac{\alpha}{z}\left(\frac{8RT}{\pi MW}\right)^{1/2} e^{(-E_d/RT)} \qquad (4.1)$$

Where α and z are the diffusion lengths and coordination numbers respectively, RT is the gas constant by temperature, MW is molecular weight of the diffusing species and E_d is the activation energy for diffusion (Y S Lin & Kanezashi, 2007; J. Xiao, 1992). For larger pore membranes, when the diffusing species is substantially smaller than the size of the pores, as is the case with larger pore MOF materials, the exponential term goes to one, which renders Knudsen diffusion as the predominant mechanism.

The level at which a membrane material adheres to Knusden diffusion can be ascertained through a trend of inversely correlated permeance with $(MW)^{1/2}$. This is shown in Figure 4.9, where a summary of the gas permeation is data plotted as a function of the inverse root of the molecular weight of the permeating species. The overall conformance to Knudsen diffusion can be roughly quantified through fitting the data

linearly with a trendline set through the origin. It was found to be quite close, with an R^2

value of 0.997. An area of divergence is shown for CO_2, where the value found for ZIF-

68 is higher than would be predicted from Knudsen diffusion. MOF and ZIF materials in

general show preferential adsorption of CO_2 due to interactions between the polar

gaseous molecule and the metal and organic portion of the framework, which manifests

in higher CO_2 permeances, where ZIF-68 is no exception (Ravichandar Babarao, Dai, &

Jiang, 2011; Millward & Yaghi, 2005).
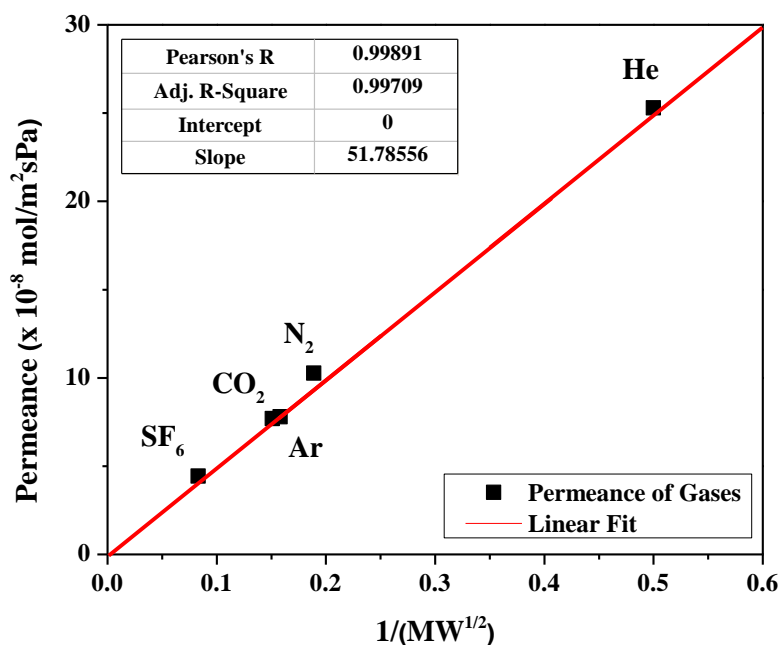
Figure 4.9.

Plot of single gas permeance of ZIF-68 as a function of the inverse molecular weight of

permeating species.

A comparison of N_2 permeance for similarly pore-sized materials is shown in

Table 4.1. Overall, the permeance for ZIF-68 on Al_2O_3 is quite low; the only value

smaller was that obtained for ZIF-68 membranes on ZnO supports.   The ZIF-68

membranes synthesized on ZnO were thicker than those synthesized on Al_2O_3, roughly 40 μm as compared to 30 μm, but the N_2 permeance was not correspondingly 25% higher. Instead, the thinner ZIF-68 membranes showed only a 14% percent increase in N_2 permeance; where ZIF-68 membrane on Al_2O_3 showed an N_2 permeance of 10.3 x 10^{-8} mol/m^{2}sPa and the thicker ZIF-68 membranes synthesized on ZnO showed an N_2 permeance of 9 x 10^{-8} mol/m^{2}sPa (Kasik et al., 2014). The permeability was obtained through the normalization of each permeance by each membrane's respective thickness, and is shown in Table 4.1. The membranes synthesized via the modified reactive seeding method show a decrease in N_2 permeability of 15% between the ZIF-68 membrane synthesized on ZnO and the membranes synthesized in this work.

One potential explanation for the non-proportional increase in permeance with decrease in thickness of the same material is that the orientation of the materials may be a factor. The membranes synthesized via reactive seeding on ZnO support were largely *c*-oriented, whereas the membranes synthesized herein are overwhelmingly *a*- and *b*-oriented. The main GME channels of ZIF-68 are located along the *c*-axis, so when the *c*-axis is orthogonal to the support, the gaseous species can travel along them with ease (J. C. Tan, Bennett, & Cheetham, 2010). These membranes, however, are strictly *a*- and *b*-oriented, which would mean the only channels available for gaseous species to travel along are the auxiliary HPR and KNO channels that characterize the *a*- and *b*- axis of the ZIF-68 structure (Yang Liu et al., 2014). So although the membrane is thinner, it does not directly correlate to an increase in permeance due to its orientation. The effect of structural orientation may extend to other MOF materials, even those not characterized by the structural disparity inherent to hexagonal materials. HKUST-1 crystals belong to

the space group Fm3m, and have a general face-centered cubic lattice, however two reports of N_2 permeation through ~25 μm thick HKUST-1 membranes on α-alumina supports were greatly varied, see Table 4.1 (Guerrero et al., 2010a; Nan et al., 2011). One report indicated the N_2 permeation was roughly 53 x 10^{-8} mol/m^{2}sPa, while another found N_2 permeation to be 20 x 10^{-8} mol/m^{2}sPa (Guerrero et al., 2010a; Nan et al., 2011). This may be a manifestation of varying crystal orientation within each membrane, as HKUST-1 is characterized by larger channels on the order of 9Å along the <100> direction and the <110> direction is characterized by smaller windows less than 4Å in size (Guerrero et al., 2010a).

Table 4.1

Summary of N$_2$ permeance and relevant material properties for similar pore sized MOF materials.

Material	Pore Size (Å)	Surface Area (m^2/g)	Membrane Thickness (μm)	Nitrogen Permeance (x 10^{-8} mol/m^{2}sPa)	Nitrogen Permeability (x10^2 Barrer)	Reference
ZIF-68	7.5	1090[1]	30	10.3	9.2	This Work (Kasik et al., 2014)
ZIF-68	7.5	1090[1]	40	9	10.8	
MOF-5	8	2304[2]	14	12	5.0	(Z. Zhao et al., 2011a)
MIL-53	7.3&7.7	1180[3]	8	13.9	3.3	(Hu et al., 2011)
HKUST-1	9	2200[4]	25	53	39.5	(Guerrero et al., 2010a)
HKUST-1	9	2200[4]	25	20	14.9	(Nan et al., 2011)

[1] (Phan et al., 2010) [2] (Z. Zhao et al., 2009) [3] (Y. Zhang et al., 2014) [4] (Wong-foy et al., 2010)

Table 4.2

Summary of ZIF-68 probing molecule properties fluxes and permeance.

Molecule	Flux (x 10^{-5} mol/m^{2}s)	Molecular Weight (g/mol)[1]	Viscosity (cP)[1]	Vapor Pressure (mm Hg at 25°C)[2]	Kinetic Diameter (nm)[1]	Permeance (x 10^{-5} mol/m^{2}sPa)
P-xylene (PX)	492.0	106.1	0.61	8.7	0.67	0.424
1,3,5-triisopropylbenzene (TIPB)	30.2	204.4	3.53	0.065	0.84	3.48
1,3-di-tert-butylbenzene (DTBB)	4.83	190.3	0.69[3]	0.074	1.1	0.493

[1]Molecular weight, viscosity and kinetic diameter information for *p*-xylene, TIPB and DTBB from reference (Z. Zhao et al., 2011a)
[2]Vapor pressure information for from *p*-xylene, TIPB and DTBB from references (Zhou, Wu, & Lemmon, 2012), ("1-3-5-Triisopropylbenzene | CasNO.717-74-8," 2015) and (Steele, Chirico, Knipmeyer, & Nguyen, 1997)

Following permeation, pervaporation with molecules of varying sizes was carried out to further elucidate membrane quality and structure. A summary of the results obtained and the molecule properties can be found in Table 4.2. Given the driving force for pervaporation is a vapor pressure gradient, the results for pervaporation flux for ZIF-68 were all normalized by the vapor pressure of the probing liquid to yield the pervaporation permeance data (vapor pressure values and pervaporation permeance provided in Table 4.2) (Wee, Tye, & Bhatia, 2008). The pervaporation permeance data however provided a confusing overview of membrane quality.

Both TIPB and DTBB pervaporation permeances were found to be higher than that of *p*-xylene, with TIPB pervaporation permeance being over 8 times as high as that found for *p*-xylene. This result is especially confounding given the TIPB molecules are larger than both the *p*-xylene molecules and the pore openings of ZIF-68. For that matter, Van der Perre et al. found through adsorption experiments that only 60% of the ZIF-68 pore volume is available to TIPB, and hypothesized that only the largest of channels can accommodate the bulky molecule through a rotation of the 2-nitroimidazole linkers around the zinc SBUs (Van der Perre et al., 2014). Due to anomalously skewed pervaporation permeance behavior wherein a molecule that is 64% larger than *p*-xylene, DTBB, can have a pervaporation permeance that is 16% larger, the applicability of using pervaporation permeance in pervaporation experiments was scrutinized. In examining this, new considerations were incorporated to take into account the contributions of not only viscous flow through non-ideal pores and defects, but also the effect that the ratio of

the size of permeating molecules compared to the size of pores/defects has on the flow through the membrane. This is shown in Equation (4.2) and Figure 4.10.

$$J_i = F_i\left(P_f^{sat} - P_p\right) + F(\lambda)\left(P_f^{hyd} - P_p\right) + \frac{\phi_d}{\mu_i}\left(P_f^{hyd} - P_p\right) \qquad (4.2)$$

In Equation (4.2) the flux of component i, J_i, is equal to the sum of the contribution from both true pervaporation and the effects of nanopores, such as defects or amorphous regions. Where P_f^{sat} is the feed saturated vapor pressure, P_f^{hyd} is the hydraulic pressure on the feed side and P_p is the permeate or downstream pressure. $F(\lambda)$ is a function of λ, where $\lambda = d_m/d_p$, and ϕ_d takes into account pore structure and is a function of $(r_p^2\varepsilon/\tau)$, where r_p is the pore radius, ε is the porosity and τ is the tortuosity. The viscosity of component i is represented by μ_i.

Figure 4.10 illustrates each of the components of pervaporation flux, as presented in Equation (4.2). Situation 1 is an ideal situation wherein pervaporation permeability occurs through ideal pores. In this situation the permeability is dependent on the solubility and diffusivity of the pervaporating molecule in the specific porous media and the driving force is entirely based on the vapor pressure of the pervaporating molecule. Situation 2 is incorporated because while the movement of molecules through the pores via pervaporation should be independent of molecular size, that is not always the case. When molecules become close to, or surpass, the size of the pore aperture, in most materials, there should be a subsequent diminishment of flux. In a system wherein the $d_m/d_p < 1$ flux may be largely attributed to the inevitable inclusion of small scale defects or amorphous regions. In Equation (4.2) this is taken into account additively to include the ratio of d_m/d_p for the system, as well as any structural pore parameters, and

pervaporation through defects is driven by hydraulic pressure. Finally a third component is incorporated additively to the equation. Illustrated as situation 3 in Figure 4.10, this component incorporates the contribution of viscous flow through larger defects or amorphous regions and, as with situation 2, the driving force behind pervaporation permeability is the hydraulic pressure. This was substantiated when the effect of viscosity on pervaporation permeability was investigated by Tsuru et al. (Tsuru, Kondo, Yoshioka, & Asaeda, 2004).

Through testing pervaporation at different temperatures and comparing both the permeability and the permeability multiplied by the viscosity across the temperature range tested, it was determined that the permeability multiplied by the viscosity, which should not be affected by a temperature change, remained constant only for those membranes with pores larger than one nanometer (Tsuru et al., 2004). This research indicates that the contribution from nanopores and various defects or amorphous regions larger than 1 nm are of substantial contribution and should not be negated.
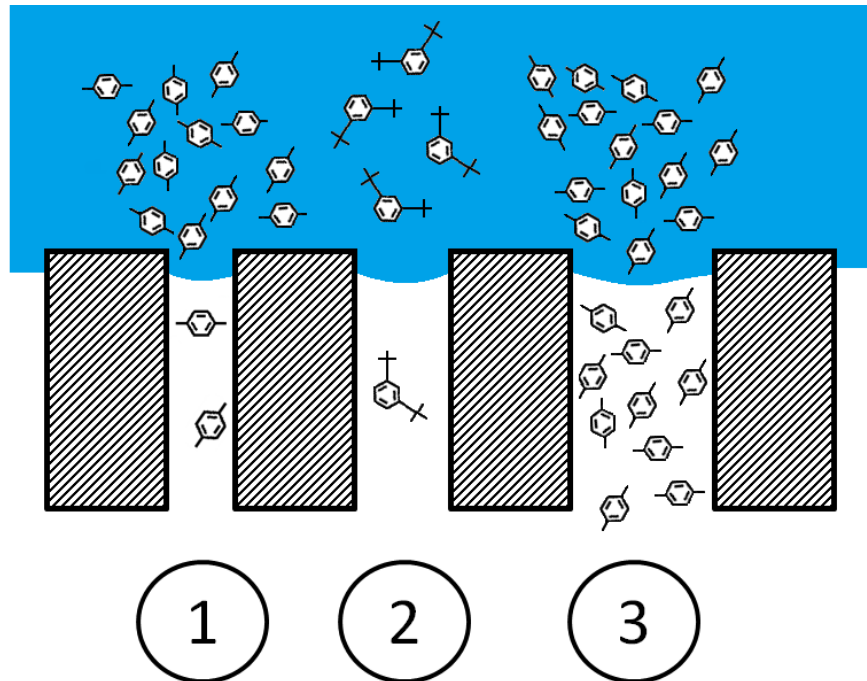
Figure 4.10

Schematic illustration of the hypothesized contributions to pervaporation flux. 1) Shows an ideal pore where pervaporation permeability is ideal and driven by the vapor pressure of the pervaporating molecule. 2) Illustrates the effect that the size of the prevaporating molecule has in relation to the pore or defect size. 3) Illustrates the non-ideal contribution to permeability from viscous flow through defects and nanopores that is driven by hydraulic pressure.

While an adherence to Knudsen diffusion can help ascertained, to an extent, the quality of a membrane, it is important to note that an adherence to Knudsen diffusion would still be exhibited even if there were defects or amorphous regions up to a few nanometers (Karger, 1992). It is in this regard that Equation (4.2) is applicable for obtaining the permeability of pervaporating molecules. It contains both the component related to ideal membrane systems where the driving force is solely based on vapor

pressure contributes, and also the added contributions from potential transport through defects and from viscous flow through non-ideal portions of the membrane. Given the complexity of quantifying the extent to which a membrane deviates from an ideal perfect membrane, pervaporation flux is used and serves as a more telling factor to membrane quality and pervaporation behavior.

When comparing pervaporation flux to that obtained previously for ZIF-68, it became clear that the flux of molecules through the ZIF-68 membranes reported herein seemed to be effected by orientation in the same manner as was evidenced for permeation. An overview of pervaporation flux data as compared to previous data by this group for ZIF-68 and MOF-5 is presented in Table 4.3. From that data, it was found that the pervaporation flux of *p*-xylene through the ZIF-68 membrane synthesized on Al_2O_3 was only 12% higher than that of the ZIF-68 membrane synthesized on ZnO, despite a 25% reduction in thickness. This indicates, as with gas permeation results, that liquid flow through the membrane may be subject to crystal orientation. The flux of *p*-xylene found by this group for both ZIF-68 membranes was substantially higher than that found for MOF-5, despite both MOF-5 iterations reported on had much smaller cross-sectional areas than the ZIF-68 membranes; ~15 μm as compared to 30 to 40 μm (Kasik et al., 2014; Kasik & Lin, 2013; Z. Zhao et al., 2011b).

Table 4.3

Comparative pervaporation data.

| Material | Flux (x 10^{-5} mol/m^{2}s) | | | Reference |
	P-xylene (PX)	1,3,5 tri-isopropylbezene (TIPB)	Di-tert-butylbenzene (DTBB)	
MOF-5	90.0	20.8	17.1	(Z. Zhao et al., 2011a)
MOF-5	117	24.0	2.58	(Kasik & Lin, 2013)
ZIF-68	440	-	-	(Kasik et al., 2014)
ZIF-68	492	30.2	4.83	This work

Initially this would appear to indicate that the ZIF-68 membranes reported on previously and herein have substantial defects that would allow for such an increased flow of *p*-xylene over MOF-5, however as larger liquid molecules were tested, there was a sharp cut off in flux. From Table 4.3, the 1,3,5-triisopropylbenzene (TIPB) flux for both MOF-5 and ZIF-68 are listed.   While the decrease in flux for both MOF-5 samples between the 0.67 nm *p*-xylene molecules and the 0.84 nm TIPB molecules was between a 4 and 5 times decrease, ZIF-68 showed a 16 times decrease in flux from *p*-xylene to TIPB. Further, when the flux of the largest molecule was tested, 1,3-di-tert-butylbenzene (DTBB) with a kinetic diameter of 1.1 nm, the ZIF-68 membrane showed one of the lower values for flux. The flux of DTBB through ZIF-68 was 3.5 times smaller than a flux previously reported for MOF-5; 17.1 x 10^{-5} mol/m^{2}s for previous MOF-5 membranes, as compared to 4.83 x 10^{-5} mol/m^{2}s for the ZIF-68 in this work. This would

indicate that the density of non-ideal pores in these ZIF-68 membranes is lower than in previous, similar pore-sized materials.

4.4 Conclusion

Through utilizing an *in situ* surface modification process that deposited a ZnO layer on an Al_2O_3 support, it was possible to reproducibly synthesize continuous ZIF-68 membranes via a modified reactive seeding on an Al_2O_3 support. The new synthesis method would likely serve as a general template for the synthesis of other zinc based MOF materials. The ZIF-68 membranes synthesized via the modified reactive seeding method were *a-* and *b*-oriented, which is in contrast to previously synthesized ZIF-68 membranes on ZnO that were *c*-oriented. The orientation appeared to have an effect on gas and liquid permeability. The membranes in this work were 25% thinner than previously synthesized ZIF-68 membranes on ZnO supports, however gas permeation data showed the permeance of the *a-* and *b*-oriented ZIF-68 membranes synthesized on Al_2O_3 were higher than those obtained for *c*-oriented ZIF-68 membranes synthesized on ZnO, but not proportional to the decrease in thickness they exhibit. Pervaporation data further duplicated this effect; *p*-xylene pervaporation flux was lower, but also did not decrease proportionately with the decrease in membrane thickness. Large fluxes for *p*-xylene were found, but the larger molecules tested exhibited impressive decreases flux, indicating the membrane quality is on par with other continuous, similar pore-sized membranes synthesized via different methods.

CHAPTER 5

BINARY GAS SEPARATION OF MOF-5 AND ZIF-68

5.1 Introduction

As was discussed in Chapter 1, there are a myriad of potential pervaporation and permeation separation processes for which metal-organic frameworks are suited. Current, pressing concerns, over global climate change have caused two in particular to stand out; the separation of CO_2 from N_2 in flue gas scenarios and the separation of CO_2 from CH_4 in the sweetening of CH_4. These two operations are extremely relevant at this juncture as it is not feasible to completely eliminate the use of nonrenewable sources for energy generation. In the interim, the amount of deleterious CO_2 that is expelled from a coal burning plant can be dramatically reduced, and the vast quantities of cleaner burning CH_4 available can be utilized with greater efficiency.

Metal-organic frameworks are especially well-suited for these applications due, in no small part, to their tendency to preferentially adsorb CO_2. This effect is especially pronounced when CO_2 is in mixtures containing stable, nonpolar molecules like N_2 and CH_4. Reports of MOF membranes used to separate CO_2/N_2 and CO_2/CH_4 are promising and indicate there is likely a future in this technology.

A remarkable initial study on MOF separation of CO_2/N_2 was reported by Zhao et al. The report outlined a thin MOF-5 membrane that showed preferential separation of CO_2 that increased from roughly that predicted by Knudsen diffusion up to 70 as CO_2 loading increased to 88% (Z. Zhao et al., 2013). When a realistic amount of H_2O is added to the testing conditions, as was done by Aguado et al. the separation is more realistically modeled (Aguado, Nicolas, et al., 2011a). In these more realistic operating

145

conditions where CO_2 is 10%, N_2 is 87% and H_2O is 3% the CO_2 selectivity is 4.5. Through incorporating hydrophobic dodecylamine into the synthesis procedure, the separation increased to 5.5 (Aguado, Nicolas, et al., 2011b). From this it is clear that hydrophobicity and stability of MOF membranes is important in maximizing the benefit of these materials.

Currently, there are limited results published for zeolitic imidazolate frameworks (ZIFs) or zeolite-like metal-organic frameworks (ZMOFs). These materials are of note due to their stability and the general hydrophobicity inherent to them, which allows them to exhibit much larger amenability to H_2O exposure than traditional MOFs. This hydrophobicity is an important consideration given the near impossibility removing the trace amounts of H_2O from the flue gas stream poses (Aguado, Nicolas, et al., 2011b). To date the work reported for CO_2/N_2 separations with MOF membranes with zeolitic topologies is limited. ZIF-90 has been studied, and this was largely due to its smaller pore size. ZIF-90 has a pore size of 0.35 nm, which, in theory, should exhibit substantial CO_2 selectivity over N_2 due to molecular sieving given CO_2 is 0.33 nm and N_2 is 0.36 nm, however, this was not the case (A. Huang, Dou, et al., 2010). The separation of CO_2 over N_2 was found to be only 1.7, which is likely an indication of the material's framework flexibility. A different zeolite-like MOF material, sod-ZMOF-1, which is characterized by a sodalite topology and a pore size of 0.41 nm, showed good selectivity both ideally, and in the binary mixture. Where ideal selectivity indicated a selectivity of 8.7 for CO_2, binary mixtures with $10CO_2/90N_2$ at 3.4 bar showed a selectivity of upwards of 10.4 (Al-Maythalony et al., 2015). Another smaller pore ZIF material, ZIF-69, with a pore size of 0.44 nm, has been tested for the separation of CO_2/CH_4 (Yunyang Liu et al.,

2011a). The results showed promise, as the selectivity for CO_2 in a CO_2/CH_4 binary system increased from 2.25 to 4.5 as the pressure increased to 3 atm. Additional reports found a CO_2/CH_4 selectivity of 4-7 for ZIF-8 tubular membranes, although the pressures reported were quite low at less than 1.5 atm (Venna & Carreon, 2010)

MOF and ZIF materials have shown that there is potential for high selectivity in both the CO_2/N_2 and CO_2/CH_4 systems. The results also indicated that the CO_2 selectivity was enhanced by increasing the transmembrane pressure drop; however, the increase in transmembrane pressure drop tested did not exceed 4 atm. Further, attempts to capitalize on the size disparity between CO_2 and N_2 and CH_4 have not proven immensely successful, largely impart to the relatively common phenomenon of framework flexibility. To make a commercially viable membrane for separation, CO_2 selectivity, as well as permeability, must be high. To maximize these, large-pore MOF materials, MOF-5 and ZIF-68, are going to be studied in tandem to isolate the effects of adsorption based separation. Further, in this work, using the synthesis method established in Chapter 4 for higher-pressure stable ZIF-68 membranes, the aim is to explore more thoroughly the effect that increasing pressure up to 9 atm has on separation.

5.2 Experimental

5.2.1 MOF-5 Membrane Synthesis

The procedure for MOF-5 membrane synthesis has been outlined extensively in other publications, so a brief overview will be presented herein (Kasik & Lin, 2013; Z. Zhao et al., 2013, 2011a). Utilizing all precursors as-received, the MOF-5 crystals were synthesized as follows. Zinc nitrate hexahydrate (1.664 g, $Zn(NO_3)_2 \cdot 6H_2O$, 99.0%,

Fluka) and terephthalic acid (0.352 g, BDC, >99.0%, Fluka) were added to a vial containing 40 mL of dimethylformamide (DMF, 99.8%, Alfa Aesar). The vial was then magnetically stirred until all constituents were dissolved and the solution was clear. The vial was next added to an oil bath held at 130°F and allowed to react for 3 hours. Following the reaction the vial was removed and left to return to room temperature naturally. The vial, now filled with an orange-hued mother liquid, now contains visible MOF-5 crystals. Once cooled, the mother liquid was carefully decanted, and the crystals were washed three times in DMF to remove any unreacted precursors. The vial containing the washed precursors was then filled with 50 mL of chloroform and placed in an oven held at 70°C to allow for solvent exchange. Every 24 hours for three days the chloroform was removed and replaced with fresh chloroform. Following the third day the chloroform/MOF-5 solution was poured into a Teflon-lined ball mill and filled with alumina balls at a weight ratio of roughly 25:1 with the MOF-5 crystals. The solution was then ball milled for 24 hours at 175 RPMs. Following ball milling the balls were removed and the crystals and chloroform were poured into a glass vial and dried under vacuum at room temperature overnight.

Once dry, the crystals were used to make a 2% MOF-5 in DMF solution for dip coating. Following four hours of ultrasonic agitation, the solution remains relatively stable. To create the membranes, homemade, polished α-alumina supports were then dip coated into the solution. The details of α-alumina support synthesis and polishing are outlined elsewhere, as well (Kasik & Lin, 2013; Z. Zhao et al., 2011a). The supports were inserted, polished side down into the solution for three seconds, then promptly removed and held sideways to allow for run off of excess solution. The supports were

then dried overnight in an oven held at 50°C. This was repeated three times. The seeded supports then underwent secondary growth to create a continuous membrane.

As with seeds synthesis, zinc nitrate hexahydrate and BDC, 0.614 g and 0.088 g, respectively, were added to 40 mL of DMF. The solution was stirred until clear, and the seeded support was placed in the solution, held vertically by a Teflon support. The vial was then capped and placed in an oil bath held at 130°C for 3 hours. After three hours the vial was removed and left to return to room temperature naturally. Once cooled, the membrane was removed and washed in DMF three times. Following washing the membrane was placed in a vial of chloroform for two days to allow for solvent exchange. After two days in chloroform, the membrane was removed and dried under vacuum at room temperature.

5.2.1 ZIF-68 Membrane Synthesis

The ZIF-68 membranes used herein were synthesized via the modified reactive seeding method, as outlined in Chapter 4. First, a thoroughly mixed solution of sodium formate (1.43 g, HCOONa, Sigma Aldrich) and zinc chloride (0.55 g, $ZnCl_2$, Sigma Aldrich) in 30 mL of methanol (MeOH, 99.8%, BDH) was placed in a Teflon-lined autoclave wherein a homemade α-alumina support was suspended polished side down by a Teflon holder. The autoclave was then sealed and placed in an oven held at 120°C for 8 hours. Following holding, the autoclave was allowed to return to room temperature naturally.

Following the ZnO coating step, the ZnO coated support was then used to create a seeds layer. First a solution of 2-nitroimidazole (0.028 g, ≥98.0%, Bosche) and

benzimidazole (0.030 g, 98%, Sigma Aldrich) was mixed in 30 mL of DMF. Once the imidazole precursors were thoroughly mixed in the DMF, it was added to a Teflon-lined autoclave where the ZnO coated support was suspended with the ZnO layer facing down by a Teflon holder. The autoclave was then sealed, and placed in an oven at 120°C for 3 hours. Following holding, the autoclave was allowed to cool in the furnace to room temperature. The seeded support was then rinsed thoroughly in DMF and left to dry under vacuum at room temperature.

Following seeding, a secondary growth synthesis was created. In a vial with 20 mL of DMF 0.113 g and 0.118 g of 2-nitroimidazole and benzimidazole, respectively, were added and thoroughly mixed. The solution was then added to a Teflon-lined autoclave where the seeded support was suspended horizontally with the seeded side facing down. The autoclave was then sealed and placed in an oven at 120°C and left to react for 8 hours. Following synthesis the autoclave was allowed to cool to room temperature and the membrane was removed, washed thoroughly in DMF and dried under vacuum overnight.

5.2.2 Binary Gas Separation

Given the overt aversion of MOF-5 to even small amounts of naturally present humidity in the air, immediately following XRD measurements the membrane was placed in the membrane cell. Once in the membrane cell, the membrane was sealed on both sides with Viton O-rings, and placed in a furnace with stainless steel tubing connecting the membrane cell to the setup, as shown in Figure 5.1. Prior to testing any gas separation behavior, the as-synthesized membranes first required activation. To activate

the membranes helium was flowed into the feed side of the membrane cell at a rate of 50 mL/min while the membrane was heated to 100°C at a ramp rate of 2°C/min. Once heated to 100°C the membrane was held at that temperature for 5 hours. Following holding, the membrane was allowed to cool to room temperature prior to beginning testing.

Once cooled, binary gas separation was then carried out. The testing gases were turned on simultaneously to jointly reach a flow rate of 150°C/min, and no sweep gas was used. Once gases were flowing, the needle valves were adjusted accordingly to reach the desired test pressure. After the pressure stabilizes and steady state has been achieved, the flow rate on the feed and permeate side were tested using bubble flow meters. Then, utilizing an Agilent 6890N Gas Chromotagraph (GC), with a HayeSep DB porous polymer 100/120 mesh and a TCD injector with Ar carrier gas at 11.5 mL/min, samples were collected from the permeate and retentate side. From this data the permeance and selectivity can be calculated as follows (Z. Zhao et al., 2013).

$$F_i = \frac{Q_P Y_i}{S(P_f X_i - P_p Y_i)} \tag{5.1}$$

$$S_{ij} = \frac{Y_i / Y_j}{X_i / X_j} \tag{5.2}$$

Where F_i is the permeance of component i, Q_p is the flow rate on the permeate side, Y_i is the molar fraction of component i in the permeate side, X_i is the molar fraction of component i in the retentate side, S is membrane surface area, S_{ij} is the selectivity of

component i over component j and P_f and P_p are the pressures on the feed and permeate side, repectively.

In between trials, the membrane was not unsealed or removed from the membrane cell. Following tests, the permeate gases were turned off, and helium was flowed through the membrane cell at a flow rate of 20 mL/min. When testing was to resume, the helium was switched off while the permeating gases were switched on, and pressure and flow rates were adjusted accordingly per the requirements of the test. In this regard, it was possible to keep the membrane on-stream for weeks at a time without experiencing membrane degradation from outside conditions. This also served to give insight into the stability of these membranes under continuous on-stream operating conditions.

5.3 Results and Discussion

5.3.1 MOF-5 Binary Gas Separation

Following synthesis per the established, outlined methods, the membranes were ready to be tested. For MOF-5 it is worth noting that extreme care went into its synthesis, storage, transportation and use. Kaye et al. showed quite starkly how immediate and irreversibly devastating atmospheric levels of water can be to MOF-5 crystallinity when they verified by XRD that after just ten minutes, there began to be permanent and quantifiable losses of crystallinity (Kaye et al., 2010) . The mechanism of which has been postulated by Saha and Deng to be the result of interactions between the polar H_2O molecules and the benzene rings of the organic ligands. Once within the structure, the water molecules then begin to form hydrogen bonds with the Zn_4N tetrahedra and the porous structure slowly begins to collapse (Saha & Deng, 2010). They went on to extrapolate this effect to virtually any polar molecule entering the structure of

152

MOF-5, or any other carboxylate-based MOF. In the current studies, the permeating molecules used are virtually all satiated, and those that are not (CO_2) do not have the hydrogen with which secondary bonding to the zinc-nitrogen tetrahedra can be facilitated. However, given these experiments were carried out in real environments, it was necessary to be meticulous about the potential exposure the MOF-5 membrane faced prior to being placed in the cell and immersed in continual flow of gases.
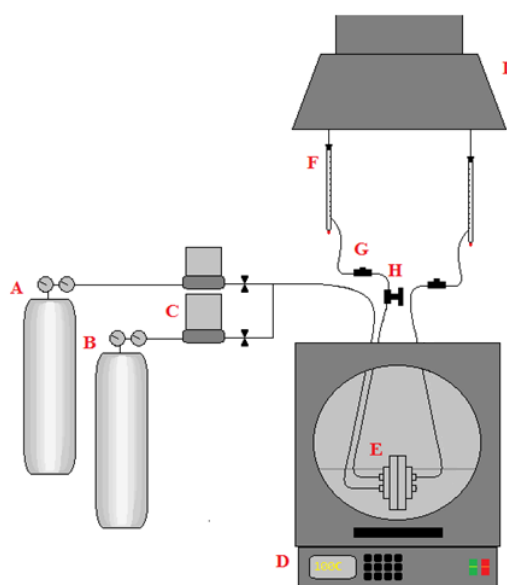
Figure 5.1

Schematic representation of binary gas separation setup. Legend: (a) *gas cylinder,* (b) *gas cylinder,* (c) *mass controller,* (d) *furnace,* (e) *membrane cell,* (f) *bubble flow meter,* (g) *sample taking port,* (h) *pressure control valve and* (i) *fume hood*

Once the MOF-5 membrane was ready for testing, it was immediately placed in the membrane cell and activated as outlined. The initial intent was to replicate earlier work carried out by Zhao *et al*. on lower pressure MOF-5 CO_2/N_2 separation with both MOF-5 and ZIF-68 membranes to determine linearity between materials. To do this, conditions were mimicked closely; no sweep gas was used, the same activation and operating temperatures were used and the pressures chosen were those used by Zhao et al. (Z. Zhao et al., 2013). The results showed similar trends, although the extent of the selectivity was not nearly as staggering in this work than it was in previous reports. For example, in Figure 5.2 the CO_2 selectivity in the CO_2/N_2 system at 4.4 atm, room temperature and at varying partial pressures of CO_2 showed a direct increase in CO_2 selectivity with an increase in CO_2 partial pressure.
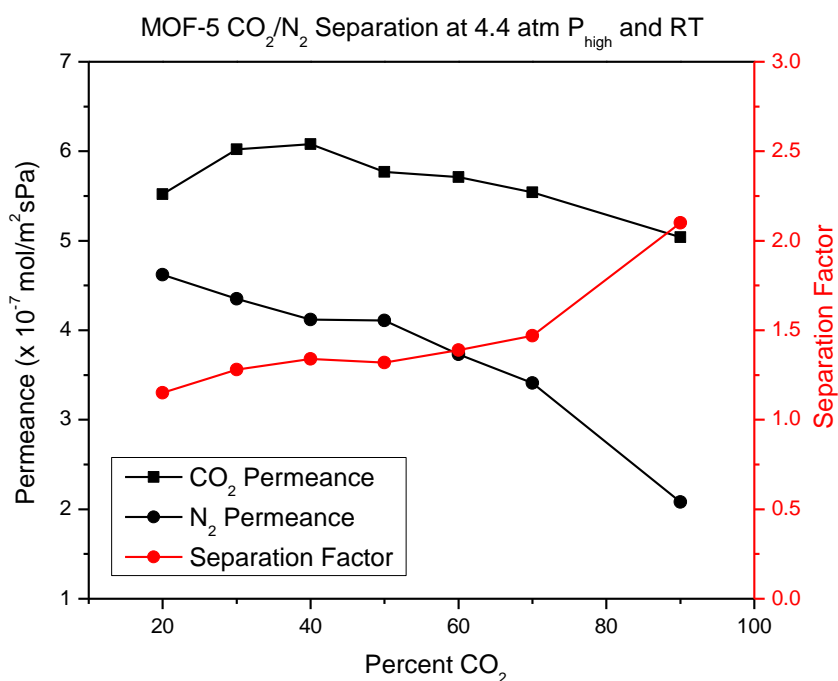
Figure 5.2

Plot of N_2 and CO_2 permeance and separation factor for MOF-5 using a binary gas feed of CO_2:N_2 at RT and 4.4 atm P_{high}.

Keskin and Sholl researched the CO_2/N_2 and CO_2/CH_4 selectivity of MOF-5 through Grand Canonical Monte Carlo (GCMC) simulations of adsorption isotherms and equilibrium molecular dynamics (MD) simulations of single component diffusion properties (Keskin & Sholl, 2009). Their results showed similar trends to those found by Zhao et al. previously and those reported herein, however, the values predicted were much more representative of those found in this work. For an equimolar stream of CO_2/N_2 at approximately 10 atm, the selectivity of CO_2 was close to 5, and in this work, as shown in Figure 5.3, the selectivity of CO_2 in an equimolar feed at 9 atm was 6 (Keskin & Sholl, 2009). Further similarities were seen with equimolar streams of

155

CO_2/CH_4 at approximately 10 atm, where Keskin and Sholl predicted a CO_2 selectivity of 2.5, this is in very good agreement with the data presented herein, where equimolar ratios of CO_2/CH_4 at 9 atm showed a separation factor of approximately 2.5 (Keskin & Sholl, 2009). These similarities indicate that these membranes can exhibit reasonable agreement with modeled data.
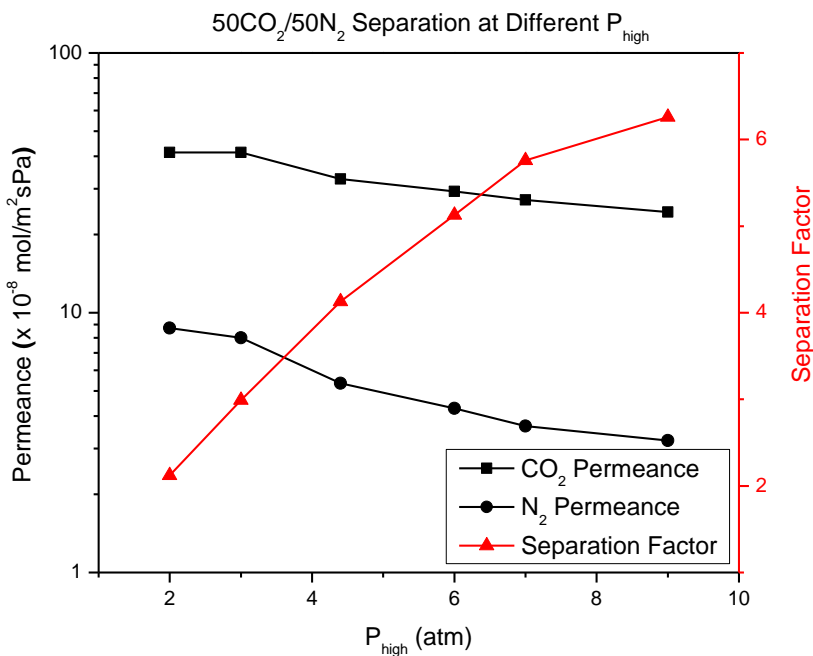
Figure 5.3

Permeance and separation factor for CO_2 and N_2 in a MOF-5 membrane with a 50CO_2:50N_2 feed at different P_{high}.

With MOF-5, the preference for CO_2 in a binary mixture of CO_2/N_2 increases with increasing CO_2 loading, as can be seen in Figure 5.5, where a CO_2 selectivity of almost 10 was shown for 80% CO_2 at a pressure of 9 atm. This increased propensity for CO_2 with increased CO_2 loading has been shown in previous work by Zhao et al. as well,

experimentally, and Zhao et al. empirically (L. Zhao et al., 2008; Z. Zhao et al., 2013). Experimentally, it was shown that as pressure increased impressive increases in CO_2 selectivity were seen; at compositions of ~10% CO_2 the selectivity was roughly 1, however, upon increasing the loading of CO_2, the selectivity increased dramatically to nearly 70. This was also shown as a trend in the review paper by Zhao et al. where the correlation with CO_2 loading and selectivity was shown to be quite frustrating, as the typical amount of CO_2 needing separation from flue gas streams is roughly 14% (L. Zhao et al., 2008; Z. Zhao et al., 2013).
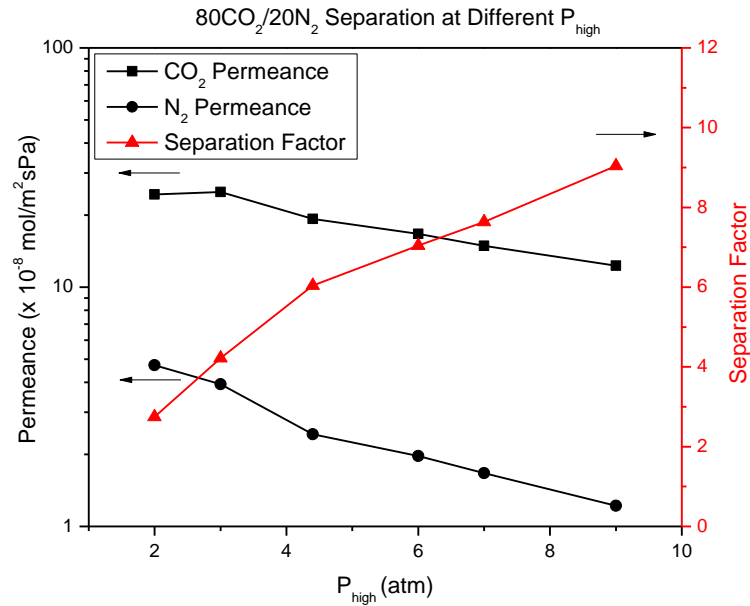
Figure 5.4

Plot of N_2 and CO_2 permeance and separation factor for MOF-5 using a binary gas feed of $80CO_2$:$20N_2$ at RT and 4.4 atm P_{high}.

In Figure 5.5 the highest CO_2 selectivity was reached, at just over 9. This selectivity was attainable by virtue of both the high CO_2 partial pressure (80% of the

157

feed) and the high overall pressure on the feed side. The correlation between CO_2 affinity and these system characteristics is likely due to some sort of framework flexibility. These materials are known, as has been alluded to in previous chapters, for their ability to accommodate and rearrange themselves when separating or adsorbing certain gases. It follows that as the overall pressure continues to increase there are arrangements in the organic BDC ligand that opens up the structure and accommodates the selective adsorption of CO_2 through revealing previously obscured adsorption sites.

Next, it was necessary to verify that this effect also extended to CO_2 in a CO_2/CH_4 binary mixture. The results, while not as pronounced, did indicate the same general patterns existed for both CO_2/N_2 and CO_2/CH_4 in a binary system through MOF-5. Results indicated that, as with CO_2/N_2, there was a direct correlation between CO_2 selectivity with increasing CO_2 partial pressure and with increasing overall pressure as well. Figure 5.6 shows the effect of increasing the percent CO_2 in the feed stream the pressure remains the same.

MOF-5 CO$_2$/CH$_4$ Separation at 4.4 atm
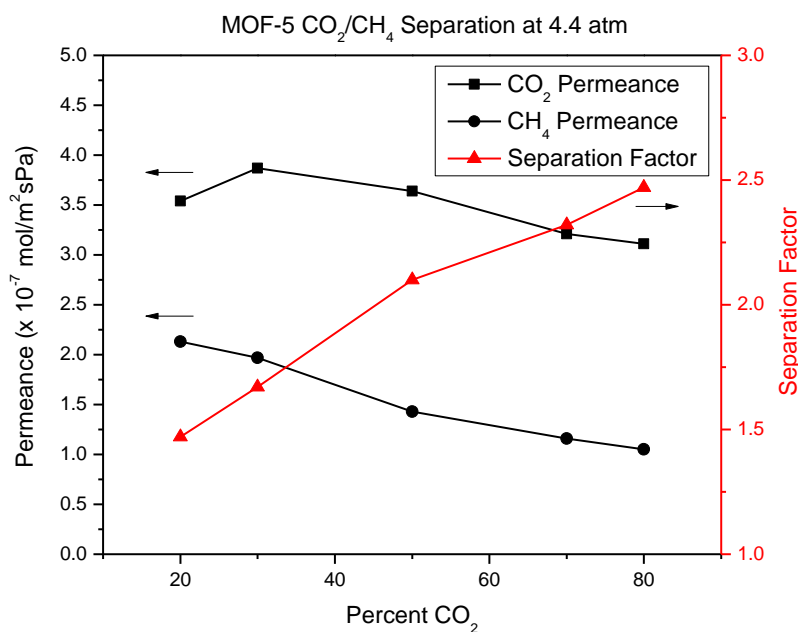
Figure 5.5

Plot of CO$_2$ and CH$_4$ permeance and separation factor for MOF-5 using a binary gas feed of CO$_2$:N$_2$ at RT and 4.4 atm P$_{high}$.

Both Figure 5.3 and Figure 5.5 show MOF-5 with CO$_2$/N$_2$ and CO$_2$/CH$_4$, respectively, at varying percent CO$_2$ in the feed compositions. When comparing the two, the first noticeable thing in testing CO$_2$/CH$_4$ separation as compared to that of CO$_2$/N$_2$ is that CH$_4$ permeances are substantially higher than those of N$_2$. This increase is to be expected given that MOF-5 exhibits permeation data that obeys Knudsen diffusion and the lower molecular weight CH$_4$ is more mobile than the N$_2$ despite being slightly larger. This correspondingly results in an overall decrease in CO$_2$ selectivity. As expected, the selectivity for CO$_2$ increases with increasing CO$_2$ partial pressure, but the closeness of

permeances between the two permeating molecules makes this effect less marked than for CO_2/N_2.

Lastly, as this testing was carried out a conscious effort was made to replicate $20CO_2/80N_2$ at 445 kPa at lulls in testing to verify the stability of MOF-5 membranes to constant permeation. In Figure 5.6 the results of 24 hours on-stream is graphed, and the results indicate reasonable stability. While there are changes that occur to the selectivity and permeances of the molecules, there is not dramatic loss of selectivity or huge spike in permeance for either molecule, as either of those would indicate a diminishment of membrane structure and quality.
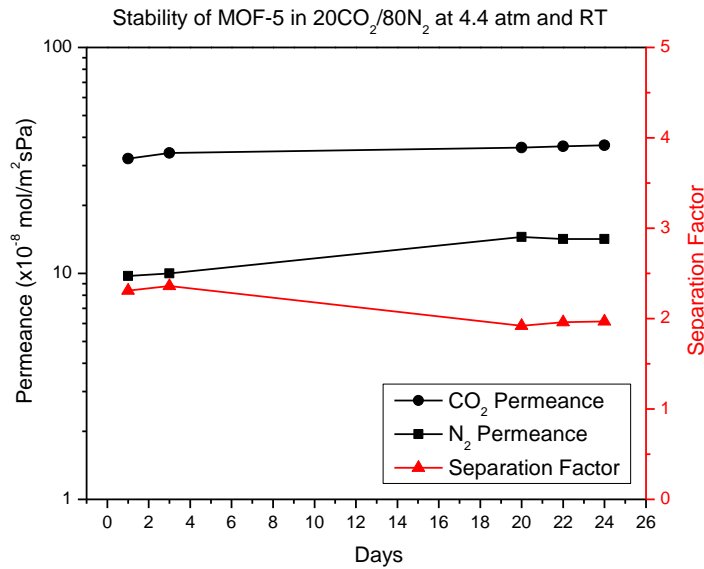
Figure 5.6

Stability of MOF-5 in $20CO_2/80N_2$ environment at 4.4 atm and RT over a period of 24 days.

From Figure 5.6, a 14-15% increase in CO_2 permeance was seen over the course of 24 days when the test was periodically revisited. This was coupled with a 13-14%

decrease in separation factor and a 45% increase in N_2 permeance. It is hypothesized that MOF-5 is, in fact, stable during continuous on-stream permeation for 24 days, but that CO_2 molecules gradually begin fouling available CO_2 bonding sites, thereby decreasing the potential of CO_2 permeance and separation, while increasing the permeance of other molecules, such as N_2.

5.3.2 ZIF-68 Binary Gas Separation

Since ZIF-68 has not previously been synthesized in a strong, useable membrane form, it was important to thoroughly test its behavior. One such test examined was its higher temperature selectivity. Given these membranes obey Knudsen diffusion, see Figure 5.7, it is hypothesized that they will begin to exhibit diminishment of permeance as temperatures increase. This was not the case, however.
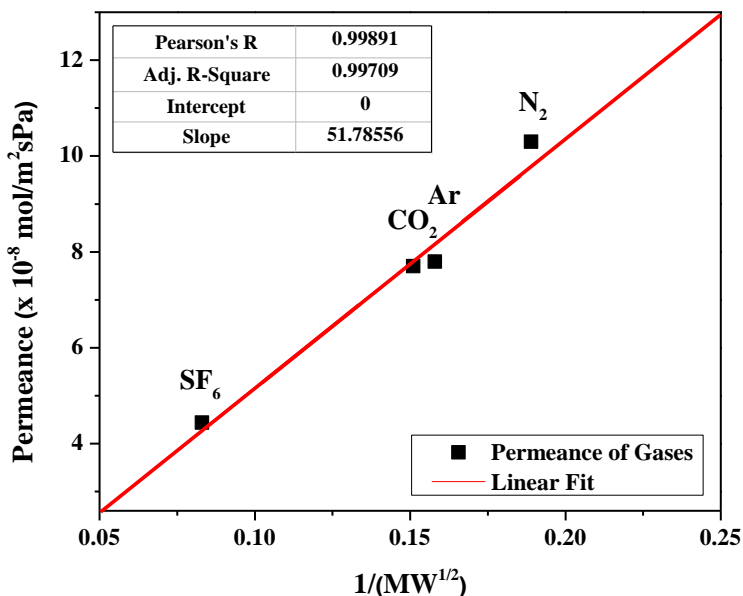
Figure 5.7

Plot of single gas permeance of ZIF-68 as a function of the inverse molecular weight of permeating species.

In Figure 5.8, the gas permeance and separation data for different percentages of CO_2 at room temperature (a) and at 100°C (b) and a feed pressure of 4.4 atm is presented. From the graph it is clear there is limited variability in the separation factor, as well as limited variability in the permeance values exhibited, however there are a few noteworthy differences:

1) An increase of 75°C (from RT to 100°C) showed an increase of 12% for CO_2 permeance and a 7% increase in N_2 permeance at $20CO_2:80N_2$. This is contrary to the assertion that permeance measurements in this regime are inversely proportional to the square root of temperature, and an increase in temperature should accordingly decrease the permeance.

2) The higher permeance at 100°C drops off dramatically at $60CO_2:40N_2$, and all remaining points show almost identical permeance for both CO_2 and N_2.

3) The highest CO_2 permeance for the RT test is at $60CO_2:40N_2$, then both CO_2 permeance and separation factor decrease.

The most probable explanation for observation 1) is that the orientation of the membrane is responsible. The membrane is a- and b- oriented, which means the pores accessible to gaseous species are different than in a c- oriented membrane. In a c-oriented membrane, the pore responsible for transport is the medium sized GME pore, while in an a- and b-oriented membrane the pores accessible to gaseous species are the HPR (small) and KNO (large) cages (Yang Liu et al., 2014). This may account for Knudsen diffusion during single gas permeance, as there are larger pores accessible to the species, however, during a slightly heated state the smaller pore can become more

162

accommodating to gaseous species and result in an increase in permeance. This logic leads to observation 2). The higher permeance drops off after $60CO_2:40N_2$, which indicates that at loadings higher than 60% CO_2 the smaller HPR cages become saturated with CO_2 molecules and only the large KNO cages are accessible to both N_2 and CO_2. The incredibly low degree of variability in both N_2 and CO_2 permeance at 100°C for $60CO_2:40N_2$, $70CO_2:30N_2$ and $80CO_2:20N_2$ indicates that the KNO cages are not susceptible to accumulation of CO_2, and if it were possible to only test gas flow through the larger cage it would not be altered across any permutation of CO_2 and N_2. The smaller variability seen at RT is a direct result of a substantially decreased mobility through the smaller pores. The HPR cages do exhibit a similar saturation at 60% CO_2, as referenced in observation 3), however the effect is minimized since the permeances were not as dramatically altered by the HPR cage at room temperature.

When discussing MOF-5, the very real possibility of framework flexibility being directly responsible for the increased CO_2 selectivity at not only higher CO_2 partial pressures, but also at higher overall feed pressures was used to substantiate the behaviors evidenced. In the case of the ZIF-68, this is likely not the case. Not only is there no correlation to speak of from viewing the CO_2 separation data presented herein, but the potential reason is largely based on potential framework flexibility, which is not known to have any influence on adsorption properties in ZIF-68 (B. Liu & Smit, 2010). Further, in ZIF-68 that is highly *a-* and *b-*oriented there is much greater restrictions to lattice movement. The largest channel, which is presented to the direct flow of permeating molecules, exhibits severely diminished movement due to the protuberance of benzyl groups into the pore, thus indicating that, again, the orientation of the material has huge

ramifications for how the material will behave in binary gas separation experiments (Van der Perre et al., 2014).

(a)

(b)
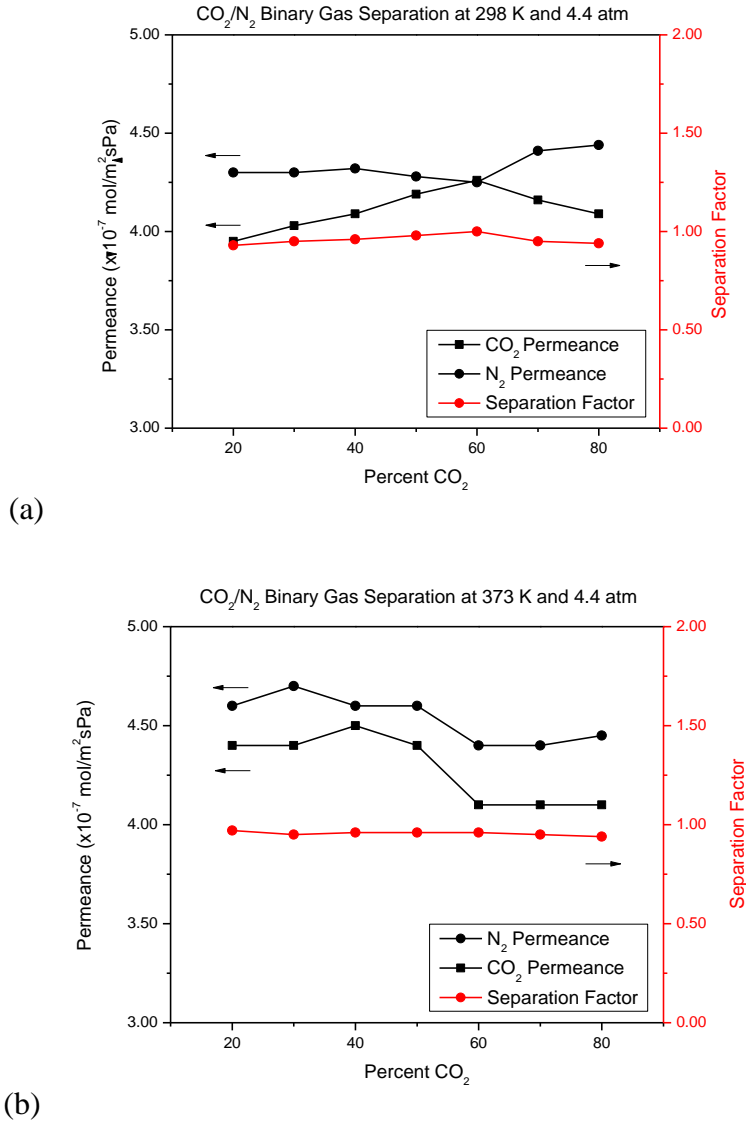
Figure 5.8

Permeance and separation factor as a function of feed composition of CO₂ in CO₂/N₂ binary system at (a) 298K and 445 kPa ΔP and (b) 373K and 445 kPa ΔP.

In Figure 5.9 (a) and (b), ZIF-68 separation of CO_2/N_2 is shown for CO_2 feed side loadings of 20% and 80%, respectively, and up to 9 atm P_{high} at room temperature. The behavior under those different loadings is reasonably similar. The permeance of both species is increased dramatically after pressures of 4.4 atm, and from there a subtle decrease is exhibited. There is also a slightly higher selectivity, 1.25 at 80%CO_2 vs. 1.0 at 20%CO_2. This indicates there may be some potential framework flexibility, but it is minimal, as these membranes are oriented along the *a-* and *b-*axis exclusively.

Figure 5.10 (a) and (b) compares similarly the selectivity of CO_2 in a CO_2/CH_4 binary mixture. There is an even less pronounced effect on CO_2 selectivity from increasing the CO_2 partial pressure or increasing the overall pressure. This is due to the difference between how N_2 and CH_4 interact within the ZIF-68 structure. CH_4 has a strong affinity to the matrix itself, almost as strong as CO_2, which results in a competition for adsorption sites. This competition for adsorption sites manifests itself in a severely diminished selectivity for CO_2 (Ozcan & Keskin, 2014). In fact, for ZIF-68 separation of CO_2/CH_4 the selectivity hovered around, and just barely beat Knudsen diffusion values. One of the most noticeable trends visible from the graphs in Figure 5.9, is that the CO_2 and CH_4 permeance values followed almost identical trends and any flux is well within experimental error. This strongly corroborates the notion that CO_2 and CH_4 have very similar and thereby, very competitive, modes of adsorption within the ZIF-68 structure.
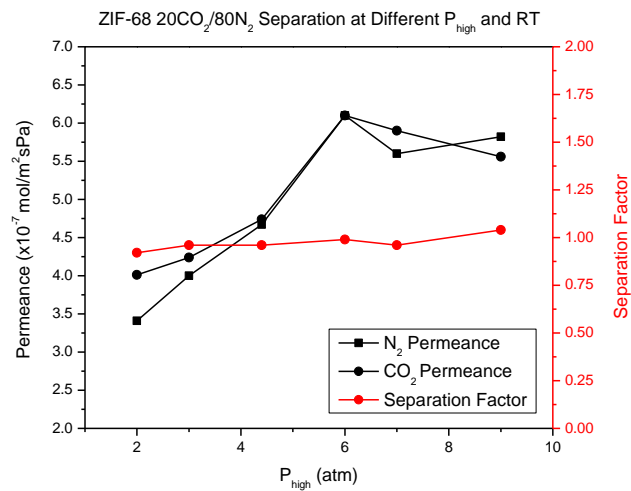
a)
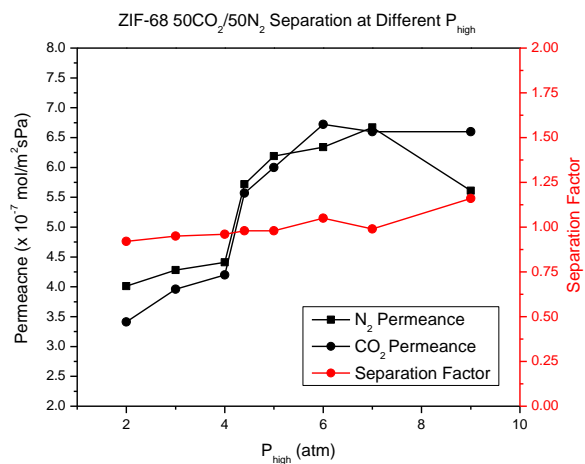
(b)

Figure 5.9

Permeance and separation factor as a function of P_{high} in CO_2/N_2 binary system at (a)

20CO_2:80N_2 and (b) 80CO_2:20N_2.
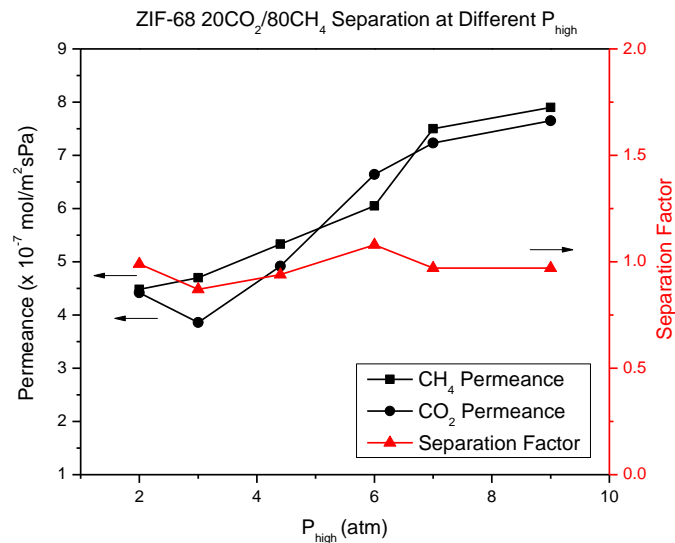
(a)
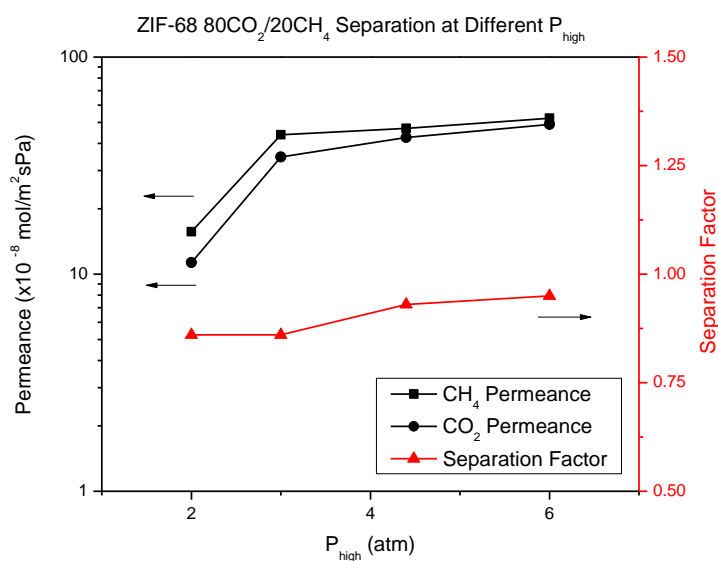
(b)

Figure 5.10

Permeance and separation factor as a function of P_{high} in CO_2/CH_4 binary system at (a) $20CO_2:80CH_4$ and (b) $80CO_2:20CH_4$.

The stability of ZIF-68 was also examined. Experiments were run continuously for over two months, with numerous cycles of activation at 100°C, and under different

pressures and permutations of CO_2/N_2. The results are shown for $20CO_2/80N_2$ at 4.4 atm P_{high} at room temperature and are shown in Figure 5.11. It is worth noting the separation factor did not change at all, it was continuously 0.93. There was a bit of variability in the actual permeance measurements, but it was all within the reasonable error of the experiment. This, coupled with XRD and SEM data presented in Chapter 2, should give a good indication that not only is ZIF-68 stable for a year in atmospheric conditions, but ZIF-68 is stable for months on stream in N_2 and CO_2 environments with thermal cycling.
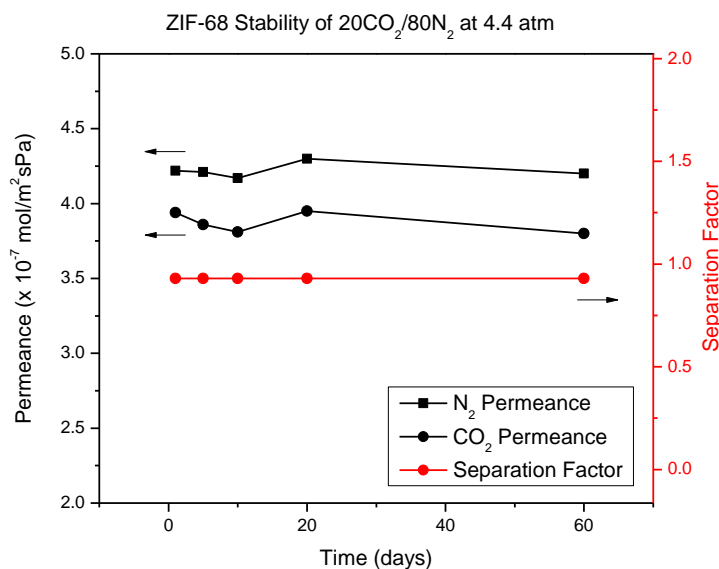
Figure 5.11

Stability of ZIF-68 in 20CO₂/80N₂ environment at 4.4 atm and RT over a period of 60 days.

5.4 Conclusions

MOF-5 and ZIF-68 membranes were synthesized per established procedure and exhibited single gas permeance per Knudsen diffusion. Binary gas separation data for MOF-5 indicated a strong preference for CO_2 over N_2 and CH_4 in CO_2/N_2 and CO_2/CH_4

binary gas mixtures. This effect was exacerbated and selectivity for CO_2 increased as the CO_2 partial pressure increased on the feed side, as well as the overall feed pressure increased. Both effects together yielded even higher CO_2 selectivities. This can be attributed to a slight rearrangement of the MOF-5 structure under higher CO_2 loadings to accommodate more CO_2 molecules. There is limited effect of framework flexibility predicted for ZIF-68, and this was seen to be true as selectivities for CO_2 from both CO_2-/N_2 and CO_2/CH_4 binary gas mixtures did not get much higher than 1. The highest CO_2 selectivity was found for CO_2 in CO_2/N_2 at 80% CO_2 and 9 atm, indicating there can be some flexibility, but the orientation likely hinders the full potential of these materials. Both MOF-5 and ZIF-68 exhibited good stability for 24 days and 60 days, respectively, of on-stream testing, with minimal changes in permeance and selectivity.

CHAPTER 6

SUMMARY AND SUGGESTIONS FOR FUTURE WORK

6.1 Summary

The research outlined within this dissertation was focused on larger pore MOF membranes. The initial focal point of this research was to be on the separation of CO_2 from CH_4 at elevated pressures, in an attempt to isolate the strictly adsorption based mode of separation that large pore membranes can exhibit due to lack of steric hindrances. Given the continually evolving nature of research, however, other, sometimes linear, sometimes tangential, objectives were considered as research progressed.

The first research objective considered was the pervaporation of MOF-5. In beginning research with MOF-5, a number of challenges were faced almost immediately. The most frustrating being the incredible and almost immediate degradation that occurs in the MOF-5 structure upon exposure to air. The effect was so immediate and seemingly insurmountable at such an early stage of research, it was decided that research into the feasibility of using MOF-5 membranes in an environment that would completely negate any exposure to air could be of immense benefit. In this vein, the pervaporation behavior of MOF-5 was studied. Through single component pervaporation studies, the stability of MOF-5 in a myriad of organic solvents was found to be quite good. This work also shed light into the fouling that occurs within the microstructure. Further, this work indicated that there was an additive effect that the fouling exhibited; as the extent of fouling worsened, the needed thermal energy and time to undo the damage increased substantially. It was also found through FTIR spectroscopy that the fouling was due to

auxiliary bonding between the pervaporation molecules and the benzene rings within the MOF-5 structure.

The second objective of this work was also directly related to the instability of MOF-5, and it was to find a linear MOF material to research in tandem to MOF-5. The qualifications for this material were that it had to have a similar pore size to MOF-5 and it needed to be characterized by a very stable structure. To narrow down candidate materials, stability was first considered. This led us to zeolitic imidazolate frameworks, which are renowned for their stability due in part to their propensity to be hydrophobic. Of ZIF materials, however, there are only reports of membrane synthesis on smaller pore ZIF materials. ZIF-68 was eventually chosen due to its pore size, and the fact that there were a few reports on membrane synthesis of a similar dual-ligand, zinc-based, gmelinite-topology ZIF known as ZIF-69. When synthesis of ZIF-68 through methods outlined in literature for similar ZIF materials proved unsuccessful, reactive seeding was tried. This method proved invaluable in creating reproducible, low-defect, c-oriented membranes that exhibited Knudsen diffusion. These membranes were then used to test the stability of ZIF-68 membranes in a variety of environments, such as a year in air, and a week in boiling water.

The third objective of this work is directly related to the reactive seeding method utilized to synthesize ZIF-68 membranes. The method requires the use of a ZnO support to contribute the needed zinc atoms to create the seeds layer. This, however, creates membranes that are incredibly weak. Given the underlying focus of this research is the high pressure separation of CO_2/CH_4, these membranes proved virtually useless. By virtue of this, the third objective of this work was to synthesize continuous ZIF-68

171

membranes on structurally sound α-alumina supports. This proved very tricky, but with time, a method was developed that could still utilize the reactive seeding principles, while still being on a strong α-alumina support. This method took a polished α-alumina support and, through an *in situ* surface modification step, created an intimately adhered layer of ZnO on the surface. Once that ZnO layer was created, reactive seeding could proceed as it did previously. This method created reproducible, continuous, *a-* and *b*-oriented membranes that exhibited Knudsen diffusion.

Finally, once ZIF-68 membranes were synthesized on supports that could stand higher transmembrane pressure drops, the first and final objective of this research was considered; the high pressure binary gas separation of CO_2/N_2 and CO_2/CH_4. Results indicated that MOF-5 has an increased preference for CO_2 in both systems as CO_2 loading increases as well as when overall feed pressure increases. This effect is postulated to be due to a slight framework flexibility that is activated when the loading of CO_2 is high, as well as when the feed pressure is high, and the rearrangement exposes more potential adsorption sites to the feed stream. It is also postulated that these mechanisms are discrete, as higher CO_2 loadings increases the CO_2 selectivity, higher feed pressures also increase the CO_2 selectivity, and when high loadings are coupled with high feed pressures, the effect is at its highest. This was not the case for ZIF-68, however. Although there were slight preferences for CO_2 evidenced that went beyond Knudsen slightly (up to 1.25), CO_2 selectivity only showed a slight dependence on overall hydraulic pressure. This further underscores the premise that these mechanisms are discrete, as only one is evidenced in ZIF-68. It is likely that the diminished selectivity of CO_2 over CH_4 and CO_2 over N_2 as compared to MOF-5 is the result of the

a- and *b-*orientation, since there is far less framework mobility along those directions due to the benzyl groups that protrude in the main cavities along those directions. Further, it is worth noting that the main channel for which CO_2 would preferentially adsorb is along the *c-*axis, further explaining the limited selectivity evidenced by these membranes.

6.2 Recommendations

Based on the research carried out herein, the following recommendations are outlined for future research.

6.2.1 MOF-5 Stability

This research really underscored two points, the first; MOF-5 is a remarkable material with a huge amount of potential. The second; none of that potential can be reached if there is not a fix to its stability issues. For this, two suggestions are immediate. The first, which is already well researched and not expounded upon herein is to create a more stable version of MOF-5 while still retaining its inherent CO_2 preference and desirably porosity. The second is to capitalize on the material as it is, through creatively implementing it in environments where normal levels of atmospheric moisture can be avoided.

In terms of negating exposure to atmosphere, it may rather quickly become a possibility to utilize these materials in environments that do not contain the atmospheric levels of moisture, because they are not being used in Earth's atmosphere. The atmosphere in Mars is 95% CO_2, 3% N_2 and 2% Ar, and with current research focusing on effective, passive ways to carry out separation processes in Martian environments, it may be entirely reasonable that these membranes can work efficiently and effectively in a number of necessary separations. A prominent example could be the use of MOF-5 to

aid in the separation processes needed to convert Martian atmosphere to breathable O_2 and CO for subsequent water-gas shift reactions (Walton & LeVan, 2004)

6.2.2 ZIF-68 C-Oriented Membranes

The selectivity of CO_2 in ZIF-68 membranes is quite directional. This has been shown through modeling, and supported through the work herein (Yang Liu et al., 2014). The membranes synthesized on ZnO supports showed almost entirely *c*-oriented microstructures; so much so in fact, almost all other peaks were missing. This was not the case when the modified reactive seeding method was utilized, and CO_2 selectivity and permeance suffered as a result. There are synthesis methods outlined for ZIF-69 on α-alumina supports that are characterized by *c*-orientation, and it would be useful to optimize those procedures as needed to be able to extrapolate that *c*-orientation to ZIF-68 membranes (Yunyang Liu et al., 2011a).

In synthesizing ZIF-68 membranes with an inherent *c*-orientation on α-alumina supports, it may be possible to reach selectivities and permeance values attainable with other similar pore size materials, such as MOF-5, and be able to capitalize on the enhanced CO_2 selectivity associated with not only increasing CO_2 feed percentage, but also overall feed pressure.

REFERENCES

1-3-5-Triisopropylbenzene | CasNO.717-74-8. (2015). *LOOKCHEM.COM*. Retrieved from http://www.lookchem.com/1-3-5-triisopropylbenzene/

Aceituno Melgar, V. M., Kwon, H. T., & Kim, J. (2014). Direct spraying approach for synthesis of ZIF-7 membranes by electrospray deposition. *Journal of Membrane Science*, *459*, 190–196. doi:10.1016/j.memsci.2014.02.020

Aguado, S., Canivet, J., & Farrusseng, D. (2010). Facile shaping of an imidazolate-based MOF on ceramic beads for adsorption and catalytic applications. *Chemical Communications (Cambridge, England)*, *46*, 7999–8001. doi:10.1039/c0cc02045a

Aguado, S., Canivet, J., & Farrusseng, D. (2011). Engineering structured MOF at nano and macroscales for catalysis and separation. *Journal of Materials Chemistry*, *21*(21), 7582. doi:10.1039/c1jm10787a

Aguado, S., Nicolas, C.-H., Moizan-Baslé, V., Nieto, C., Amrouche, H., Bats, N., … Farrusseng, D. (2011a). Facile synthesis of an ultramicroporous MOF tubular membrane with selectivity towards CO2. *New Journal of Chemistry*, *35*(1), 41. doi:10.1039/c0nj00667j

Aguado, S., Nicolas, C.-H., Moizan-Baslé, V., Nieto, C., Amrouche, H., Bats, N., … Farrusseng, D. (2011b). Facile synthesis of an ultramicroporous MOF tubular membrane with selectivity towards CO2. *New Journal of Chemistry*, *35*, 41. doi:10.1039/c0nj00667j

Al-Maythalony, B. a., Shekhah, O., Swaidan, R., Belmabkhout, Y., Pinnau, I., & Eddaoudi, M. (2015). Quest for Anionic MOF Membranes: Continuous   sod - ZMOF Membrane with CO 2 Adsorption-Driven Selectivity. *Journal of the American Chemical Society*, *137*(5), 1754–1757. doi:10.1021/ja511495j

Amirjalayer, S., & Schmid, R. (2009). Mechanism of benzene diffusion in MOF-5: A molecular dynamics investigation. *Microporous and Mesoporous Materials*, *125*(1-2), 90–96. doi:10.1016/j.micromeso.2009.02.006

Amirjalayer, S., Tafipolsky, M., & Schmid, R. (2007). Molecular dynamics simulation of benzene diffusion in MOF-5: importance of lattice dynamics. *Angewandte Chemie (International Ed. in English)*, *46*(3), 463–6. doi:10.1002/anie.200601746

Babarao, R., Dai, S., & Jiang, D. (2011). Effect of Pore Topology and Accessibility on Gas Adsorption Capacity in Zeolitic− Imidazolate Frameworks: Bringing Molecular Simulation Close to Experiment. *The Journal of Physical Chemistry C*, *115*, 8126–8135. Retrieved from http://pubs.acs.org/doi/abs/10.1021/jp1117294

Babarao, R., Eddaoudi, M., & Jiang, J. W. (2010). Highly porous ionic rht metal-organic framework for H2 and CO2 storage and separation: A molecular simulation study. *Langmuir*, *26*(13), 11196–11203. doi:10.1021/la100509g

Babarao, R., & Jiang, J. (2009). Unprecedentedly High Selective Adsorption of Gas Mixtures in rho Zeolite-like Metal - Organic Framework : A Molecular, (10), 11417–11425.

Baker, R. W. (2004). *Membrane Technology and Applications*. John Wiley & Sons, Inc.

Ban, Y., Li, Y., Liu, X., Peng, Y., & Yang, W. (2013). Microporous and Mesoporous Materials Solvothermal synthesis of mixed-ligand metal – organic framework ZIF-78 with controllable size and morphology. *Microporous and Mesoporous Materials*, *173*, 29–36. doi:10.1016/j.micromeso.2013.01.031

Banerjee, R., Furukawa, H., Britt, D., Knobler, C., Keeffe, M. O., & Yaghi, O. M. (2009). Control of Pore Size and Functionality in Isoreticular Zeolitic Imidazolate Frameworks and their Carbon Dioxide Selective Capture Properties. *Journal of the American Chemical Society*, *131*, 3875–3877.

Banerjee, R., Furukawa, H., Britt, D., Knobler, C., Yaghi, O. M., & Angeles, L. (n.d.). Control of Pore Size and Functionality in Isoreticular Zeolitic Imidazolate Frameworks and their Carbon Dioxide Selective Capture Properties, 1–95.

Banerjee, R., Phan, A., Wang, B., Knobler, C., Furukawa, H., O'Keeffe, M., & Yaghi, O. M. (2008). High-throughput synthesis of zeolitic imidazolate frameworks and application to CO2 capture. *Science (New York, N.Y.)*, *319*(5865), 939–43. doi:10.1126/science.1152516

Battisti, A., Taioli, S., & Garberoglio, G. (2011). Zeolitic imidazolate frameworks for separation of binary mixtures of CO2, CH4, N2 and H2: A computer simulation investigation. *Microporous and Mesoporous Materials*, *143*(1), 46–53. doi:10.1016/j.micromeso.2011.01.029

Bertazzo, S., & Rezwan, K. (2010). Control of alpha-alumina surface charge with carboxylic acids. *Langmuir : The ACS Journal of Surfaces and Colloids*, *26*(5), 3364–71. doi:10.1021/la903140k

Bhatia, S. C., Rani, R., & Bhatia, R. (2011). Viscosities, densities, speeds of sound and refractive indices of binary mixtures of o-xylene, m-xylene, p-xylene, ethylbenzene and mesitylene with 1-decanol at 298.15 and 308.15K. *Journal of Molecular Liquids*, *159*(2), 132–141. doi:10.1016/j.molliq.2010.12.011

Bowen, T. C., Noble, R. D., & Falconer, J. L. (2004). Fundamentals and applications of pervaporation through zeolite membranes. *Journal of Membrane Science*, *245*(1-2), 1–33. doi:10.1016/j.memsci.2004.06.059

Breck, D. . (1974). *Zeolite Molecular Sieves*. New York: Wiley.

Brown, A. J., Johnson, J. R., Lydon, M. E., Koros, W. J., Jones, C. W., & Nair, S. (2012). Continuous polycrystalline zeolitic imidazolate framework-90 membranes on polymeric hollow fibers. *Angewandte Chemie - International Edition*, *51*, 10615–10618. doi:10.1002/anie.201206640

Bux, H., Liang, F., Li, Y., Cravillon, J., & Wiebcke, M. (2009). Zeolitic Imidazolate Framework Membrane with Molecular Sieving Properties by Microwave-Assisted Solvothermal Synthesis, 16000–16001. doi:10.1021/cm902032y.

Chmelik, C., van Baten, J., & Krishna, R. (2012). Hindering effects in diffusion of CO2/CH4 mixtures in ZIF-8 crystals. *Journal of Membrane Science*, *397-398*, 87–91. doi:10.1016/j.memsci.2012.01.013

Choi, J. Y., Huang, R., Uribe-romo, F. J., Chae, H. K., Park, K. S., Ni, Z., … Yaghi, O. M. (2006). Exceptional chemical and thermal stability of zeolitic imidazolate frameworks. *PNAS*, *103*(27), 8–13.

Collodi, G. (2008). Hydrogen Production via Steam Reforming with CO 2 Capture, 1–6.

Diestel, L., Bux, H., Wachsmuth, D., & Caro, J. (2012). Pervaporation studies of n-hexane, benzene, mesitylene and their mixtures on zeolitic imidazolate framework-8 membranes. *Microporous and Mesoporous Materials*, *164*, 288–293. doi:10.1016/j.micromeso.2012.06.031

Dong, X., Huang, K., Liu, S., Ren, R., Jin, W., & Lin, Y. S. (2012). Synthesis of zeolitic imidazolate framework-78 molecular-sieve membrane: defect formation and elimination. *Journal of Materials Chemistry*, *22*(36), 19222. doi:10.1039/c2jm34102f

Dong, X., & Lin, Y. S. (2013). Synthesis of an organophilic ZIF-71 membrane for pervaporation solvent separation. *Chemical Communications (Cambridge, England)*, *49*(12), 1196–8. doi:10.1039/c2cc38512k

Eddaoudi, M., Li, H., & Yaghi, O. (2000). Highly porous and stable metal-organic frameworks: structure design and sorption properties. *Journal of the American Chemical Society*, 1391–1397. Retrieved from http://pubs.acs.org/doi/abs/10.1021/ja9933386

Faibish, R. S., & Cohen, Y. (2001). Fouling and rejection behavior of ceramic and polymer-modified ceramic membranes for ultrafiltration of oil-in-water emulsions and microemulsions. *Colloids and Surfaces A: Physicochemical and Engineering Aspects*, *191*(1-2), 27–40. doi:10.1016/S0927-7757(01)00761-0

Férey, G., & Serre, C. (2009). Large breathing effects in three-dimensional porous hybrid matter: facts, analyses, rules and consequences. *Chemical Society Reviews*, *38*(5), 1380–99. doi:10.1039/b804302g

First, E. L., Gounaris, C. E., & Floudas, C. a. (2013). Predictive framework for shape-selective separations in three-dimensional zeolites and metal-organic frameworks. *Langmuir*, *29*(18), 5599–5608. doi:10.1021/la400547a

Fox, S. (2009). The Top Ten Greenhouse Gases. *Popular Science*.

Freemantle, M. (2005). Advanced organic and inorganic materials being developed for separations offer cost benefits for environmental and energy-related processes. *Chemical & Engineering News*, *83*(40), 49–57.

Frunza, S., Schönhals, A., Frunza, L., Ganea, P., Kosslick, H., Harloff, J., & Schulz, A. (2010). Molecular relaxation processes in a MOF-5 structure revealed by broadband dielectric spectroscopy: signature of phenylene ring fluctuations. *The Journal of Physical Chemistry. B*, *114*(40), 12840–6. doi:10.1021/jp1071617

Garcia-Martinez, J., Johnson, M., Valla, J., Li, K., & Ying, J. Y. (2012). Mesostructured zeolite Y- high hydrothermal stability and superior FCC catalytic performance. *Catalysis Science & Technology*, *2*, 987–994.

Guerrero, V. V., Yoo, Y., McCarthy, M. C., & Jeong, H.-K. (2010a). HKUST-1 membranes on porous supports using secondary growth. *Journal of Materials Chemistry*, *20*(19), 3938. doi:10.1039/b924536g

Guerrero, V. V., Yoo, Y., McCarthy, M. C., & Jeong, H.-K. (2010b). HKUST-1 membranes on porous supports using secondary growth. *Journal of Materials Chemistry*, *20*, 3938. doi:10.1039/b924536g

Herm, Z., Krishna, R., Long, J. R., Smit, B., & Swisher, J. A. (2011). Metalorganic frameworks for h2/co2 separation. *Office of Intellectual Property and Industry Research Alliances*.

178

Hermes, S., Schröder, F., Chelmowski, R., Wöll, C., & Fischer, R. a. (2005). Selective nucleation and growth of metal-organic open framework thin films on patterned COOH/CF3-terminated self-assembled monolayers on Au(111). *Journal of the American Chemical Society*, *127*(40), 13744–5. doi:10.1021/ja053523l

Hoskins, B., & Robson, R. (1989). Infinite polymeric frameworks consisting of three dimensionally linked rod-like segments. *Journal of the American Chemical …*, *111*(15), 5962–5964. Retrieved from http://pubs.acs.org/doi/abs/10.1021/ja00197a079

Hou, X., & Li, H. (2010). Unraveling the High Uptake and Selectivity of CO 2 in the Zeolitic Imidazolate Frameworks ZIF-68 and ZIF-69. *J Chem Phys C*, 13501–13508.

Houghton, J. (2005). Global warming. *Reports on Progress in Physics*, *68*(6), 1343–1403. doi:10.1088/0034-4885/68/6/R02

Hu, Y., Dong, X., Nan, J., Jin, W., Ren, X., Xu, N., & Lee, Y. M. (2011). Metal-organic framework membranes fabricated via reactive seeding. *Chemical Communications (Cambridge, England)*, *47*(2), 737–9. doi:10.1039/c0cc03927f

Huang, A., Bux, H., Steinbach, F., & Caro, J. (2010). Molecular-sieve membrane with hydrogen permselectivity: ZIF-22 in LTA topology prepared with 3-aminopropyltriethoxysilane as covalent linker. *Angewandte Chemie (International Ed. in English)*, *49*(29), 4958–61. doi:10.1002/anie.201001919

Huang, A., Chen, Y., Liu, Q., Wang, N., Jiang, J., & Caro, J. (2014). Synthesis of highly hydrophobic and permselective metal–organic framework Zn(BDC)(TED)0.5 membranes for H2/CO2 separation. *Journal of Membrane Science*, *454*, 126–132. doi:10.1016/j.memsci.2013.12.018

Huang, A., Chen, Y., Wang, N., Hu, Z., Jiang, J., & Caro, J. (2012). A highly permeable and selective zeolitic imidazolate framework ZIF-95 membrane for H2/CO2 separation. *Chemical Communications*, *48*(89), 10981. doi:10.1039/c2cc35691k

Huang, A., Dou, W., & Caro, J. (2010). Steam-stable zeolitic imidazolate framework ZIF-90 membrane with hydrogen selectivity through covalent functionalization. *Journal of the American Chemical Society*, *132*(44), 15562–15564. doi:10.1021/ja108774v

Huang, A., Liu, Q., Wang, N., & Caro, J. (2013). Organosilica functionalized zeolitic imidazolate framework ZIF-90 membrane for CO2/CH4 separation. *Microporous and Mesoporous Materials*, 1–5. doi:10.1016/j.micromeso.2013.09.025

Huang, A., Wang, N., Kong, C., & Caro, J. (2012). Organosilica-functionalized zeolitic imidazolate framework ZIF-90 membrane with high gas-separation performance. *Angewandte Chemie (International Ed. in English)*, *51*(42), 10551–5. doi:10.1002/anie.201204621

Huang, L., Wang, H., Chen, J., Wang, Z., Sun, J., Zhao, D., & Yan, Y. (2003). Synthesis , morphology control , and properties of porous metal – organic coordination polymers, *58*, 105–114.

James, S. L. (2003). Metal-organic frameworks. *Chemical Society Reviews*, *32*(5), 276. doi:10.1039/b200393g

Karger, J. (1992). *Diffusion in Zeolites and Other Microporous Solids*. New York: John Wiley & Sons, Inc.

Kasik, A., Dong, X., & Lin, Y. S. (2014). Synthesis and Stability of Zeolitic Imidazolate Framework-68 Membranes. *Microporous and Mesoporous Materials*, *204*, 99–105. doi:10.1016/j.micromeso.2014.10.050

Kasik, A., & Lin, Y. S. (2013). Organic solvent pervaporation properties of MOF-5 membranes. *Separation and Purification Technology*. doi:10.1016/j.seppur.2013.04.033

Kaye, S. S., Dailly, A., Yaghi, O. M., & Long, J. R. (2010). Impact of Preparation and Handling on the Hydrogen Storage Properties of Zn4O(w,4-benzendicarboxylate)3 (MOF-5). *JACS*, *3*, 14176–14177.

Keskin, S., & Sholl, D. S. (2009). Assessment of a Metal-Organic Framework Membrane for Gas Separations Using Atomically Detailed Calculations : CO 2 , CH 4 , N 2 , H 2 Mixtures in MOF-5. *Society*, 914–922.

Khodakov, Y. S., Mikheikin, I. D., Nakhshunov, V. S., Shvets, V. A., Kazanskii, V. B., & Minachev, K. M. (1969). Investigation of the structure and thermal stability of zeolites of types A, X and Y containing trivalent chromium. *Russian Chemical Bulletin*, *18*(3), 465–470.

Kim, T. W. (2008). *STUDIES OF TRANSPORT PHENOMENA IN HYDROTALCITE MEMBRANES, AND THEIR USE IN DIRECT METHANOL FUEL CELLS*. Los Angeles: University of Southern California Libraries.

Koros, W. J., & Fleming, G. K. (1993). Membrane-based gas separation. *Journal of Membrane Science*, *83*(1), 1–80. doi:10.1016/0376-7388(93)80013-N

Krishna, R. (2012). Adsorptive separation of CO 2/CH 4/CO gas mixtures at high pressures. *Microporous and Mesoporous Materials*, *156*, 217–223. doi:10.1016/j.micromeso.2012.02.034

Lee, T., Choi, J., & Tsapatsis, M. (2013). On the performance of c-oriented MFI zeolite Membranes treated by rapid thermal processing. *Journal of Membrane Science*, *436*, 79–89. doi:10.1016/j.memsci.2013.02.028

Li, J.-R., Ma, Y., McCarthy, M. C., Sculley, J., Yu, J., Jeong, H.-K., … Zhou, H.-C. (2011a). Carbon dioxide capture-related gas adsorption and separation in metal-organic frameworks. *Coordination Chemistry Reviews*, *255*(15-16), 1791–1823. doi:10.1016/j.ccr.2011.02.012

Li, J.-R., Ma, Y., McCarthy, M. C., Sculley, J., Yu, J., Jeong, H.-K., … Zhou, H.-C. (2011b). Carbon dioxide capture-related gas adsorption and separation in metal-organic frameworks. *Coordination Chemistry Reviews*, *255*(15-16), 1791–1823. doi:10.1016/j.ccr.2011.02.012

Li, Y., Liang, F., Bux, H., Yang, W., & Caro, J. (2010). Zeolitic imidazolate framework ZIF-7 based molecular sieve membrane for hydrogen separation. *Journal of Membrane Science*, *354*(1-2), 48–54. doi:10.1016/j.memsci.2010.02.074

Li, Y.-S., Liang, F.-Y., Bux, H., Feldhoff, A., Yang, W.-S., & Caro, J. (2010). Molecular sieve membrane: supported metal-organic framework with high hydrogen selectivity. *Angewandte Chemie (International Ed. in English)*, *49*(3), 548–51. doi:10.1002/anie.200905645

Lin, Y. S., & Kanezashi, M. (2007). *Gas permeation and diffusion in small and intermediate pore zeolite membranes*. *Studies in Surface Science and Catalysis* (Vol. 170). Elsevier B.V. doi:10.1016/S0167-2991(07)80931-1

Lin, Y. S., Kumakiri, I., Nair, B. N., & Alsyouri, H. (2007). Microporous Inorganic Membranes. *Separation & Purification Reviews*, *31*(2), 229–379. doi:10.1081/SPM-120017009

Liu, B., & Smit, B. (2010). Molecular Simulation Studies of Separation of CO 2 / N 2 , CO 2 / CH 4 , and CH 4 / N 2 by ZIFs, 8515–8522.

Liu, Q., Wang, N., Caro, J., & Huang, A. (2013). Bio-inspired polydopamine: a versatile and powerful platform for covalent synthesis of molecular sieve membranes. *Journal of the American Chemical Society*, *135*(47), 17679–82. doi:10.1021/ja4080562

Liu, X., Jin, H., Li, Y., Bux, H., Hu, Z., Ban, Y., & Yang, W. (2013). Metal–organic framework ZIF-8 nanocomposite membrane for efficient recovery of furfural via pervaporation and vapor permeation. *Journal of Membrane Science*, *428*, 498–506. doi:10.1016/j.memsci.2012.10.028

Liu, Y., Hu, E., Khan, E. A., & Lai, Z. (2010). Synthesis and characterization of ZIF-69 membranes and separation for CO 2 / CO mixture. *Journal of Membrane Science*, *353*(1-2), 36–40. doi:10.1016/j.memsci.2010.02.023

Liu, Y., Kasik, A., Linneen, N., Liu, J., & Lin, Y. S. (2014). Adsorption and diffusion of carbon dioxide on ZIF-68. *Chemical Engineering Science*, *118*, 32–40. doi:10.1016/j.ces.2014.07.030

Liu, Y., Liu, J., Chang, M., & Zheng, C. (2012). E ff ect of Functionalized Linker on CO 2 Binding in Zeolitic Imidazolate Frameworks : Density Functional Theory Study. *The Journal of Physical Chemistry C*, (116), 16985–16991.

Liu, Y., Ng, Z., Khan, E. a., Jeong, H.-K., Ching, C., & Lai, Z. (2009). Synthesis of continuous MOF-5 membranes on porous α-alumina substrates. *Microporous and Mesoporous Materials*, *118*(1-3), 296–301. doi:10.1016/j.micromeso.2008.08.054

Liu, Y., Zeng, G., Pan, Y., & Lai, Z. (2011a). Synthesis of highly c-oriented ZIF-69 membranes by secondary growth and their gas permeation properties. *Journal of Membrane Science*, *379*(1-2), 46–51. doi:10.1016/j.memsci.2011.05.041

Liu, Y., Zeng, G., Pan, Y., & Lai, Z. (2011b). Synthesis of highly c-oriented ZIF-69 membranes by secondary growth and their gas permeation properties. *Journal of Membrane Science*, *379*(1-2), 46–51. doi:10.1016/j.memsci.2011.05.041

Mccarthy, M. C., Varela-guerrero, V., Barnett, G. V, & Jeong, H. (2010). Synthesis of Zeolitic Imidazolate Framework Films and Membranes with Controlled Microstructures. *Langmuir*, *26*(11), 14636–14641. doi:10.1021/la102409e

McLeary, E. E., Jansen, J. C., & Kapteijn, F. (2006). Zeolite based films, membranes and membrane reactors: Progress and prospects. *Microporous and Mesoporous Materials*, *90*(1-3), 198–220. doi:10.1016/j.micromeso.2005.10.050

Meek, S. T., Greathouse, J. a, & Allendorf, M. D. (2011). Metal-organic frameworks: a rapidly growing class of versatile nanoporous materials. *Advanced Materials*, *23*(2), 249–67. doi:10.1002/adma.201002854

Millward, A. R., & Yaghi, O. M. (2005). Metal-Organic Frameworks with Exceptionally High Capacity for Storage of Carbon Dioxide at Room Temperature, 17998–17999.

Morris, W., Doonan, C. J., Furukawa, H., Banerjee, R., & Yaghi, O. M. (2008). Crystals as molecules: postsynthesis covalent functionalization of zeolitic imidazolate frameworks. *Journal of the American Chemical Society*, *130*(38), 12626–7. doi:10.1021/ja805222x

Nalaparaju, A., Zhao, X. S., & Jiang, J. W. (2011). Biofuel purification by pervaporation and vapor permeation in metal–organic frameworks: a computational study. *Energy & Environmental Science*, *4*(207890), 2107. doi:10.1039/c0ee00630k

Nan, J., Dong, X., Wang, W., & Jin, W. (2012). Formation mechanism of metal–organic framework membranes derived from reactive seeding approach. *Microporous and Mesoporous Materials*, *155*(3), 90–98. doi:10.1016/j.micromeso.2012.01.010

Nan, J., Dong, X., Wang, W., Jin, W., & Xu, N. (n.d.). Supporting Information for A step-by-step seeding procedure for preparing HKUST-1 membrane on porous α - alumina support.

Nan, J., Dong, X., Wang, W., Jin, W., & Xu, N. (2011). Step-by-Step Seeding Procedure for Preparing HKUST-1 Membrane on Porous a -Alumina Support, 4309–4312.

Natural Gas and the Environment. (2013). *Naturalgas.org*.

Nuwer, R. (2012). A 20-Year Low in U.S. Carbon Emissions. *The New York Times*.

O'Brien-Abraham, J., Kanezashi, M., & Lin, Y. S. (2008). Effects of adsorption-induced microstructural changes on separation of xylene isomers through MFI-type zeolite membranes. *Journal of Membrane Science*, *320*(1-2), 505–513. doi:10.1016/j.memsci.2008.04.023

Ozcan, A., & Keskin, S. (2014). Effects of molecular simulation parameters on predicting gas separation performance of ZIFs. *Journal of Chemical Technology & Biotechnology*, (May), n/a–n/a. doi:10.1002/jctb.4482

Pan, Y., Wang, B., & Lai, Z. (2012). Synthesis of ceramic hollow fiber supported zeolitic imidazolate framework-8 (ZIF-8) membranes with high hydrogen permeability. *Journal of Membrane Science*, *421-422*, 292–298. doi:10.1016/j.memsci.2012.07.028

Panella, B., Hirscher, M., Pütter, H., & Müller, U. (2006). Hydrogen Adsorption in Metal–Organic Frameworks: Cu-MOFs and Zn-MOFs Compared. *Advanced Functional Materials*, *16*(4), 520–524. doi:10.1002/adfm.200500561

Park, K. S. (2006). Supporting Info Exceptional stability ZIFS. *PNAS*, *103*(27), 10188. doi:10.1093/her/cyt145

Peng, Y., Li, Y., Ban, Y., Jin, H., Jiao, W., Liu, X., & Yang, W. (2014). Metal-organic framework nanosheets as building blocks for molecular sieving membranes. *Science*, *346*(6215), 1356–1359.

Phan, A., Doonan, C. J., Uribe-romo, F. J., Knobler, C. B., Keeffe, M. O., & Yaghi, O. M. (2010). Synthesis, Structure and Carbon Dioxide Capture Properties of Zeolitic Imidazolate Frameworks, *43*(1).

Rankin, R. B., Liu, J., Kulkarni, A. D., & Johnson, J. K. (2009). Adsorption and Diffusion of Light Gases in ZIF-68 and ZIF-70 : A Simulation Study, 16906–16914.

Rapp, D. (2013). *Use of Extaterrestrial Resources for Human Space Missions*. Heidelberg.

Resources. (2013). *Naturalgas.org*.

Robeson, L. M. (1991). Correlation of separation factor versus permeability for polymeric membranes. *Journal of Membrane Science*, *62*(2), 165–185. doi:10.1016/0376-7388(91)80060-J

Rosi, N. L., Eckert, J., Eddaoudi, M., & Vodak, D. T. (2013). Hydrogen Storage in Microporous Metal-Organic Frameworks Kim , Michael O ' Keeffe and Omar M . Yaghi Reviewed work (s): Source : Science , New Series , Vol . 300 , No . 5622 (May 16 , 2003), pp . 1127-1129 Published by : American Association for the A, *300*(5622), 1127–1129.

Saha, D., & Deng, S. (2010). Ammonia adsorption and its effects on framework stability of MOF-5 and MOF-177. *Journal of Colloid and Interface Science*, *348*(2), 615–20. doi:10.1016/j.jcis.2010.04.078

Saint Remi, J. C., Rémy, T., Vanhunskerken, V., Vandeperre, S., Duerinck, T., Maes, M., … Denayer, J. F. M. (2011). Biobutanol separation with the metal-organic framework ZIF-8. *ChemSusChem*, *4*, 1074–1077. doi:10.1002/cssc.201100261

Schrock, K., Schroder, F., Heyden, M., Fischer, R. A., & Havenith, M. (2008). Characterization of interfacial water in MOF-5 (Zn4(O)(BDC)3)- a combined spectroscopic and theoretical study. *Physical Chemistry Chemical Physics : PCCP*, *10*(32), 4732–4739. doi:10.1039/b812223g

Seader, J. D., & Henley, E. J. (1998). *Separation Process Principles*. New York: John Wiley & Sons, Inc.

Shah, M., Kwon, H. T., Tran, V., Sachdeva, S., & Jeong, H.-K. (2013). One step in situ synthesis of supported zeolitic imidazolate framework ZIF-8 membranes: Role of sodium formate. *Microporous and Mesoporous Materials*, *165*, 63–69. doi:10.1016/j.micromeso.2012.07.046

Shah, M., Mccarthy, M. C., Sachdeva, S., Lee, A. K., & Jeong, H. (2012). Current Status of Metal À Organic Framework Membranes for Gas Separations : Promises and Challenges, 2179–2199.

Shao, P., & Huang, R. Y. M. (2007). Polymeric membrane pervaporation. *Journal of Membrane Science*, *287*(2), 162–179. doi:10.1016/j.memsci.2006.10.043

Shekhah, O., Liu, J., Fischer, R. a, & Wöll, C. (2011). MOF thin films: existing and future applications. *Chemical Society Reviews*, *40*(2), 1081–106. doi:10.1039/c0cs00147c

Shimekit, B., & Mukhtar, H. (2012). Natural Gas Purification Technologies–Major Advances for CO2 Separation and Future Directions. *Advances in Natural Gas Technology*. Retrieved from http://cdn.intechopen.com/pdfs-wm/35293.pdf

Sirjoosingh, A., Alavi, S., & Woo, T. K. (2010). Grand-Canonical Monte Carlo and Molecular-Dynamics Simulations of Carbon-Dioxide and Carbon-Monoxide Adsorption in Zeolitic Imidazolate Framework Materials, 2171–2178.

Smith, B., Longanathan, M., & Shantha, M. S. (2010). A Review of the Water Gas Shift Reaction Kinetics. *International Journal of Chemical Reactor Engineering*, *8*, 1–32.

Smitha, B. (2004). Separation of organic-organic mixtures by pervaporation-a review*. *Journal of Membrane Science*, *241*(1), 1–21. doi:10.1016/j.memsci.2004.03.042

Steele, W. V, Chirico, R. D., Knipmeyer, S. E., & Nguyen, A. (1997). Vapor Pressure , Heat Capacity , and Density along the Saturation Line , Measurements for Cyclohexanol , 2-Cyclohexen-1-one , Acid , 2- (Methylamino) ethanol , Perfluoro-n -heptane , and Sulfolane. *J. Chem. Eng. Data*, *9568*(97), 1021–1036.

Tan, J., Bennett, T. D., & Cheetham, A. K. (2010). Chemical structure, network topology, and porosity effects on the mechanical properties of Zeolitic Imidazolate Frameworks. *Proceedings of the …*, *107*(22), 9938–9943. doi:10.1073/pnas.1003205107/-/DCSupplemental.www.pnas.org/cgi/doi/10.1073/pnas.1003205107

Tan, J. C., Bennett, T. D., & Cheetham, A. K. (2010). Chemical structure, network topology, and porosity effects on the mechanical properties of Zeolitic Imidazolate Frameworks. *Proceedings of the National Academy of Sciences of the United States of America*, *107*(22), 9938–43. doi:10.1073/pnas.1003205107

185

Tavolaro, A., & Drioli, E. (1999a). Zeolite membranes. *Advanced Materials*, *11*(12), 975–996. doi:10.1002/(SICI)1521-4095(199908)11:12<975::AID-ADMA975>3.0.CO;2-0

Tavolaro, A., & Drioli, E. (1999b). Zeolite Membranes. *Advanced Materials*, *11*(12), 975–996. doi:10.1002/(SICI)1521-4095(199908)11:12<975::AID-ADMA975>3.0.CO;2-0

Tsuru, T., Kondo, H., Yoshioka, T., & Asaeda, M. (2004). Permeation of Nonaqueous Solution through Organic/Inorganic Hybrid Nanoporous Membranes. *AIChE Journal*, *50*(5), 1080–1087. doi:10.1002/aic.10092

Ulbricht, M. (2006). Advanced Polymer Membranes. *Polymer*, *47*(7), 2217–2262.

Van der Perre, S., Van Assche, T., Bozbiyik, B., Lannoeye, J., De Vos, D. E., Baron, G. V, & Denayer, J. F. M. (2014). Adsorptive characterization of the ZIF-68 metal-organic framework: a complex structure with amphiphilic properties. *Langmuir : The ACS Journal of Surfaces and Colloids*, *30*(28), 8416–24. doi:10.1021/la501594t

Venna, S. R., & Carreon, M. A. (2010). Highly Permeable Zeolite Imidazolate Framework-8 Membranes for CO 2 / CH 4 Separation, 76–78.

Venna, S. R., Zhu, M., Li, S., & Carreon, M. a. (2013). Knudsen diffusion through ZIF-8 membranes synthesized by secondary seeded growth. *Journal of Porous Materials*, *21*(2), 235–240. doi:10.1007/s10934-013-9768-1

Waite, J. H. (1999). Reverse engineering of bioadhesion in marine mussels. *Annals of the New York Academy of Sciences*, *875*, 301–309. doi:10.1111/j.1749-6632.1999.tb08513.x

Walton, K. S., & LeVan, M. D. (2004). Separation of Carbon Monoxide and Carbon Dioxide for Mars ISRU, *2*, 500–502. Retrieved from http://hdl.handle.net/2060/20040161229

Wee, S.-L., Tye, C.-T., & Bhatia, S. (2008). Membrane separation process—Pervaporation through zeolite membrane. *Separation and Purification Technology*, *63*(3), 500–516. doi:10.1016/j.seppur.2008.07.010

Wegner, K., Dong, J., & Lin, Y. S. (1999). Polycrystalline MFI zeolite membranes : xylene pervaporation and its implication on membrane microstructure, *158*, 17–27.

Wessling, M. (1991). Plasticization of gas separation membranes. *Gas Separation & Purification*, *5*, 222–228.

Wong-foy, A. G., Matzger, A. J., & Yaghi, O. M. (2010). Exceptional H 2 Saturation Uptake in Microporous Metal - Organic Frameworks, 3494–3495.

Xiao, J. (1992). Diffusion Mechanism of Hydrocarbon in Zeolites-I Theory. *Chemical Engineering Science*, *47*, 1123–1141.

Xiao, Y., Low, B. T., Hosseini, S. S., Chung, T. S., & Paul, D. R. (2009). The strategies of molecular architecture and modification of polyimide-based membranes for CO2 removal from natural gas—A review. *Progress in Polymer Science*, *34*(6), 561–580. doi:10.1016/j.progpolymsci.2008.12.004

Xie, Z., Li, T., Rosi, N. L., & Carreon, M. a. (2014). Alumina-supported cobalt–adeninate MOF membranes for CO2/CH4 separation. *Journal of Materials Chemistry A*, *2*(5), 1239. doi:10.1039/c3ta14058j

Yampolskii, Y. (2012). Polymeric Gas Separation Membranes. *Macromolecules*, *45*(8), 3298–3311. doi:10.1021/ma300213b

Yao, J., & Wang, H. (2013). Zeolitic imidazolate framework composite membranes and thin films: Synthesis and applications. *Chemical Society Reviews*.

Yao, J., & Wang, H. (2014). Zeolitic imidazolate framework composite membranes and thin films: synthesis and applications. *Chemical Society Reviews*, 4470–4493. doi:10.1039/c3cs60480b

Yu, M., Noble, R. D., & Falconer, J. L. (2011). Zeolite membranes: microstructure characterization and permeation mechanisms. *Accounts of Chemical Research*, *44*(11), 1196–206. doi:10.1021/ar200083e

Zhang, X., Liu, Y., Kong, L., Liu, H., Qiu, J., Han, W., … Zhu, W. (2013). A simple and scalable method for preparing low-defect ZIF-8 tubular membranes. *Journal of Materials Chemistry A*, *1*(36), 10635. doi:10.1039/c3ta12234d

Zhang, X., Liu, Y., Li, S., Kong, L., Liu, H., Li, Y., … Qiu, J. (2014). New Membrane Architecture with High Performance : ZIF - 8 Membrane Supported on Vertically Aligned ZnO Nanorods for Gas Permeation and Separation. *Chemistry*, *26*, 1975–1981.

Zhang, Y., Gao, Q., Lin, Z., Zhang, T., Xu, J., Tan, Y., … Jiang, L. (2014). Constructing free standing metal organic framework MIL-53 membrane based on anodized aluminum oxide precursor. *Scientific Reports*, *4*, 4947. doi:10.1038/srep04947

Zhao, L., Riensche, E., Menzer, R., Blum, L., & Stolten, D. (2008). A parametric study of CO2/N2 gas separation membrane processes for post-combustion capture. *Journal of Membrane Science*, *325*(1), 284–294. doi:10.1016/j.memsci.2008.07.058

Zhao, Z., Li, Z., & Lin, Y. S. (2009). Adsorption and Diffusion of Carbon Dioxide on Metal−Organic Framework (MOF-5). *Industrial & Engineering Chemistry Research*, *48*(22), 10015–10020. doi:10.1021/ie900665f

Zhao, Z., Ma, X., Kasik, A., Li, Z., & Lin, Y. S. (2013). Gas Separation Properties of Metal Organic Framework (MOF-5) Membranes. *Industrial & Engineering Chemistry Research*, *52*(3), 1102–1108. doi:10.1021/ie202777q

Zhao, Z., Ma, X., Li, Z., & Lin, Y. S. (2011a). Synthesis, characterization and gas transport properties of MOF-5 membranes. *Journal of Membrane Science*, *382*(1-2), 82–90. doi:10.1016/j.memsci.2011.07.048

Zhao, Z., Ma, X., Li, Z., & Lin, Y. S. (2011b). Synthesis, characterization and gas transport properties of MOF-5 membranes. *Journal of Membrane Science*, *382*(1-2), 82–90. doi:10.1016/j.memsci.2011.07.048

Zhou, Y., Wu, J., & Lemmon, E. W. (2012). Thermodynamic Properties of o -Xylene , m -Xylene , p -Xylene , and Ethylbenzene. *J. Phys. Chem. Ref. Data*, *41*(2).

APPENDIX A

PROCEDURE FOR SYNTHESIS OF HOMEMADE ALPHA ALUMINA SUPPORTS

Table A.1 *Main chemicals and experimental materials*

Chemicals	Molecular formula	Purity	MW (g/mol)	From
A16 Alumina Powder	Al_2O_3	$\geq 99.0\%$ (KT)	101.96	Alcoa
Deionized Water	H_2O	-	18.02	-

(1) Measure out 21 g of A16 Al_2O_3 powder and 2.1 g of deionized water.

(2) Mix thoroughly with a mortar and pestle.

(3) Measure out 3.1 grams of the mixture and put it into the 22 mm mold and press to an applied load of 20,000 lb.

(4) The pressure is held for a minute and then slowly released.

(5) Following pressing, the green bodies are held at 40°C for 2 days.

(6) The green bodies are then sintered per Table A.2.

(7) The sintered supports are then polished with 500, 800 and 1200 grit sandpaper.

Table A.2 *Furnace ramp rates and holding times for alumina support sintering*

STEP	RATE (°C/HR)	T_{SP} (°C)	T_{HOLD} (HR)
1	60	600	0.1
2	96	1260	0.1
3	96	200	0.1
4	60	1150	30
5	60	200	0.1

APPENDIX B

PROCEDURE FOR MOF-5 MEMBRANE SYNTHESIS VIA SEEDING AND

SECONDARY GROWTH

Table B.1 *Main chemicals and experimental materials*

Chemicals	Molecular formula	Purity	MW (g/mol)	From
Zinc nitrate	$Zn(NO_3) \cdot 6H_2O$	$\geq 99.0\%$ (KT)	297.48	Fluka
Terephthalic	$C_8H_6O_4$	$\geq 99\%$ (NT)	166.14	Fluka
Dimethylformamide	$HCON(CH_3)_2$	99.8%	73.09	Mallinckrodt
Chloroform	$CHCl_3$	99.8%	119.38	Mallinckrodt
Ethyldiisopropylamine		--	--	Alfa Aeasar

Synthesis of MOF-5 membranes utilized terephthalic acid (BDC, +99%, from Aldrich) and zinc nitrate ($Zn(NO_3)_2$, 99.5%, from Fluka), and dimethylformamide (DMF, 99%, from Mallinckrodt) as the organic solvent. All chemicals used in this work were purchased from these vendors and used without further purification. The synthesis occurs in three separate stages; MOF-5 crystal synthesis, support seeding and secondary growth.

MOF-5 Crystal Synthesis

(1) First 60 mL of DMF was degassed in argon for 60 minutes.

(2) 5.6 mmol of zinc nitrate hexahydrate (1.664g) and 2.12 mmol of terephthalic acid (0.352g) were measured out and added to 40 mL of the degassed DMF in a sealable vial.

(3) The solution was thoroughly mixed, and the vial was then capped.

(4) The vial was then placed in an oil bath heated to 130°C for 4 hours.

(5) After 4 hours, the vial was taken out of the oil bath and allowed to return to room

temperature naturally.

(6) The mother liquid was decanted and fresh DMF was added to remove any unreacted precursors.

(7) That DMF was then decanted and chloroform was added to the vial, which was then sealed tightly and put into the oven at 70°C for three days. During the heating process, the solvent was decanted and replenished every day, to facilitate solvent exchange.

(8) After three days the chloroform was decanted and the crystals were dried at room temperature overnight under vacuum.

Procedure for Seeding the Support

(9) The dried crystals were then ball milled in chloroform with zirconia balls at a ratio of 25:1 with the dried powder for 24 hours at 175 RPMs.

(10) Following 24 hours, the ball milling media was removed and the remaining chloroform was removed overnight at room temperature under vacuum.

(11) The dried ball-milled crystals were then used to make a dip-coating solution; 2% MOF-5 crystals in DMF.

(12) Once measured out, the solution was ultrasonically agitated for 4 hours.

(13) The agitated solution was then used to dip-coat α-alumina supports.

  a) Clean and polished supports were placed on the surface of the dip-coating solution, polished side down, for five seconds.

  b) The excess solution was allowed to run off.

  c) The support was then placed in an oven at 50°C for 24 hours.

  d) This was repeated three times.

Procedure for Secondary Growth

(14) First 60 mL of DMF was degassed in argon for 60 minutes.

(15) 1.4 mmol of zinc nitrate hexahydrate (0.416g) and 0.485 mmol of terephthalic acid (0.088g) were measured out and added to 40 mL of the degassed DMF in a sealable vial.

(16) The solution was thoroughly mixed, and while mixing 0.53 mmol of ethyldiisopropylamine was added drop-wise to the still stirring solution. Once thoroughly mixed, a seeded support was added to the vial, suspended vertically by a Teflon holder. The vial was then capped.

(17) The vial was then placed in an oil bath heated to 130°C for 4 hours.

(18) After 4 hours, the vial was taken out of the oil bath and allowed to return to room temperature naturally.

(19) The membrane was then removed, rinsed in DMF, and placed in chloroform for solvent exchange.

(20) After two days in chloroform, the membrane was removed and dried overnight under vacuum at room temperature.

APPENDIX C

PROCEDURE FOR SYNTHESIS OF HOMEMADE ZINC OXIDE SUPPORTS

Table C.1 *Main chemicals and experimental materials*

Chemicals	Molecular Formula	Purity	MW (g/mol)	From
Zinc Oxide	ZnO	$\geq$ 99.0% (KT)	297.48	Alfa Aesar
PVA (3% in water)	$(C_4H_6O_2)_n$		86.09	Alfa Aesar

(1) 75 grams of ZnO powder and 8 grams PVA 3% solution is measured out.

(2) Combine the ingredients and mix thoroughly with a mortar and pestle.

(3) Measure out 3.2 grams of the mixture and put it into the 22 mm mold and press to an applied load of 12,500 lb.

(4) The pressure is held for a minute and then slowly released.

(5) Following pressing, the green bodies are sintered at 570°C for 5 hours.

(6) The sintered supports are then gently polished manually with 800 and 1200 grit sandpaper.

APPENDIX D

PROCEDURE FOR ZIF-68 MEMBRANE SYNTHESIS VIA REACTIVE SEEDING

Table D.1 Main chemicals and experimental materials

Chemicals	Molecular Formula	Purity	MW (g/mol)	From
Zinc nitrate hexahydrate	$Zn(NO_3) \cdot 6H_2O$	$\geq 99.0\%$	297.48	Fluka
Benzimidazole	$C_7H_6N_2$	98%	118.14	Sigma-Aldrich
2-Nitroimidazole	$C_3H_3N_3O_2$	$\geq 98.0\%$	113.07	Bosche
Dimethylformamide	$HCON(CH_3)_2$	99%	73.09	Alfa Aesar

Reactive seeding synthesis of ZIF-68 membranes will utilize dimethylformamide, zinc nitrate hexahydrate, 2-nitroimidazole and benzimidazole (with purities of 99%, $\geq 98.0\%$, $\geq 98.0\%$ and 99% respectively). All chemicals used in this work were purchased from these vendors and used without further purification. The synthesis occurs in two stages; seeding and secondary growth.

Procedure for ZIF-68 support seeding

(8) 0.25 mmol of 2-nitroimidazole (~0.028g) and 0.25 mmol of benzimidazole (~0.030g) were added to 30 mL of DMF and stirred vigorously.

(9) Once thoroughly stirred, the solution was poured into a Teflon lined autoclave where a polished ZnO support is suspended, polished side down.

(10) The autoclave is sealed and inserted into a low-temperature oven set to 120°C and allowed to react for 8 hours.

(11) Once the autoclave has completely cooled, the seeded support is removed and washed gently with fibrous cotton in DMF, and allowed to soak in DMF for three hours.

(12) The seeded support is then dried for 2 hours or so at 100°C.

Procedure for ZIF-68 secondary growth

(13) 1 mmol each of zinc nitrate hexahydrate, 2-nitroimidazole and benzimidazole are measured out.

(14) The 2-nitroimidazole and benzimidazole are added to a vial containing 20 mL of DMF and left to stir vigorously.

(15) The zinc nitrate hexahydrate is added to a vial containing 10 mL of DMF and is stirred vigorously.

(16) Once the zinc nitrate hexahydrate is dissolved completely, it is added dropwise to the still stirring mixture of the imidazole precursors and DMF.

(17) Once thoroughly stirred, the solution was poured into a Teflon lined autoclave where the seeded ZnO support is suspended, seeded side down.

(18) The autoclave is sealed and inserted into a low-temperature oven set to 120°C and allowed to react for 8 hours.

(19) Once the autoclave has completely cooled, the membrane is removed and washed gently with fibrous cotton in DMF, and allowed to soak in DMF for three hours.

(20) The membrane is then dried overnight at room temperature under vacuum.

APPENDIX E

SYNTHESIS OF ZIF-68 MEMBRANES VIA MODIFIED REACTIVE SEEDING

METHOD

Table E.1 *Main chemicals and experimental materials*

Chemicals	Molecular Formula	Purity	MW (g/mol)	From
Zinc nitrate hexahydrate	$Zn(NO_3)\cdot6H_2O$	$\geq 99.0\%$	297.48	Fluka
Benzimidazole	$C_7H_6N_2$	98%	118.14	Sigma-Aldrich
2-Nitroimidazole	$C_3H_3N_3O_2$	$\geq 98.0\%$	113.07	Bosche
Zinc Chloride	$ZnCl_2$		136.32	Alfa Aesar
Sodium Formate	$HCOONa$		68.01	Alfa Aesar
Dimethylformamide	$HCON(CH_3)_2$	99%	73.09	Alfa Aesar
Methanol	$MeOH$	99.8%	32.05	BDH

The surface modification step will require sodium formate, zinc chloride and methanol to create a homogeneous layer of ZnO on a homemade Al_2O_3 support$_s$ Reactive seeding synthesis of ZIF-68 membranes will utilize dimethylformamide, zinc nitrate hexahydrate, 2-nitroimidazole and benzimidazole (with purities of 99%, $\geq 98.0\%$, $\geq 98.0\%$ and 99% respectively). All chemicals used in this work were purchased from these vendors and used without further purification. The synthesis occurs in three stages; *in situ* coating of ZnO, reactive seeding and secondary growth.

Procedure for *in situ* coating of ZnO on α-Al_2O_3 support

(1) 6.3 mmol of sodium formate (1.43g) and 4 mmol of zinc chloride (0.55g) were added to 30 mL of MeOH and stirred vigorously.

(2) Once the solution was well mixed, it was poured into a Teflon lined autoclave where two polished Al_2O_3 supports are suspended vertically, polished sides outward and unpolished sides flush with one another.

(3) The autoclave is then sealed and placed in an oven at 120°C for 4 hours.

(4) Following the reaction, the autoclave is allowed to return to room temperature naturally.

(5) The coated supports are then removed, rinsed in methanol and allowed to dry

overnight under vacuum.

Procedure for ZIF-68 support seeding

(6) 0.25 mmol of 2-nitroimidazole (~0.028g) and 0.25 mmol of benzimidazole (~0.030g) were added to 30 mL of DMF and stirred vigorously

(7) The solution was then poured into a Teflon-lined autoclave where a ZnO coated Al_2O_3 support is suspended, polished side down.

(8) The autoclave is then sealed and inserted into a low-temperature oven set to 120°C and allowed to react for 8 hours.

(9) Once the autoclave has completely cooled, the seeded support is removed and washed gently with fibrous cotton in DMF, and allowed to soak in DMF for three hours.

(10) The seeded support is then dried for 2 hours or so at 100°C.

Procedure for ZIF-68 secondary growth

(11) 1 mmol each of zinc nitrate hexahydrate, sodium formate, 2-nitroimidazole and benzimidazole are measured out.

(12) The 2-nitroimidazole and benzimidazole are added to a vial containing 20 mL of DMF and left to stir vigorously.

(13) The zinc nitrate hexahydrate and sodium formate are added to a vial containing 10 mL of DMF and is stirred vigorously.

(14) Once the zinc nitrate hexahydrate and sodium formate are dissolved completely, the solution is added dropwise to the still stirring mixture of the imidazole precursors and DMF.

(15) Once thoroughly stirred, the solution was poured into a Teflon-lined autoclave where the seeded ZnO support is suspended, seeded side down.

(16) The autoclave is sealed and inserted into a low-temperature oven set to 120°C and allowed to react for 8 hours.

(17) Once the autoclave has completely cooled, the membrane is removed and washed gently with fibrous cotton in DMF, and allowed to soak in DMF for three hours.

(18) The membrane is then dried overnight at room temperature under vacuum.

APPENDIX F

SYNTHESIS OF ZIF-68 CRYSTALS

Table F.1 *Main chemicals and experimental materials*

Chemicals	Molecular Formula	Purity	MW (g/mol)	From
Zinc nitrate hexahydrate	$Zn(NO_3) \cdot 6H_2O$	$\geq 99.0\%$	297.48	Fluka
Benzimidazole	$C_7H_6N_2$	98%	118.14	Sigma-Aldrich
2-Nitroimidazole	$C_3H_3N_3O_2$	$\geq 98.0\%$	113.07	Bosche
Dimethylformamide	$HCON(CH_3)_2$	99%	73.09	Alfa Aesar

Synthesis of ZIF-68 crystals will utilize dimethylformamide, zinc nitrate hexahydrate, 2-nitroimidazole and benzimidazole (with purities of 99%, $\geq 98.0\%$, $\geq 98.0\%$ and 99% respectively). All chemicals used in this work were purchased from these vendors and used without further purification.

(1)   1 mmol of 2-nitroimidazole (~0.113g) and 1 mmol of benzimidazole (~0.118g) were added to 10 mL of DMF and stirred vigorously in a sealable vial. And in a separate vial 1 mmol of zinc nitrate hexahydrate (~0.297g) was added to 5 mL of DMF and stirred vigorously.

(2)   Once both were dissolved in the DMF, the solution of zinc nitrate hexahydrate in DMF was added drop-wise to the still stirring solution of the imidazole precursors in DMF.

(3)   The solution was then left to stir for 20 minutes.

(4)   The vial containing the solution was then capped and placed in an oven at 85°C and left to react for 52 hours.

(5)   Following 52 hours, the solution was allowed to return to room temperature naturally.

(6)   The solution was then ultrasonicated and added to a centrifuge tube. Following 20 minutes at 3.9 RPMs the mother liquid was decanted and fresh DMF was added to the tube. The crystals were then ultrasonically agitated and centrifuged as before. The DMF was decanted following centrifuging.

(7)   Methanol was then placed in the tube.   This was ultrasonically agitated, centrifuged and decanted as before.   This was repeated three times.   The third time the methanol was ultrasonically agitated and left to sit overnight for solvent exchange.

(8)   The following day, the methanol was centrifuged and decanted, and the crystals were allowed to dry at room temperature under vacuum.

APPENDIX G

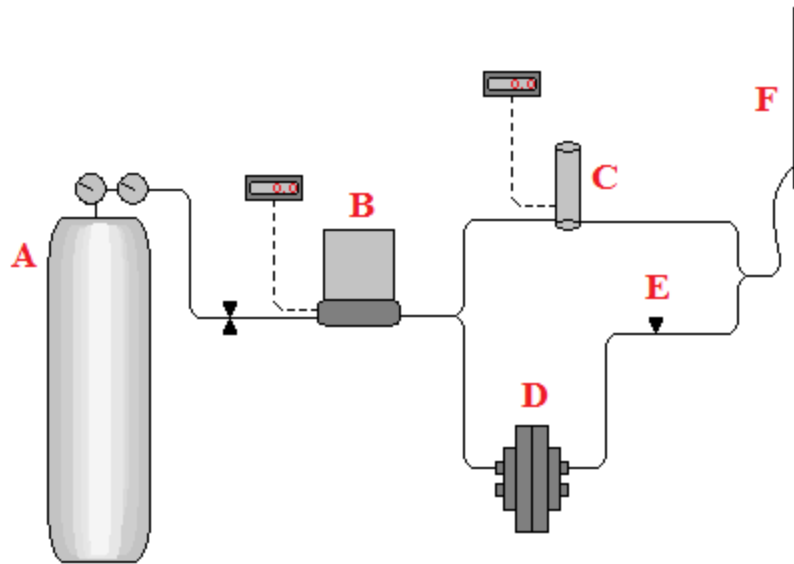# PROCEDURE FOR TESTING SINGLE COMPONENT GAS PERMEATION

Figure G.1

Schematic representation of the steady-state permeation setup. Legend: (A) helium

cylinder, (B) mass flow controller, (C) pressure sensor, (D) membrane cell, (E) needle

valve, (F) bubble flow meter.

(1)   Activate membrane under vacuum at 100°C for five hours prior to testing.

(2)   Following activation, remove the membrane from vacuum and place it in the membrane cell, secured by Viton O-rings.

(3)   Once the membrane is sealed in the membrane cell, connect the feed side to the gas being tested.

(4)   Tighten the needle valve (E on the diagram in Figure G.1) 12.5 turns.

(5)   Allow the system to reach steady state by monitoring the stability of the pressure read out on the pressure sensor (C on the diagram in Figure G.1).

(6)   Once steady state has been reached, note the P_h and ΔP on the pressure sensor and measure the flux with the bubble flow meter.

(7)   Obtain four more points by repeating steps (4) through (6) for each additional point.

(8)   The points should be measured first with the needle valve turned 12.5 times, then

the remaining points taken with the needled valve closed 13, 13.5 and 14 times. Take the final point with the needle valve completely closed. To allow for a wide cross-section of points to be obtained at differing average pressures.

APPENDIX H

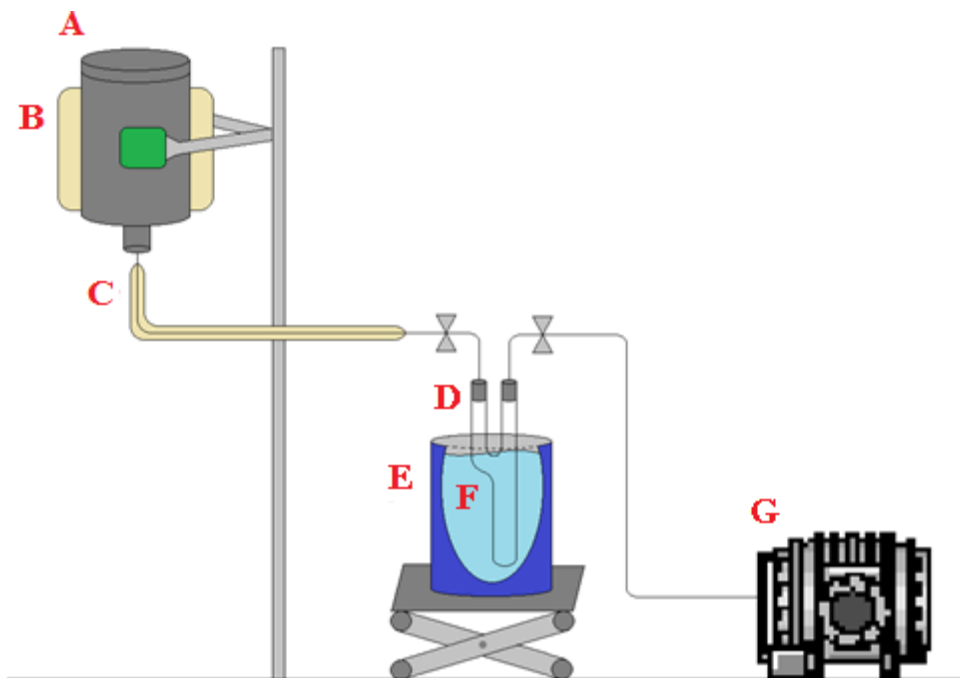PROCEDURE FOR TESTING SINGLE COMPONENT PERVAPORATION

Figure H.1

Schematic representation of the pervaporation setup. Legend: (A) membrane cell, (B) heating jacket, (C) heating coil, (D) cold trap, (E) liquid nitrogen dewar, (F) liquid nitrogen, (G) vacuum pump.

(1) Activate membrane under vacuum at 100°C for five hours prior to testing.

(2) Following activation, remove the membrane from vacuum and place it in the membrane cell with the membrane layer facing the open containment portion of the membrane cell.

(3) Seal the membrane in the cell with chemical resistant Viton O-rings.

(4) Once the membrane is sealed in the cell, fill the containment portion with the necessary probing molecules. If the molecules are liquid at room temperature, the membrane cell may be sealed and used as is, if the molecules are solid at room temperatures, follow the procedure below:

   a) Place solid molecules in the containment portion of the membrane cell and

seal thoroughly.

b) Put heating jacket on the membrane cell and heat to just above the melting point of the molecules.

c) Allow the cell to remain at that temperature for a half hour prior to testing, and throughout the entire pervaporation run.

(5) Once the cell is filled with the appropriate probing molecules and sealed, it can be affixed to the pervaporation set up.

(6) Prior to beginning pervaporation, measure the starting weight of the clean and dry cold trap that is to be used for testing.

(7) Once the cold trap is secured in the setup, a vacuum can be drawn throughout the entire system, with the exception of the membrane cell, which is closed off with a needle valve from the rest of the set up at this stage.

(8) Following the attainment of an adequate vacuum in the system, the cold trap is placed in liquid nitrogen, the valve to the membrane cell is opened and the time is noted to signal testing has begun.

(9) Following testing, take note of the time, close the valve to the membrane cell and turn off vacuum.

(10) Remove the cold trap from liquid nitrogen and allow it to warm up, removing all condensation.

(11) Finally, take the weight of the cold trap.

Pervaporation flux is calculated as follows:

$$Q_i = [(W_f - W_i)/MW_i]/(A \cdot \Delta T) \qquad \text{(H.1)}$$

Where W_f and W_i are the final and initial weight of the cold trap, MW_i is the molecular weight of probing molecule i, A is the membrane area and ΔT is the length of testing.

APPENDIX I

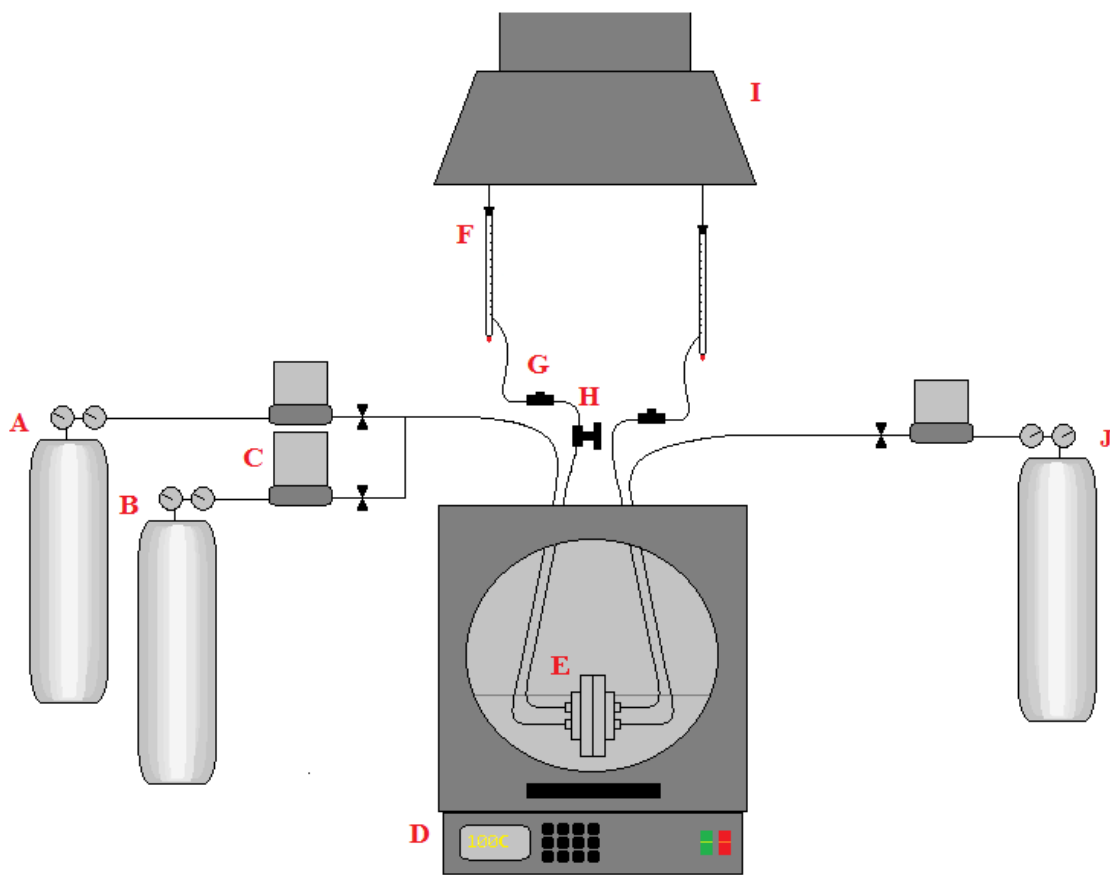## PROCEDURE FOR TESTING BINARY GAS SEPARATION

Figure I.1

Schematic representation of the pervaporation setup. Legend: (A) gas cylinder, (B) gas cylinder, (C) mass controller, (D) furnace, (E) membrane cell, (F) bubble flow meter, (G) sample taking port, (H) pressure control valve, (I) fume hood and (J) sweep gas.

(1) Place membrane in membrane cell with membrane layer on feed side. Place membrane cell in oven. Connect feed side to sweep gas (helium) and activate membrane under helium flow at 100°C for five hours prior to testing.

(2) Following activation, allow the membrane cell to return to room temperature (or whatever temperature at which testing is to occur) prior to switching gases.

(3) Once testing is ready to begin, set the appropriate flow of gas A and gas B using the mass controllers and allow steady state to be reached. Usually an hour or so is necessary for the first point.

(4) Once steady state has been reached, measure and record the flow rates on the permeate and retentate side with the attached bubble flow meters.

(5) To determine the concentration on the permeate and retentate sides, obtain gas samples at the sample ports on the set up.

(6) Take sample and inject it into the Agilent 6890N, which uses a HayeSep DB porous polymer 100/120 mesh packing material, with Ar carrier gas at 11.5 mL/min.
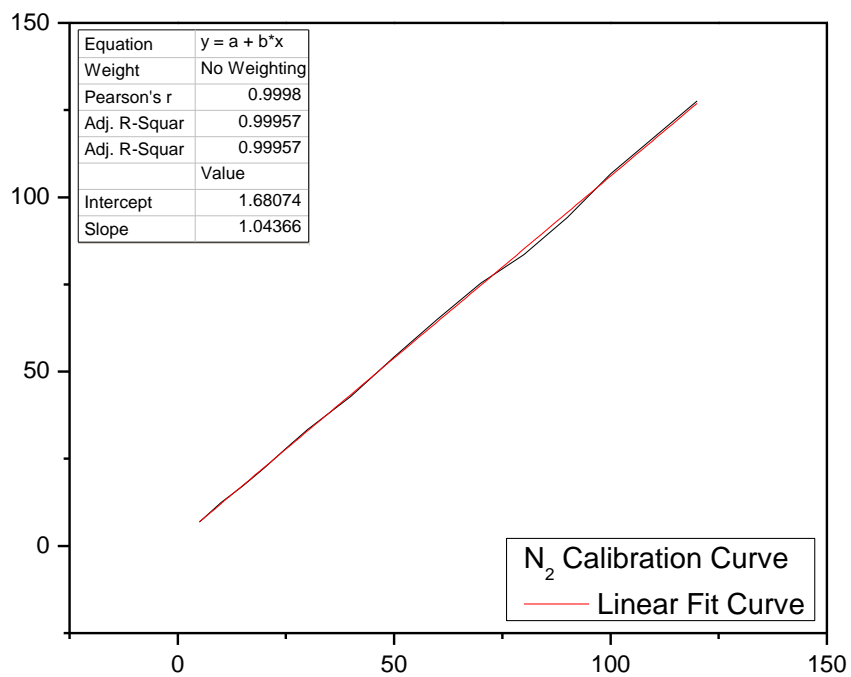

Equation	y = a + b*x
Weight	No Weighting
Pearson's r	0.9998
Adj. R-Squar	0.99957
Adj. R-Squar	0.99957
	Value
Intercept	1.68074
Slope	1.04366

N_2 Calibration Curve

Linear Fit Curve

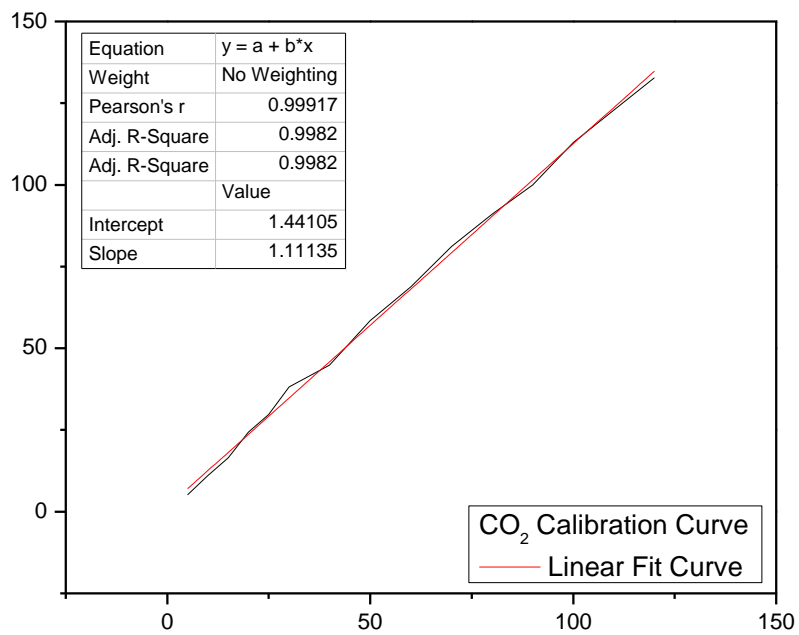Figure I.2

Calibration Curve for N_2 for GC.
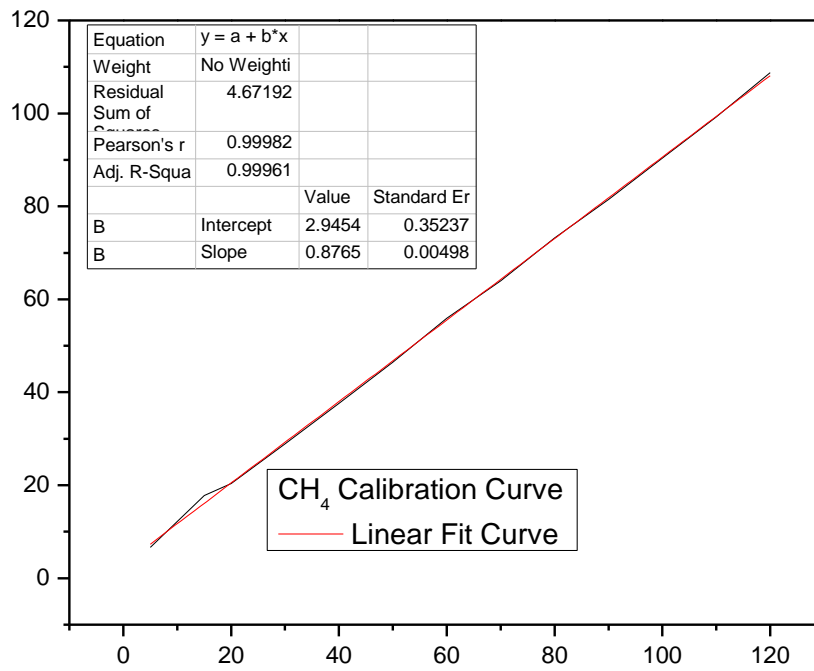
Figure I.3

Calibration Curve for CO₂ for GC.

Figure I.4

Calibration Curve for CH₄ for GC.